US008504135B2

(12) **United States Patent**
Bourqui et al.

(10) **Patent No.: US 8,504,135 B2**
(45) **Date of Patent: Aug. 6, 2013**

(54) **TRAVELING-WAVE ANTENNA**

(75) Inventors: **Jeremie Bourqui**, Calgary (CA); **Elise C. Fear**, Calgary (CA); **Michal Okoniewski**, Calgary (CA)

(73) Assignee: **UTI Limited Partnership**, Calgary, Alberta (CA)

(*) Notice: Subject to any disclaimer, the term of this patent is extended or adjusted under 35 U.S.C. 154(b) by 609 days.

(21) Appl. No.: **12/606,853**

(22) Filed: **Oct. 27, 2009**

(65) **Prior Publication Data**

US 2010/0145190 A1 Jun. 10, 2010

Related U.S. Application Data

(60) Provisional application No. 61/197,560, filed on Oct. 27, 2008.

(51) **Int. Cl.**
H01Q 13/00 (2006.01)

(52) **U.S. Cl.**
USPC **600/407**; 343/785

(58) **Field of Classification Search**
USPC 600/407, 425, 430; 343/767
See application file for complete search history.

(56) **References Cited**

U.S. PATENT DOCUMENTS

5,949,382	A	9/1999	Quan	343/767
6,208,308	B1	3/2001	Lemons	343/785
6,351,246	B1	2/2002	McCorkle	343/795
6,911,951	B2	6/2005	Dotto et al.	343/767
7,088,300	B2	8/2006	Fisher	343/767
7,193,575	B2	3/2007	Mohammadian	343/767
7,454,242	B2	11/2008	Fear et al.	600/430
2005/0107693	A1 *	5/2005	Fear et al.	600/430
2005/0219126	A1 *	10/2005	Rebeiz et al.	343/700 MS

OTHER PUBLICATIONS

Bourqui et al., "Balanced antipodal vivaldi antenna for breast cancer detection," *2nd Eur. Conf Antennas Propag.*, Edinburgh, UK, Nov. 11-16, 2007.

Bourqui et al., "Balanced antipodal vivaldi antenna with dielectric director for near-field microwave imaging," to appear in *IEEE Trans. Antennas Propag.*, 52 (7): 2010.

Bourqui et al., "Antenna performance for ultra-wideband microwave imaging," in *IEEE Radio and Wireless Symposium*, San Diego, CA, pp. 522-525, Jan. 18-22, 2009.

Bourqui, "Director effect on the radiation behaviour of the BAVA_ ID4," *Interrnal Technical Report*, University of Calgary, 2007.

Craddock et al., "An improved hemispherical antenna array design for breast imaging," in *EurAAP—The Second European Conference on Antennas and Propagation, Edinburgh, UK*, Nov. 11-16, 2007.

(Continued)

Primary Examiner — Parikha Mehta
(74) *Attorney, Agent, or Firm* — Fogarty, L.L.C.

(57) **ABSTRACT**

Embodiments of endfire aperture-based traveling-wave antennas are described. For example, an embodiment, including a Vivaldi antenna, may have a director incorporated into the aperture region of the antenna to provide enhanced radiation directivity. The director may be a shaped dielectric that interacts with an electromagnetic field to reduce the divergence of the resultant beam as it exits the antenna. Additional dielectric substrate layers may be stacked on both sides of the antenna in order to balance the dielectric loading between the different conductors. The dielectric substrates may also eliminate contact between the antenna metallization and the lossy environment. Certain disclosed Vivaldi antennas may be used in tissue screening applications.

21 Claims, 32 Drawing Sheets

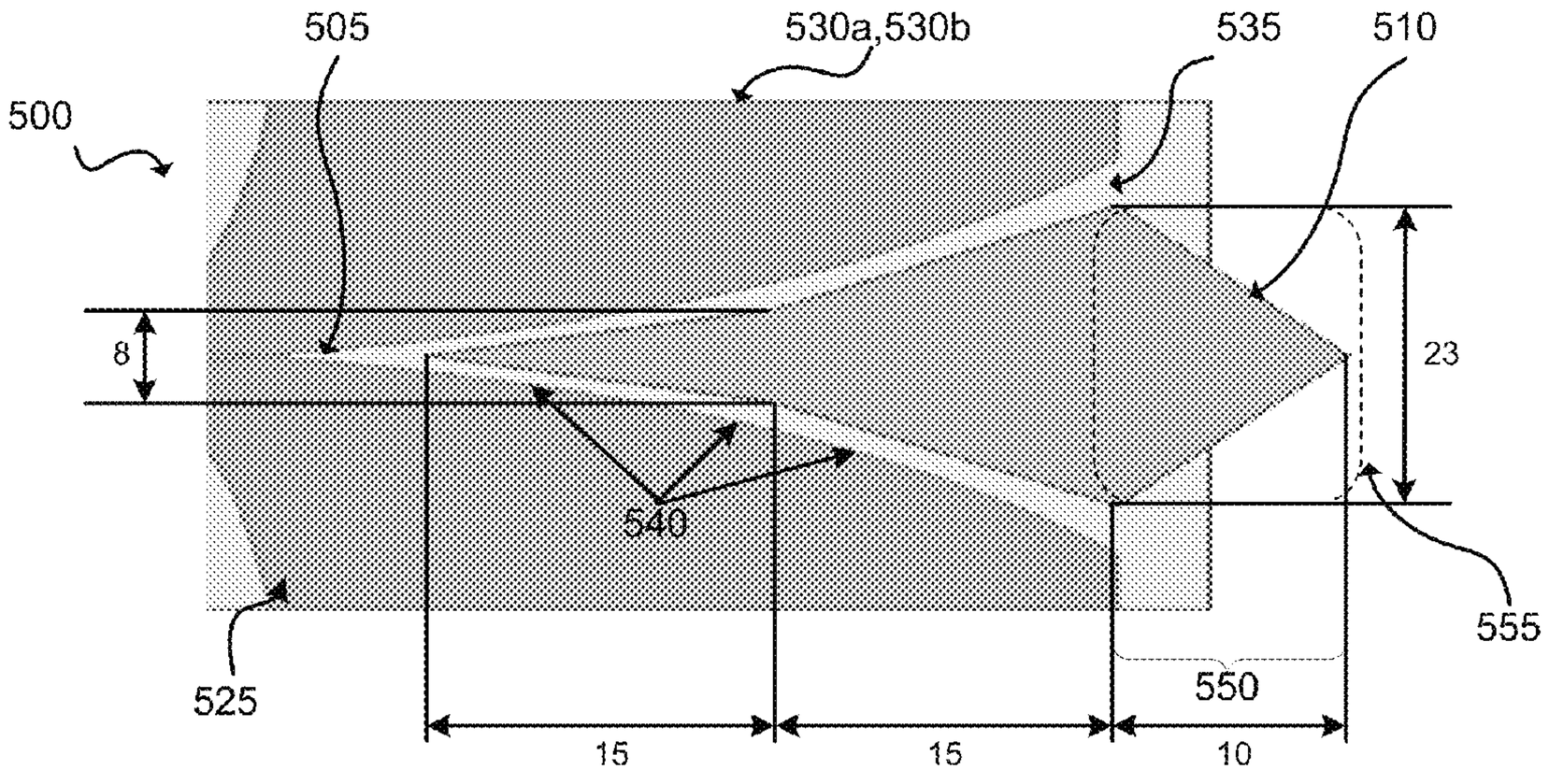

OTHER PUBLICATIONS

Elsherbini et al., "Uwb antipodal vivaldi antennas with protruded dielectric rods for higher gain, symmetric patterns and minimal phase center variations," in *Proc. IEEE Antennas and Propagation Society International Symposium*, 1973-1976, 2007.

Fear et al., "Confocal microwave imaging for breast cancer detection: localization of tumors in three dimensions," *IEEE Transactions on Biomedical Engineering*, 49 (8): 812-822, 2002.

Gibbens et al., "The design of a wide slot antenna for the transmission of UWB signals into the human body using FDTD simulation," *2nd European Conference on Antennas and Propagation, Edinburgh*, UK, 1: 1-5, Nov. 11-16, 2007.

Guillanton et al., "A new design tapered slot antenna for ultra-wideband applications," *Microwave and optical Technology Letters*, 19 (4): 286-289, 1998.

Khor et al., "An ultra wideband microwave imaging system for breast cancer detection," *IEICE Trans. Commun.*, E90-B (9): 2376-2381, 2007.

Kim and Chang, "Ultra wideband exponentially-tapered antipodal vivaldi antennas," *IEEE Antennas Propag. Soc. Int. Symp.*, 3: 2004.

Langley et al., "Balanced antipodal vivaldi antenna for wide bandwidth phased arrays," *IEE Proceedings—Microwaves, Antennas and Propagation*, 143 (2): 97-102, 1996.

Langley et al., "Multi-octave phased array for circuit integration using balanced antipodal vivaldi antenna elements," *IEEE Antennas Propag. Soc. Int. Symp.*, 1: 178-181, 1995.

Langley et al., "Novel ultrawide-bandwidth vivaldi antenna with low crosspolarisation," *Electronic Letters*, 29 (23): 2004-2005, 1993.

Lazebnik et al., "A large-scale study of the ultrawideband microwave dielectric properties of normal breast tissue obtained from reduction surgeries," *Physics in Medicine and Biology*, 52 (10): 2637-2656, 2007.

Lazebnik et al., "Highly accurate debye models for normal and malignant breast tissue dielectric properties at microwave frequencies," *IEEE Microwave and Wireless Components Letters*, 17 (12): 822-824, 2007.

Li et al., "Numerical and experimental investigation of an ultrawideband ridged pyramidal horn antenna with curved launching plane for pulse radiation," *IEEE Antennas and Wireless Propagation Letters*, 2: 259-262, 2003.

Montoya et al., "A study of pulse radiation from several broad-band loaded monopoles," *IEEE Transactions on Antennas and Propagation*, 44 (8): 1172-1182, 1996.

Nilavalan et al., "Wideband microstrip patch antenna design for breast cancer tumour detection," *IET Microwave, Attennas & Propagation*, 1: 277-281, 2007.

Rubaek et al., "Three-dimensional microwave imaging for breast-cancer detection using the log-phase formulation," *Proc. IEEE Antennas and Propagation Society International Symposium*, 2184-2187, 2007.

Schuneman et al., "Decade bandwidth tapered notch antenna array element," in *Antenna Applications Symposium*, 280-294, 2001.

Sill and Fear, "Tissue sensing adaptive radar for breast cancer detection: study of immersion liquids," *Electronic Letters*, 41: 113-115, 2005.

Sill and Fear, "Tissue sensing adaptive radar for breast cancer detection—experimental investigation of simple tumor models," *IEEE Transactions on Microwave Theory and Techniques*, 53 (11): 3312-3319, 2005.

Sill, "Second generation experimental system for tissue sensing adaptive radar," Master's thesis, Department of Electrical and Computer Engineering, Schulich School of Engineering, University of Calgary, Alberta, Canada, 2005.

Wang et al., "Analysis of ultra wideband antipodal vivaldi antenna design," *Loughborough Antennas and Propagation Conference*, 129-132, Apr. 2-3, 2007.

Winters et al., "Estimation of the frequency-dependent average dielectric properties of breast tissue using a time-domain inverse scattering technique," *IEEE Transactions on Antennas and Propagation*, 54 (11): 3517-3528, 2006.

* cited by examiner

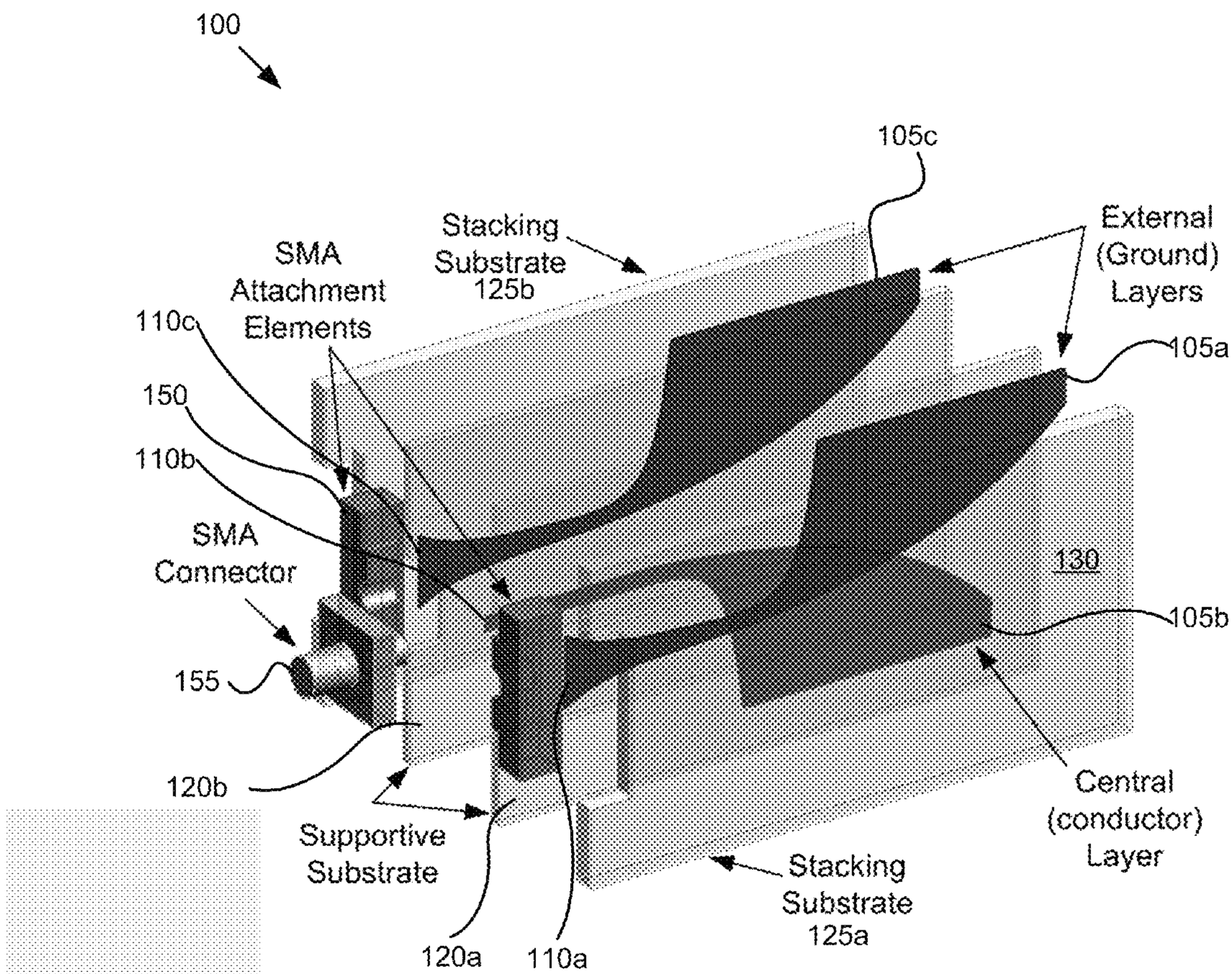
100
105c
Stacking Substrate 125b
External (Ground) Layers
SMA Attachment Elements
110c
105a
150
110b
SMA Connector
130
105b
155
120b
Supportive Substrate
Central (conductor) Layer
Stacking Substrate 125a
120a
110a

FIG. 1

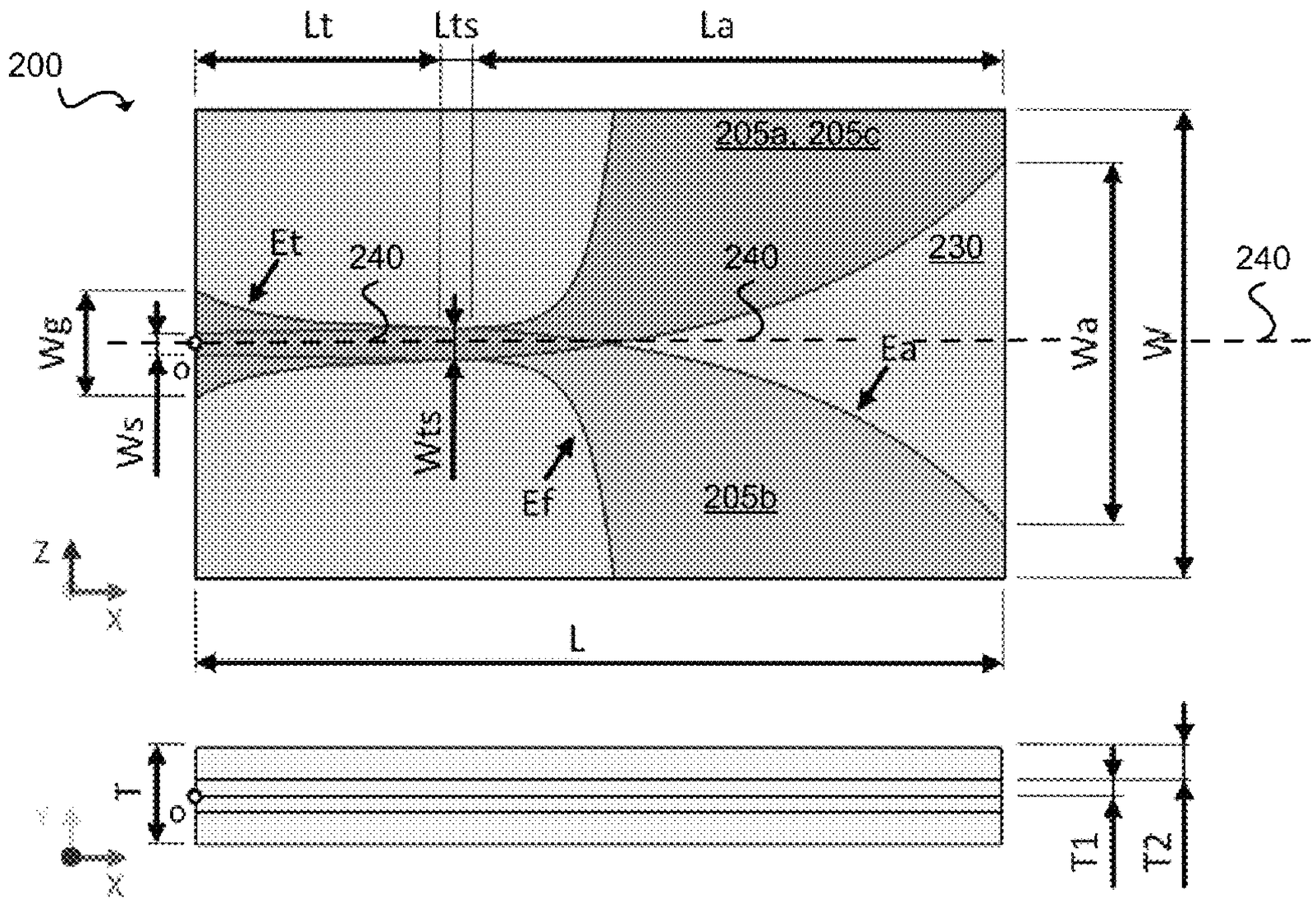
Lt
Lts
La
200
205a, 205c
Et
240
240
230
240
Wg
t
o
Ws
Wts
Ea
Wa
W
Ef
205b
Z
X
L
T
o
T1
T2

FIG. 2

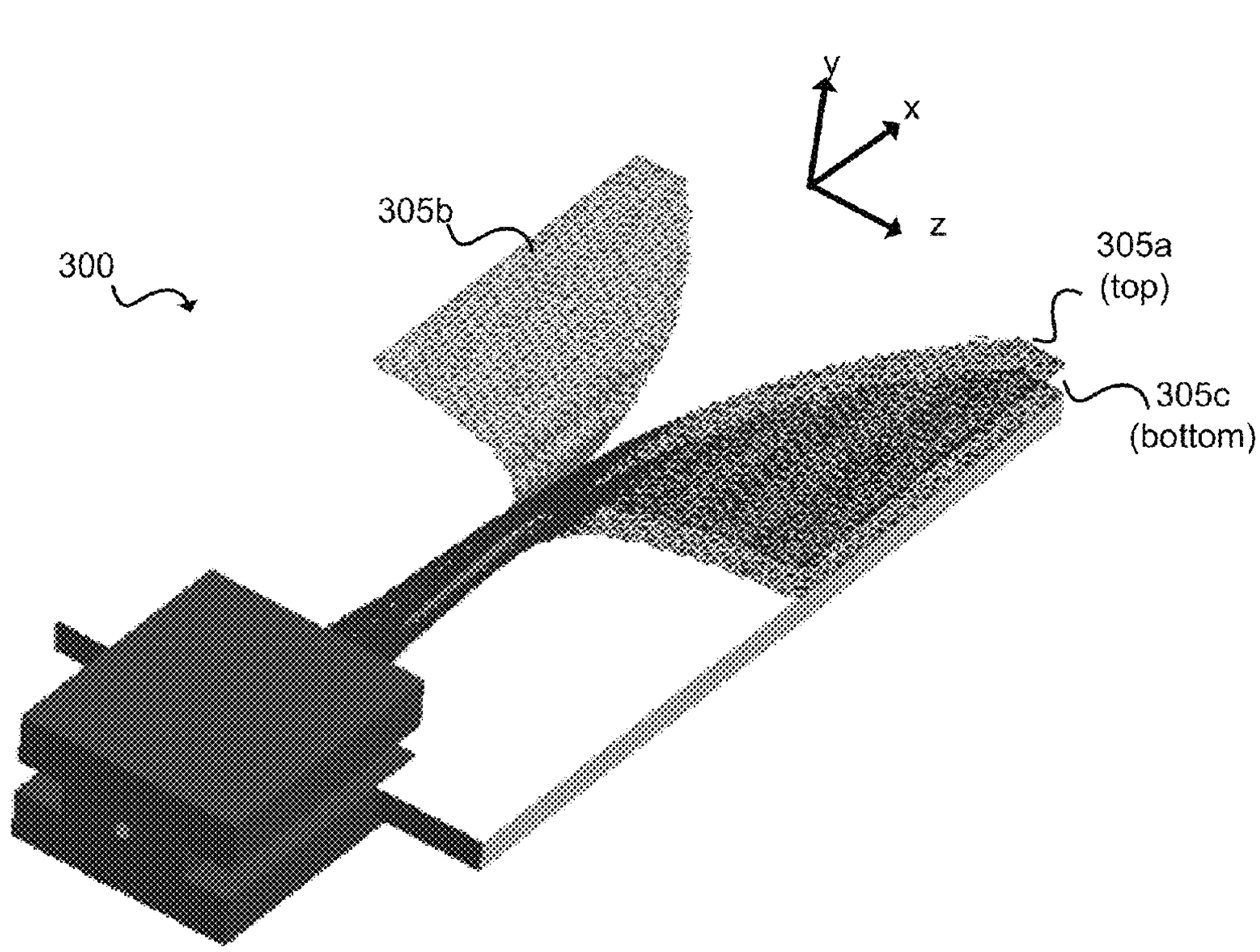

FIG. 3

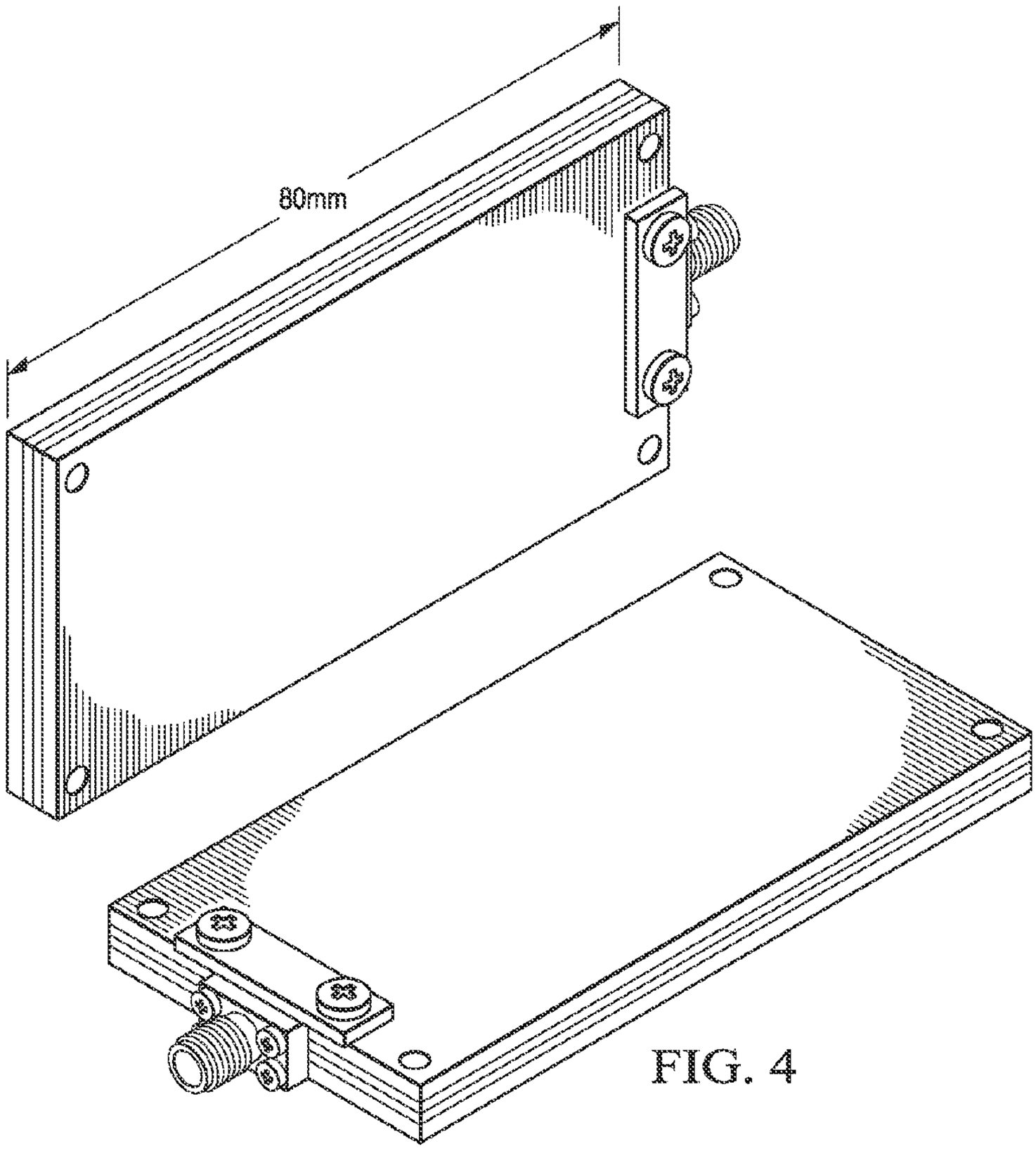

FIG. 4

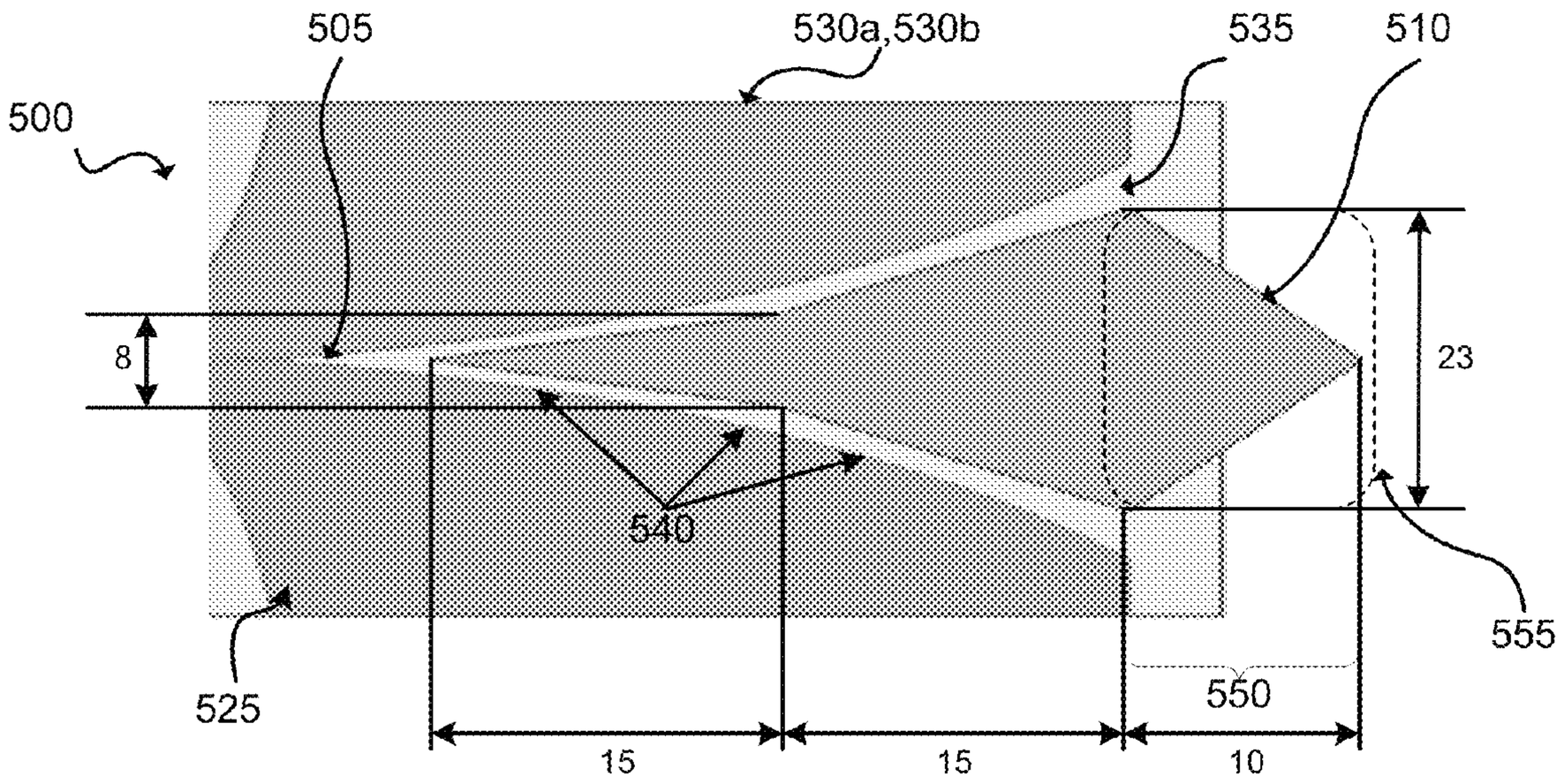

FIG. 5a

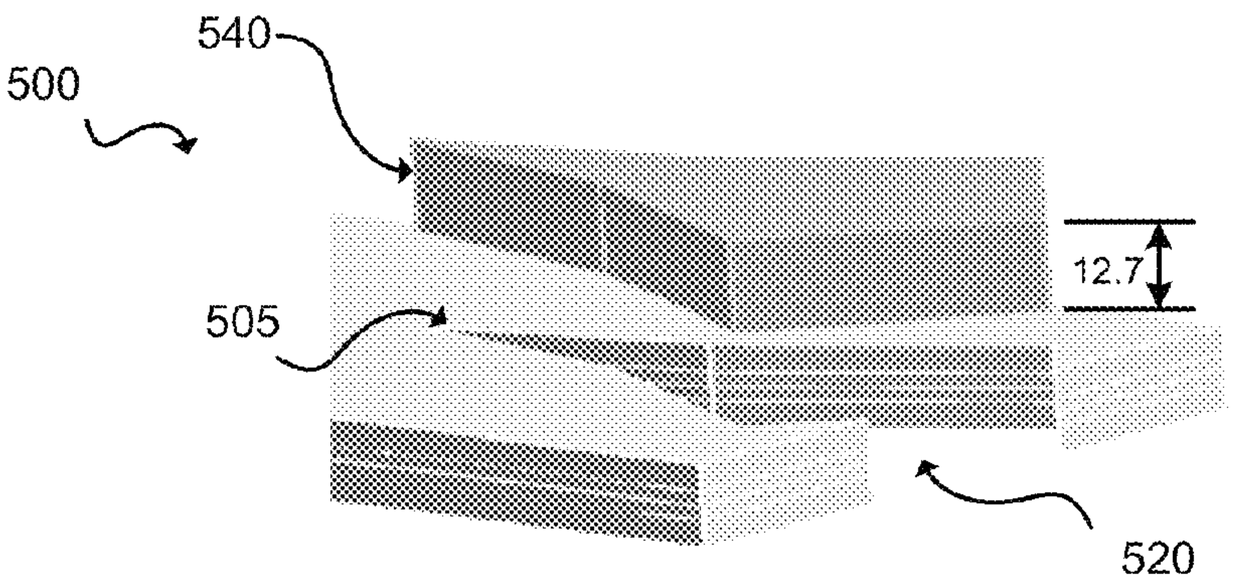

FIG. 5b

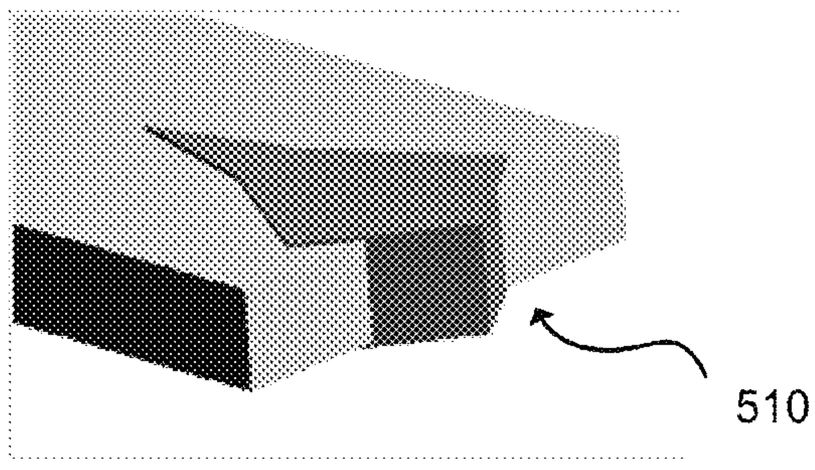

FIG. 5c

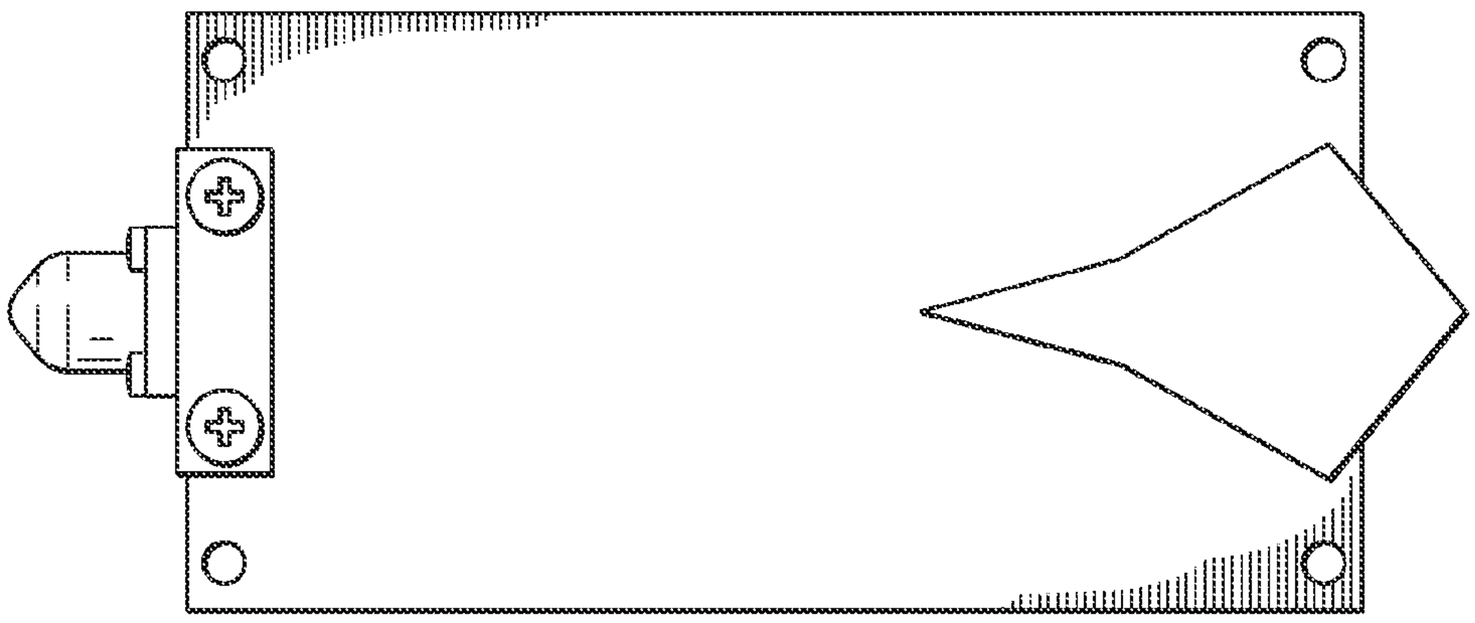

FIG. 6

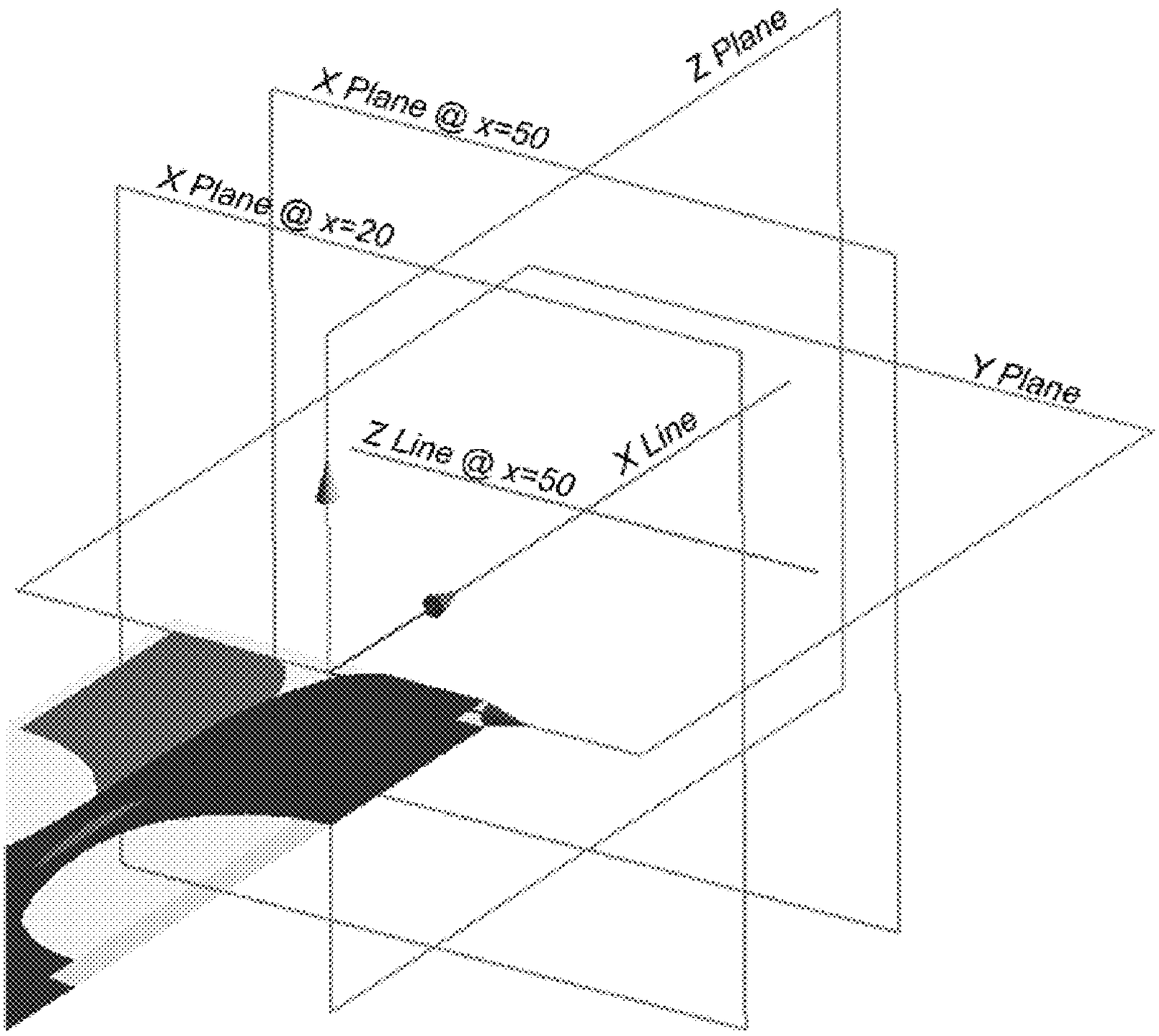

FIG. 7

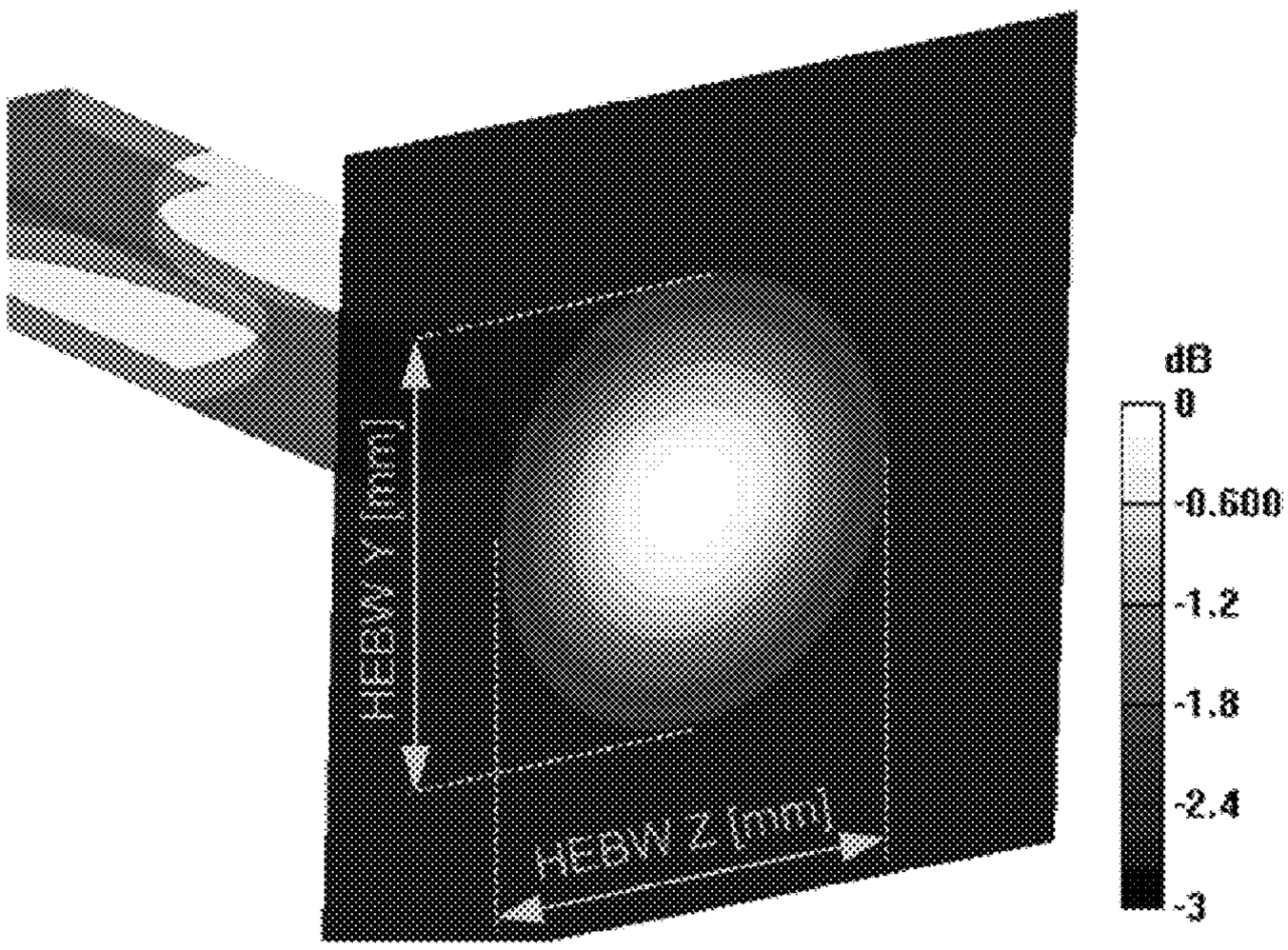

(a)
Energy Flux Density (x,y,z) in dB

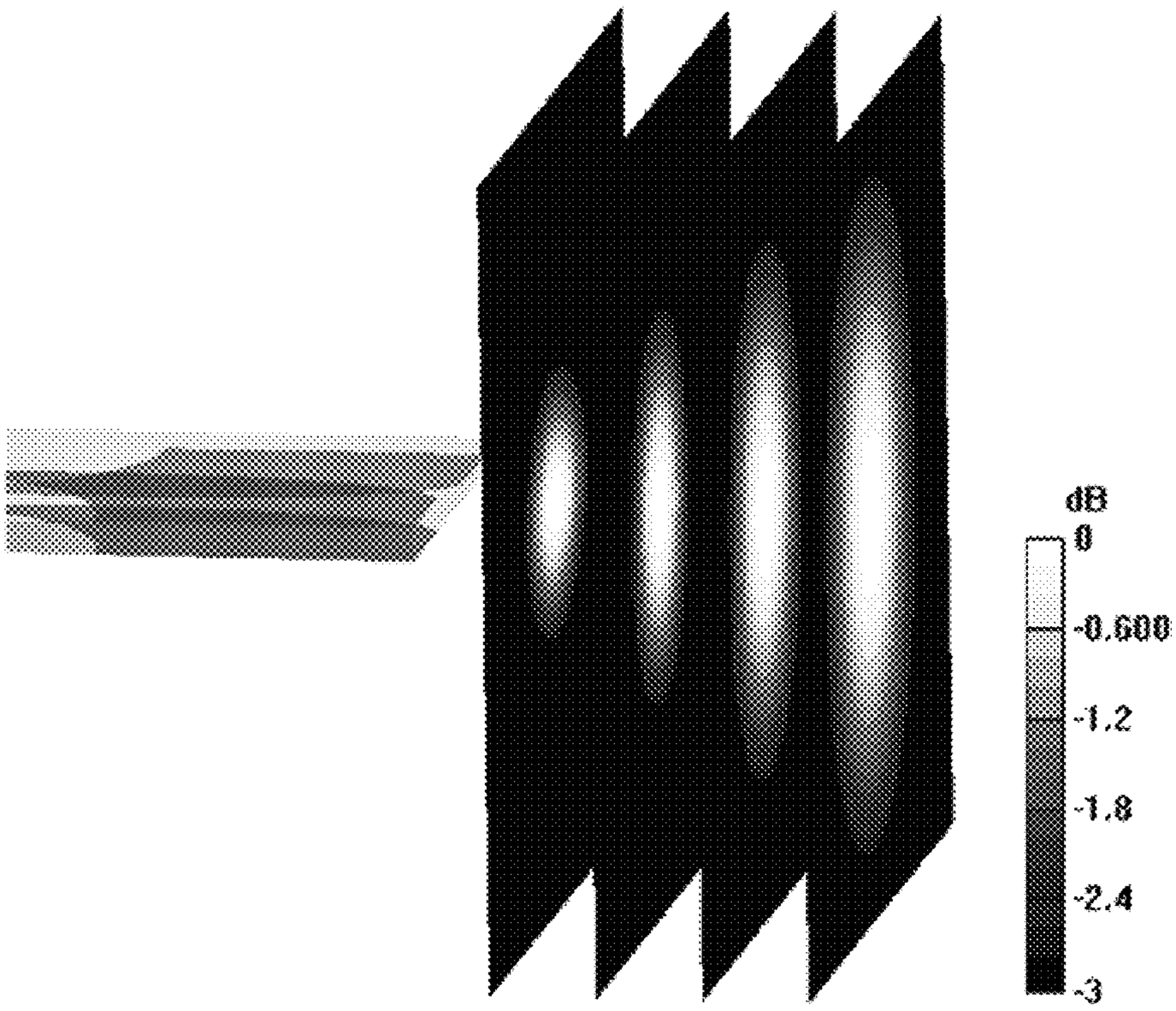

(b)
Energy Flux Density (x,y,z) in dB

FIG. 8

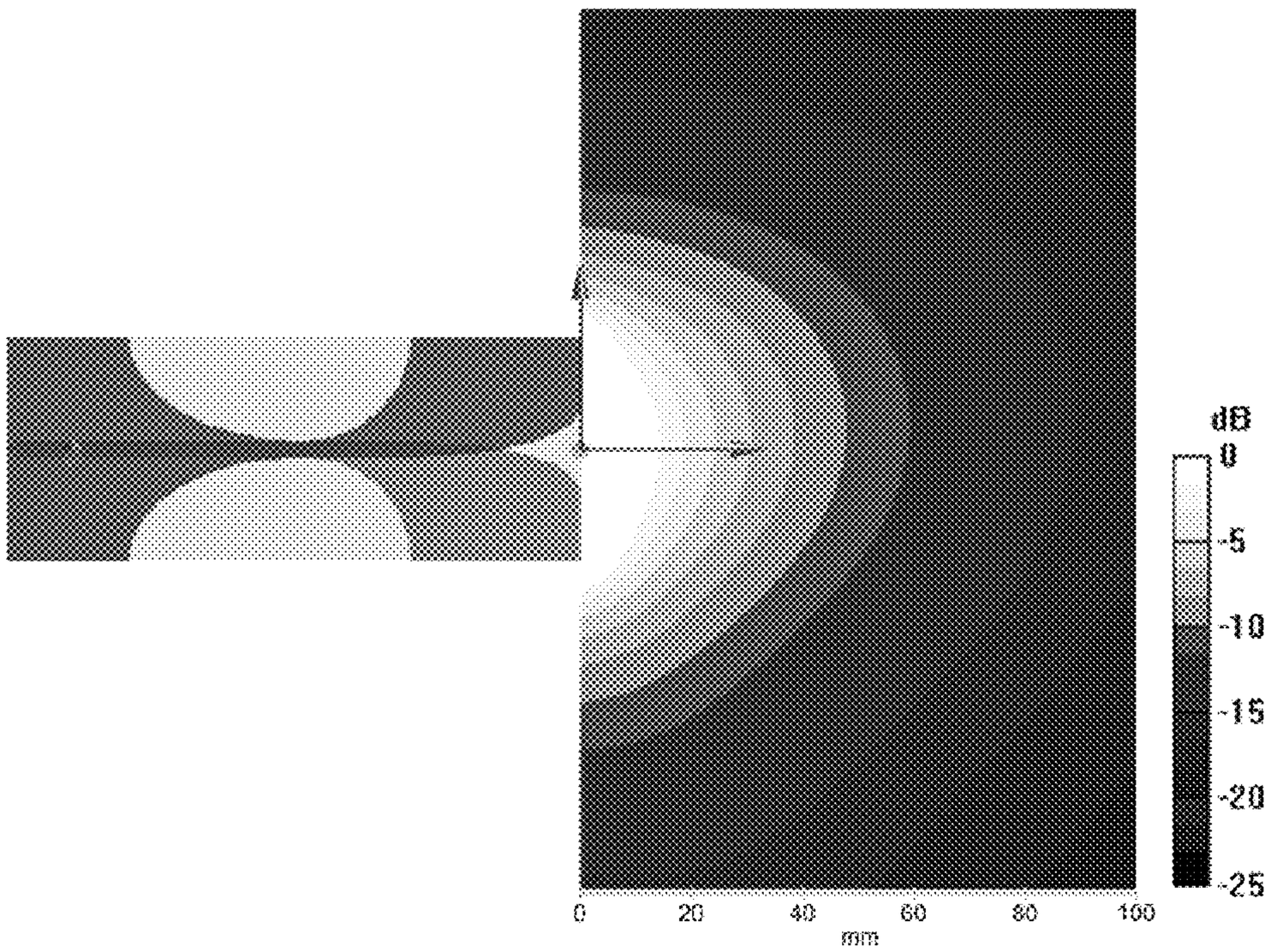

(a)

Energy Flux Density (x,y,z) in dB

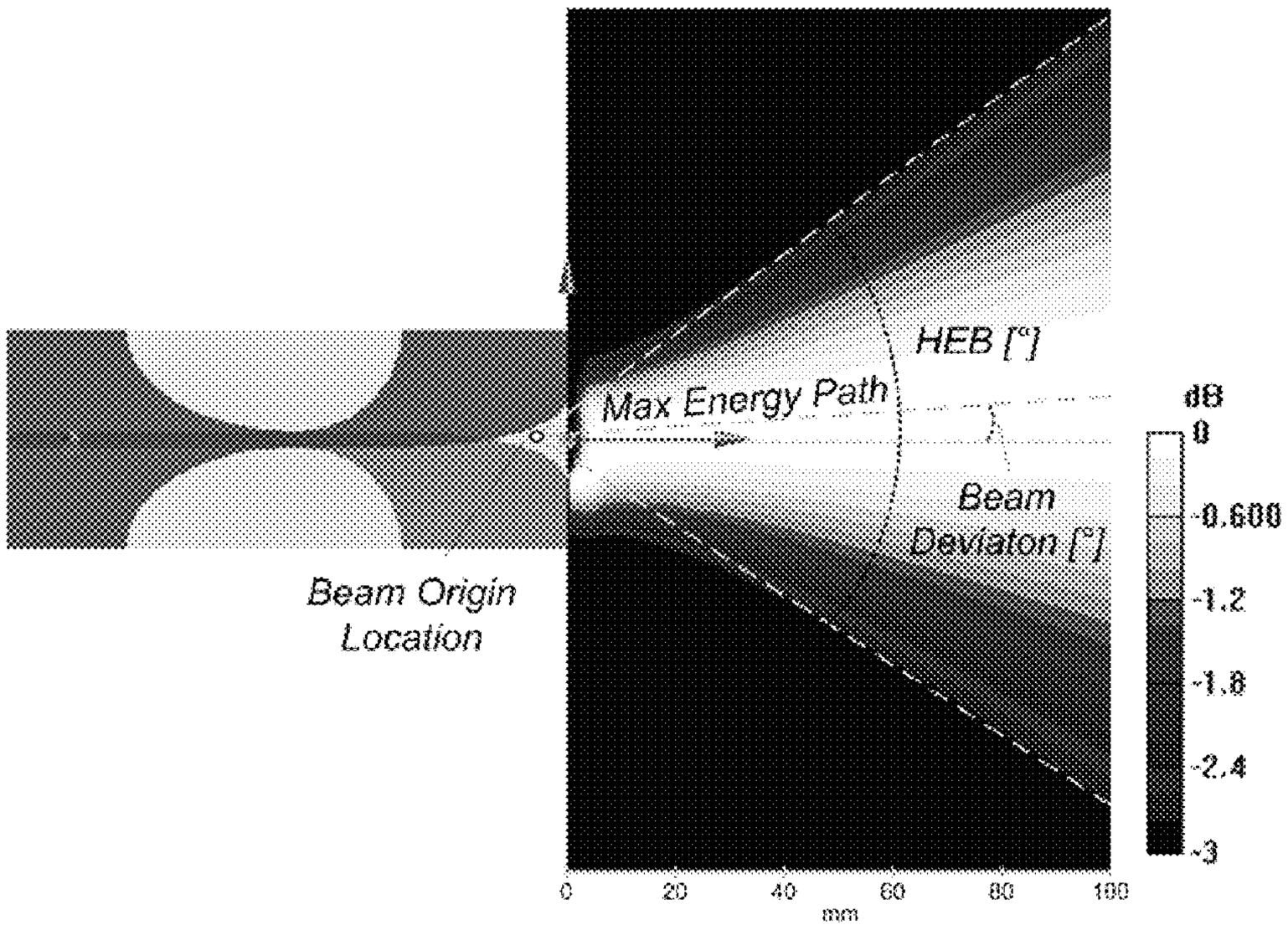

(b)

HEB (x,y,z) in dB

FIG. 9

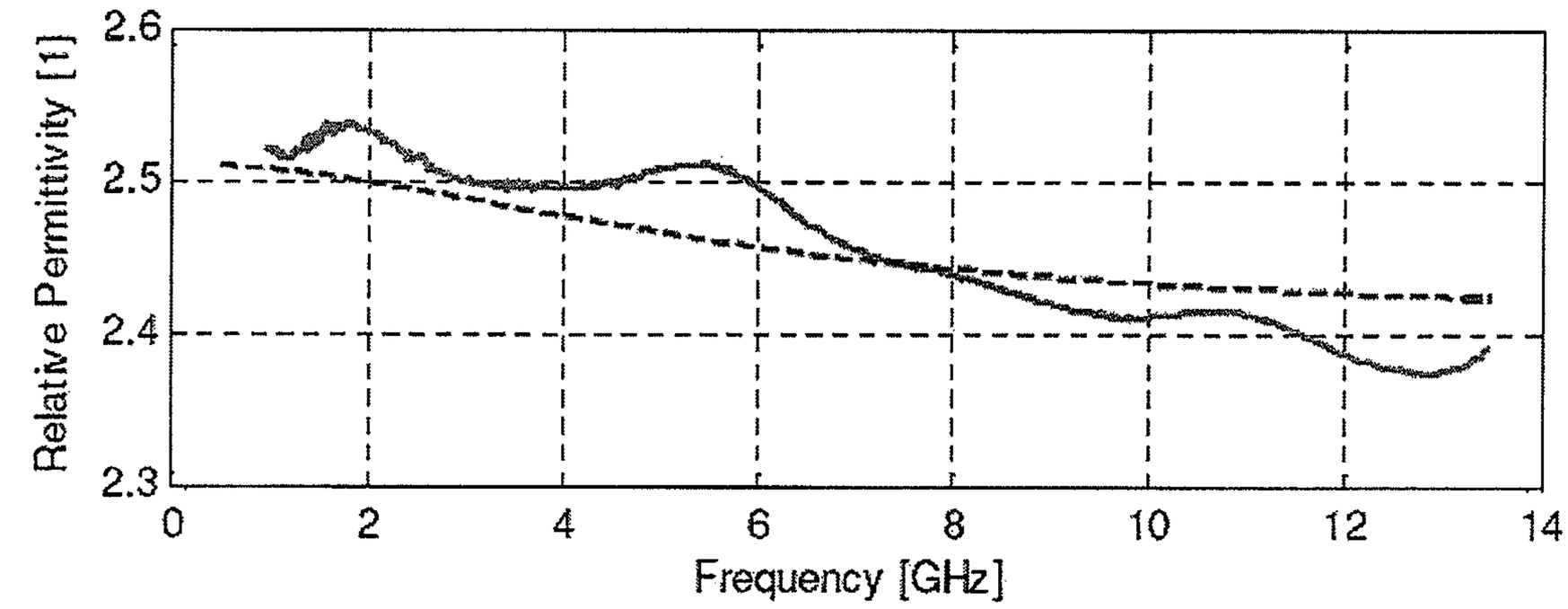
Relative Permittivity [1]
2.6
2.5
2.4
2.3
0
2
4
6
8
10
12
14
Frequency [GHz]

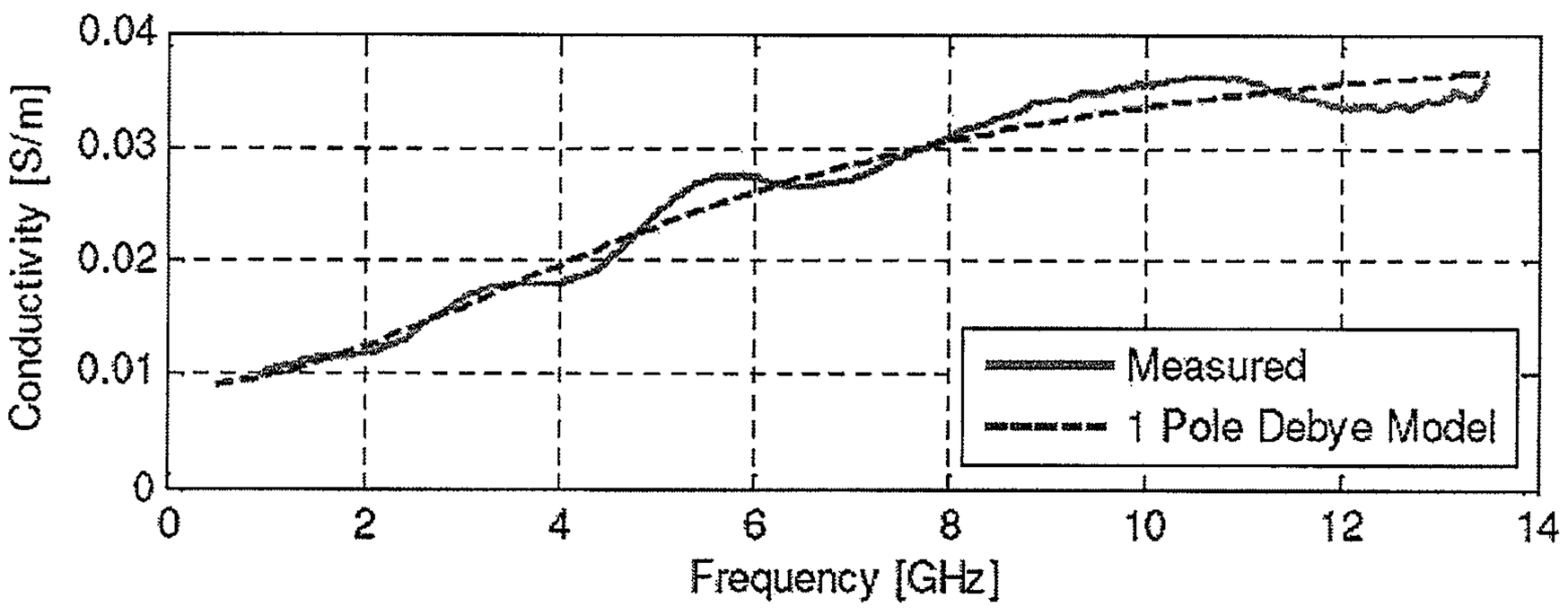
Conductivity [S/m]
0.04
0.03
0.02
0.01
0
Measured
1 Pole Debye Model
0
2
4
6
8
10
12
14
Frequency [GHz]

FIG. 10

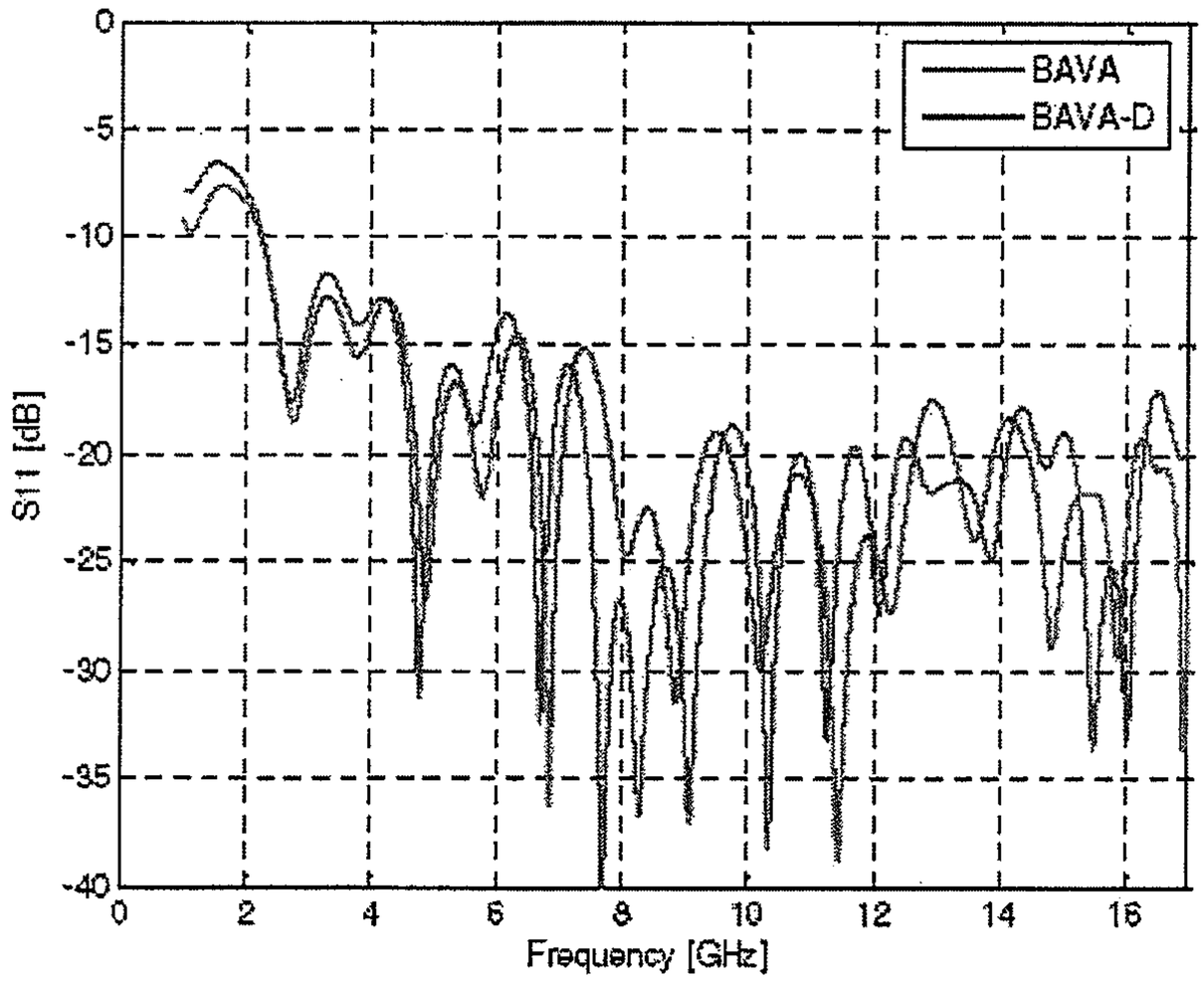
BAVA
BAVA-D
S11 [dB]
Frequency [GHz]
0
-5
-10
-15
-20
-25
-30
-35
-40
0
2
4
6
8
10
12
14
16

FIG. 11

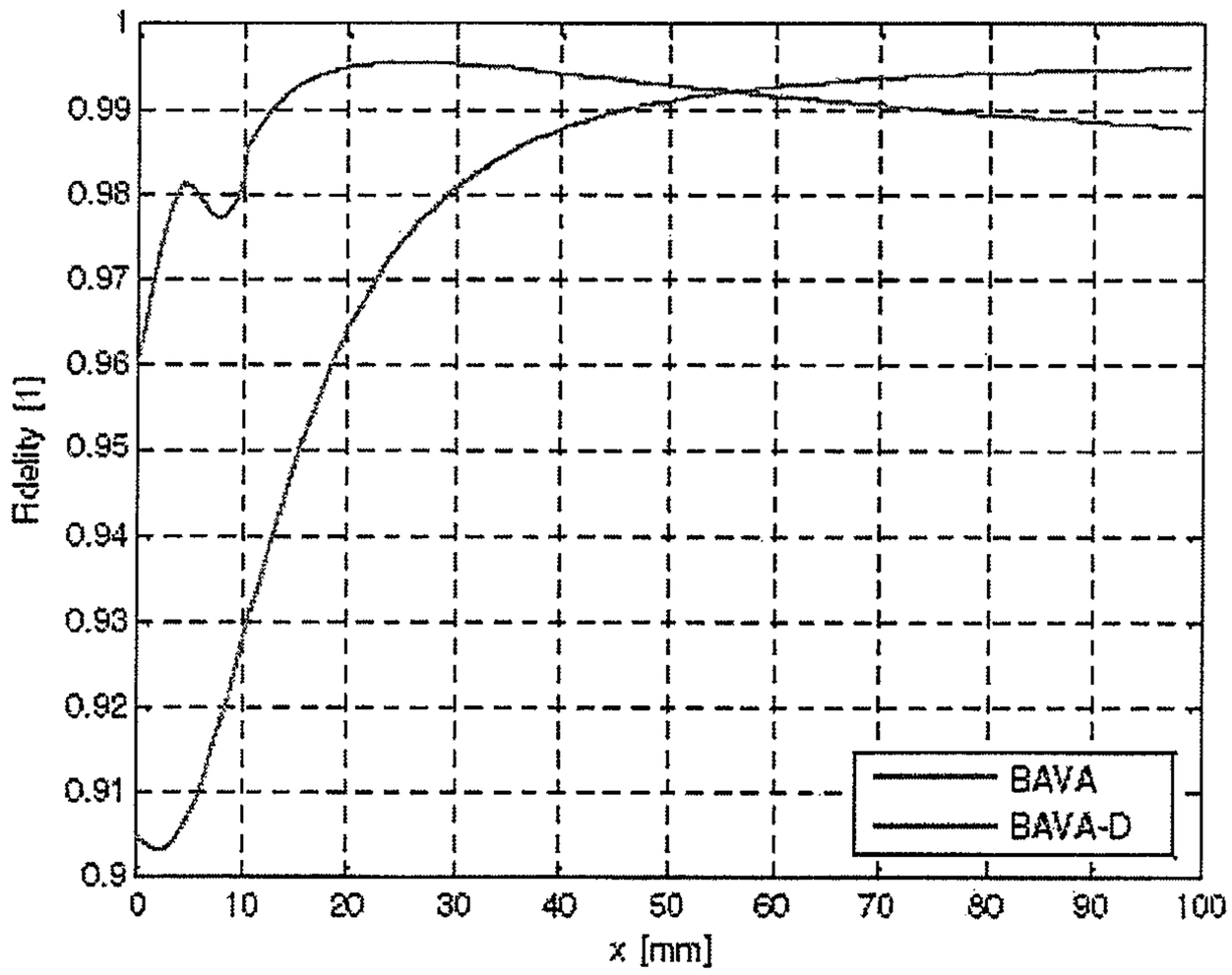
BAVA
BAVA-D
Fidelity [1]
x [mm]
1
0.99
0.98
0.97
0.96
0.95
0.94
0.93
0.92
0.91
0.9
0
10
20
30
40
50
60
70
80
90
100

FIG. 12

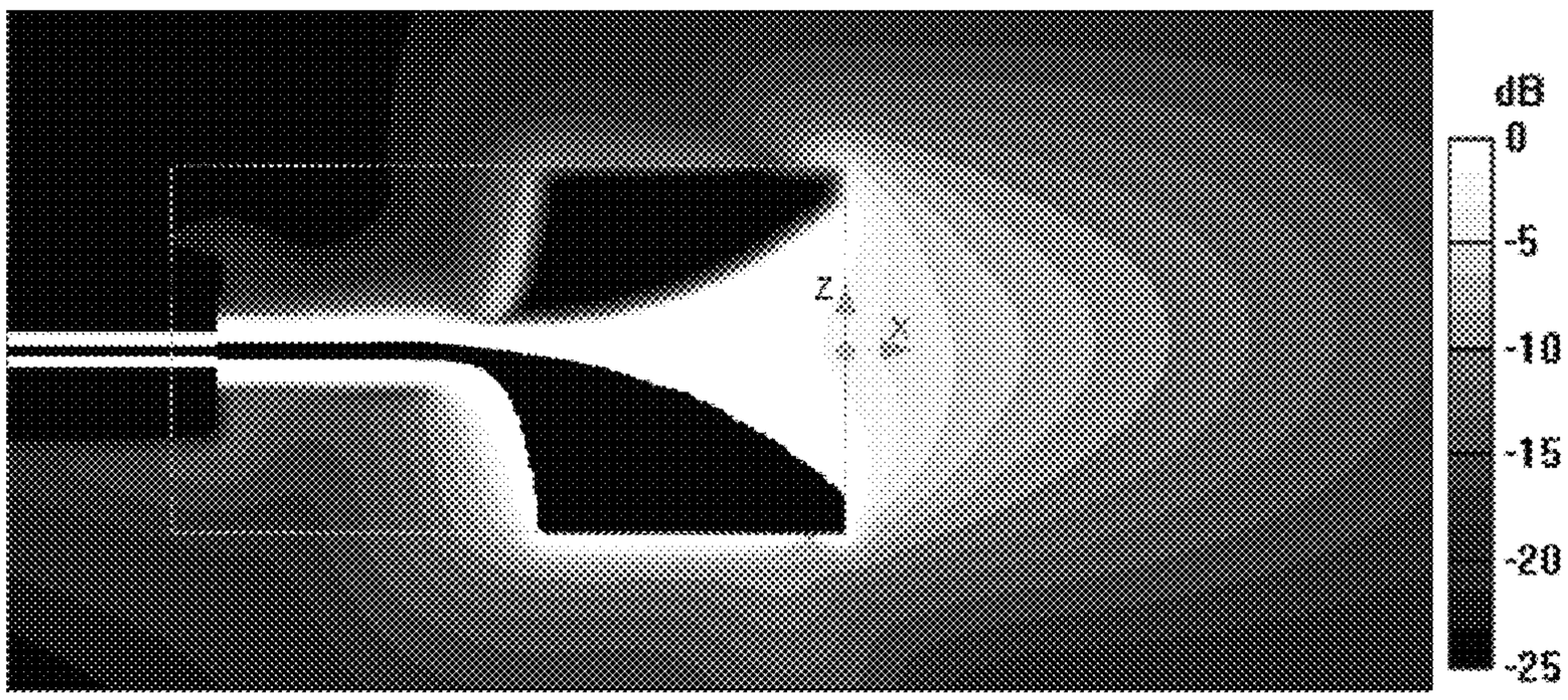

(a)

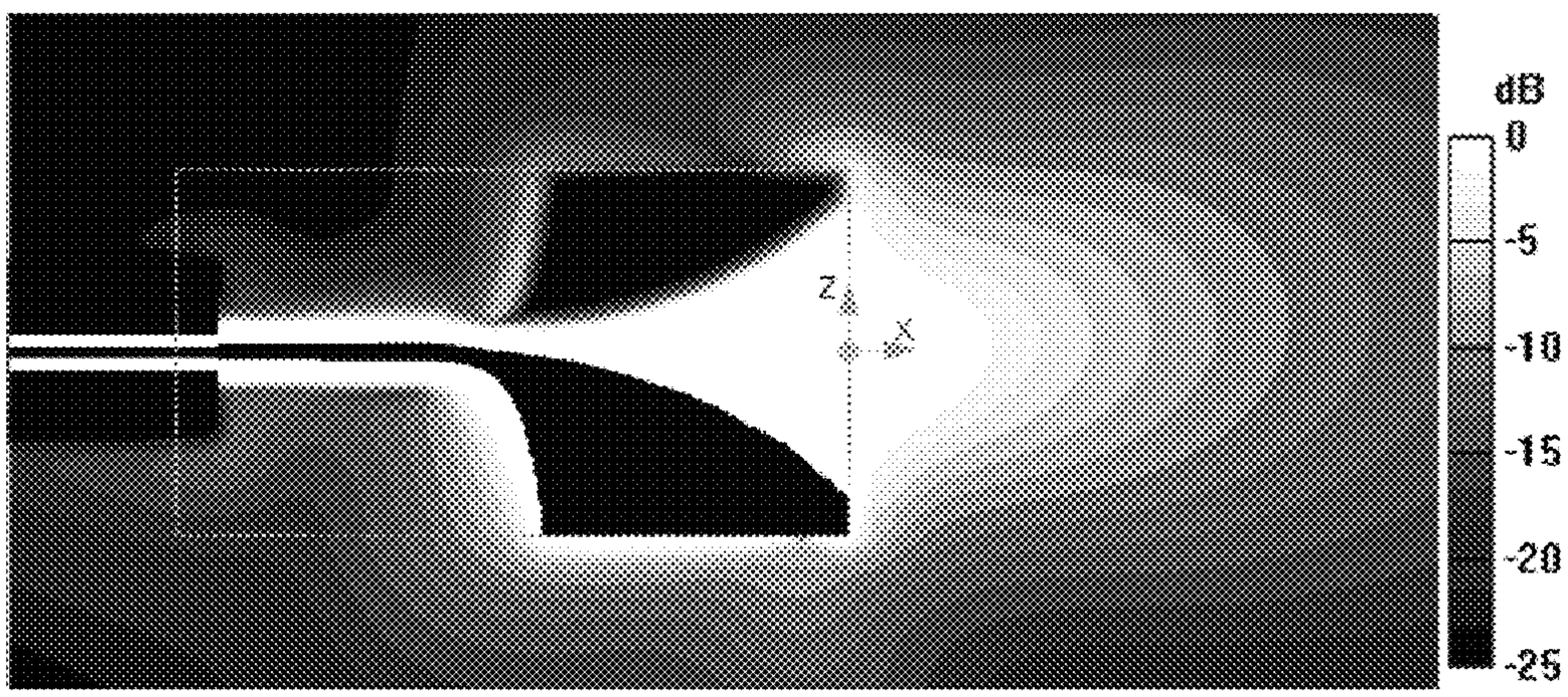

(b)

FIG. 13

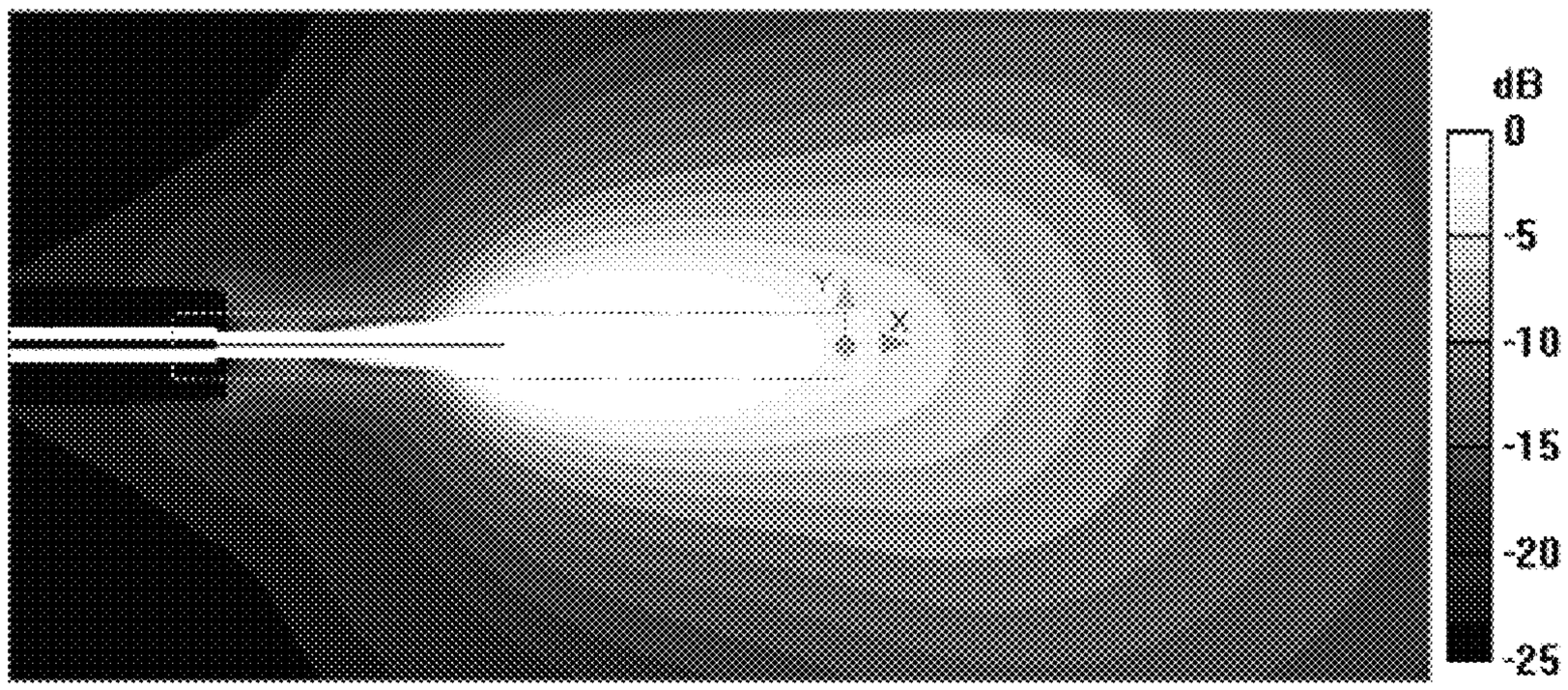

(a)

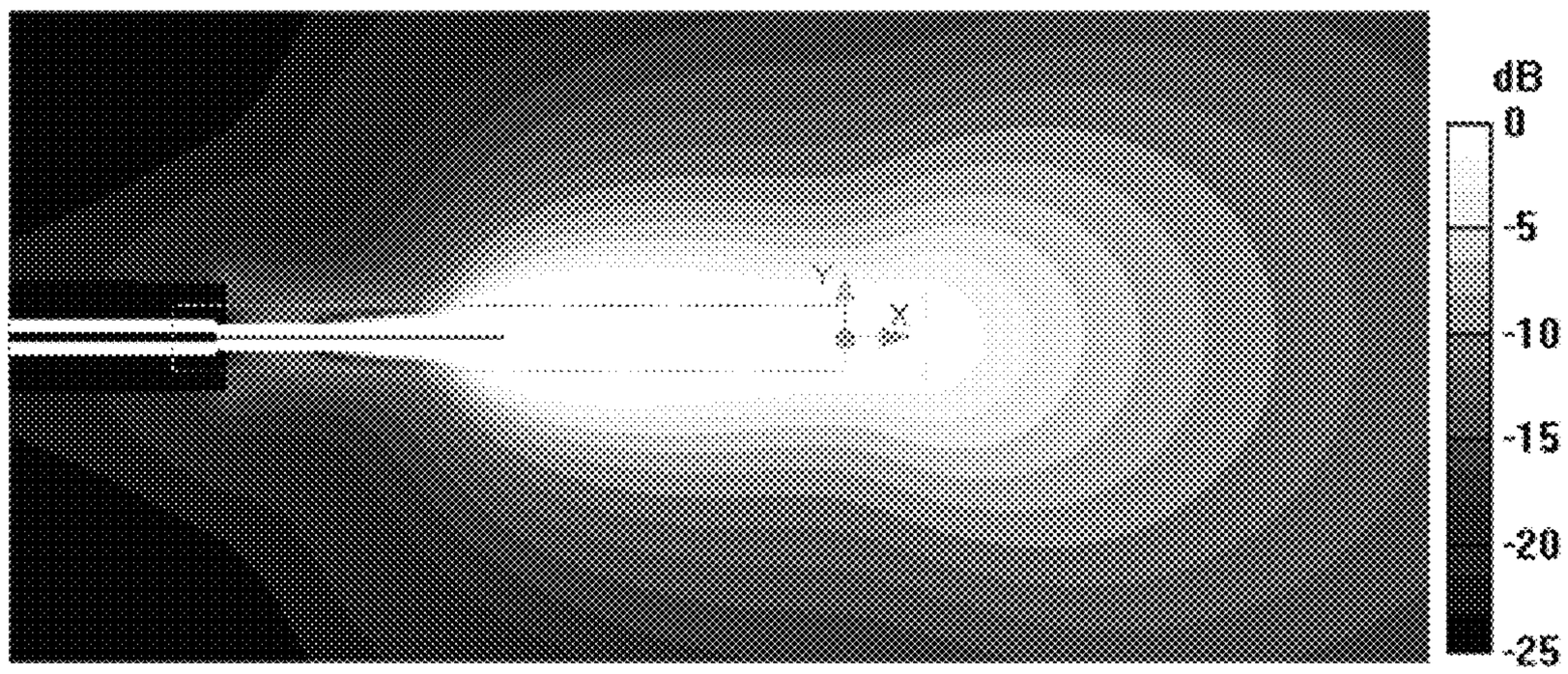

(b)

FIG. 14

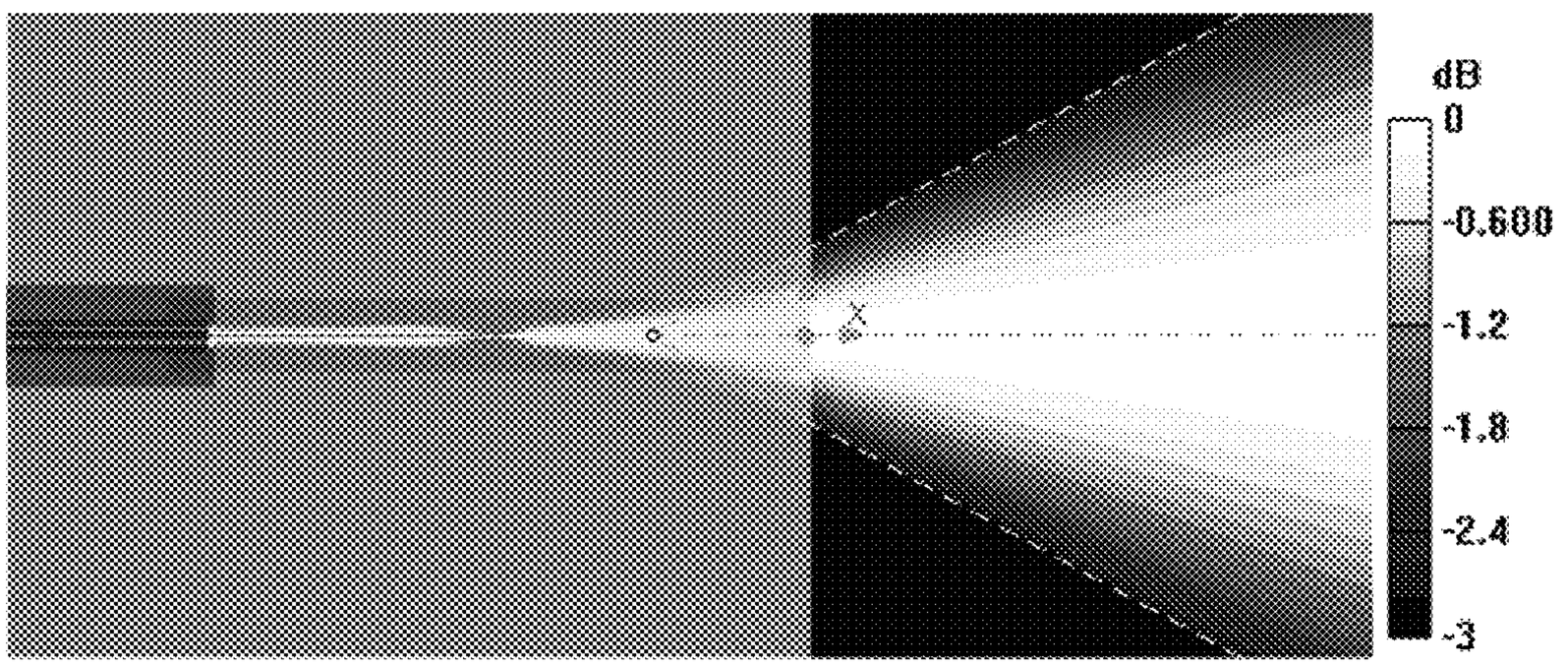

(a)

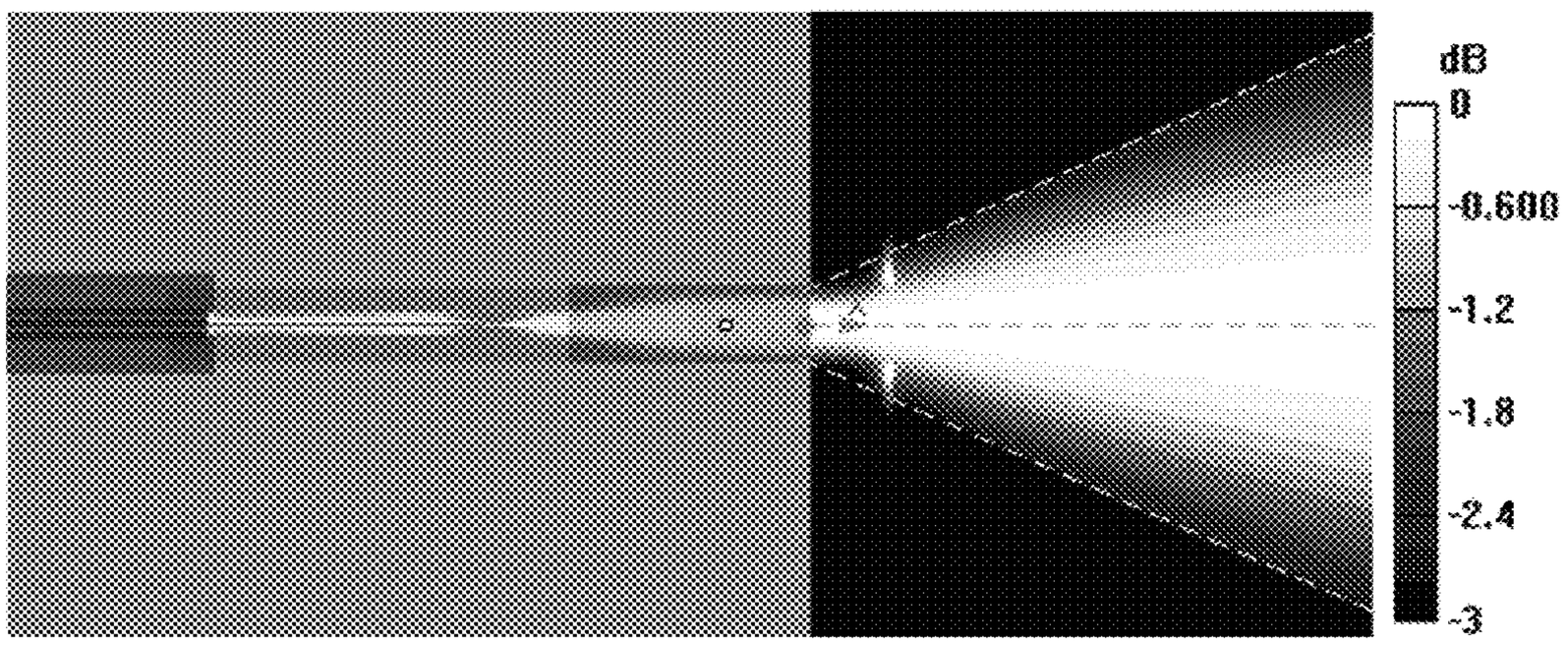

(b)

FIG. 15

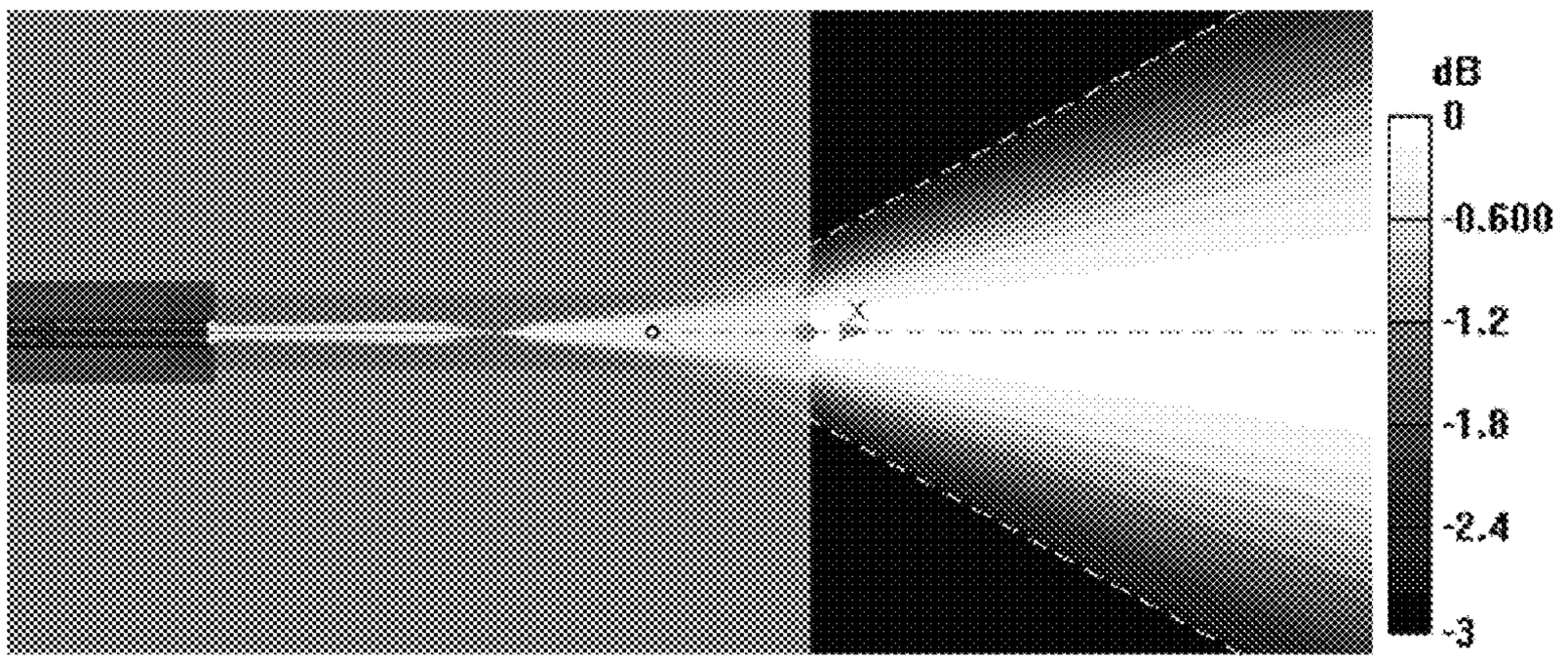

(a)

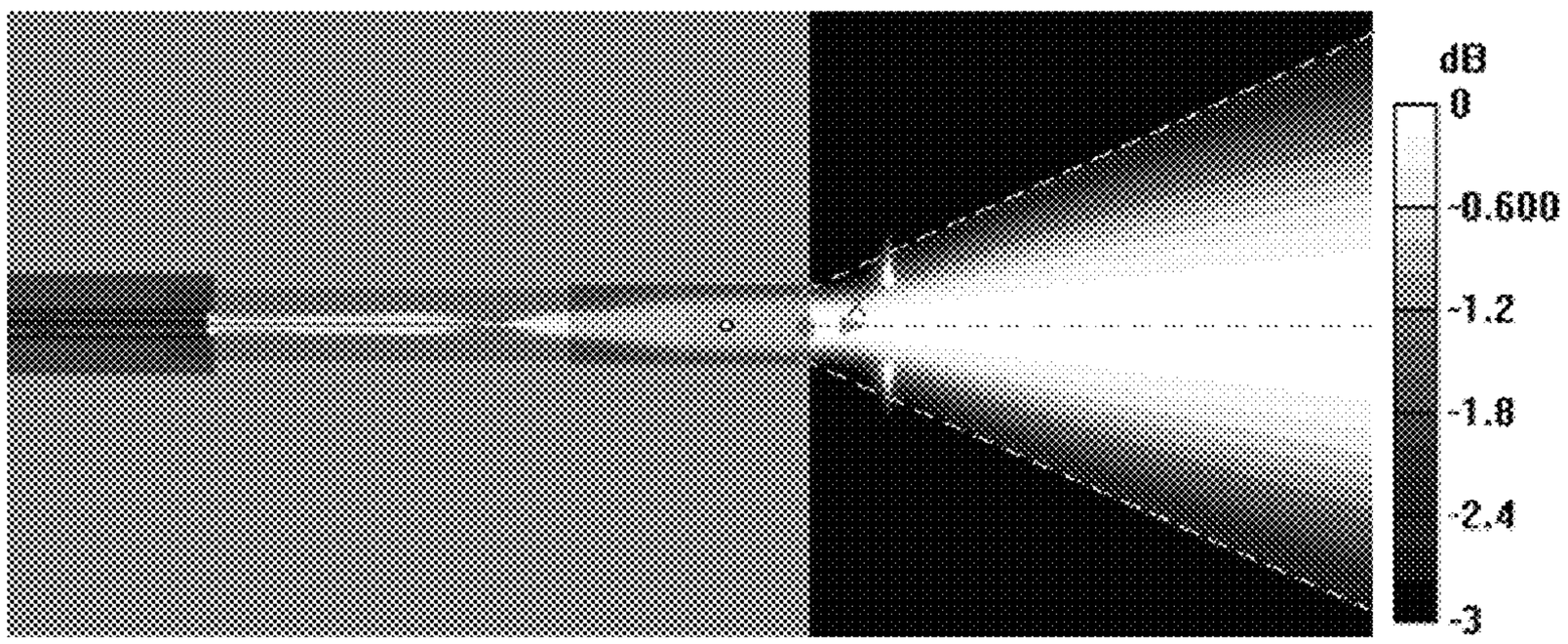

(b)

FIG. 16

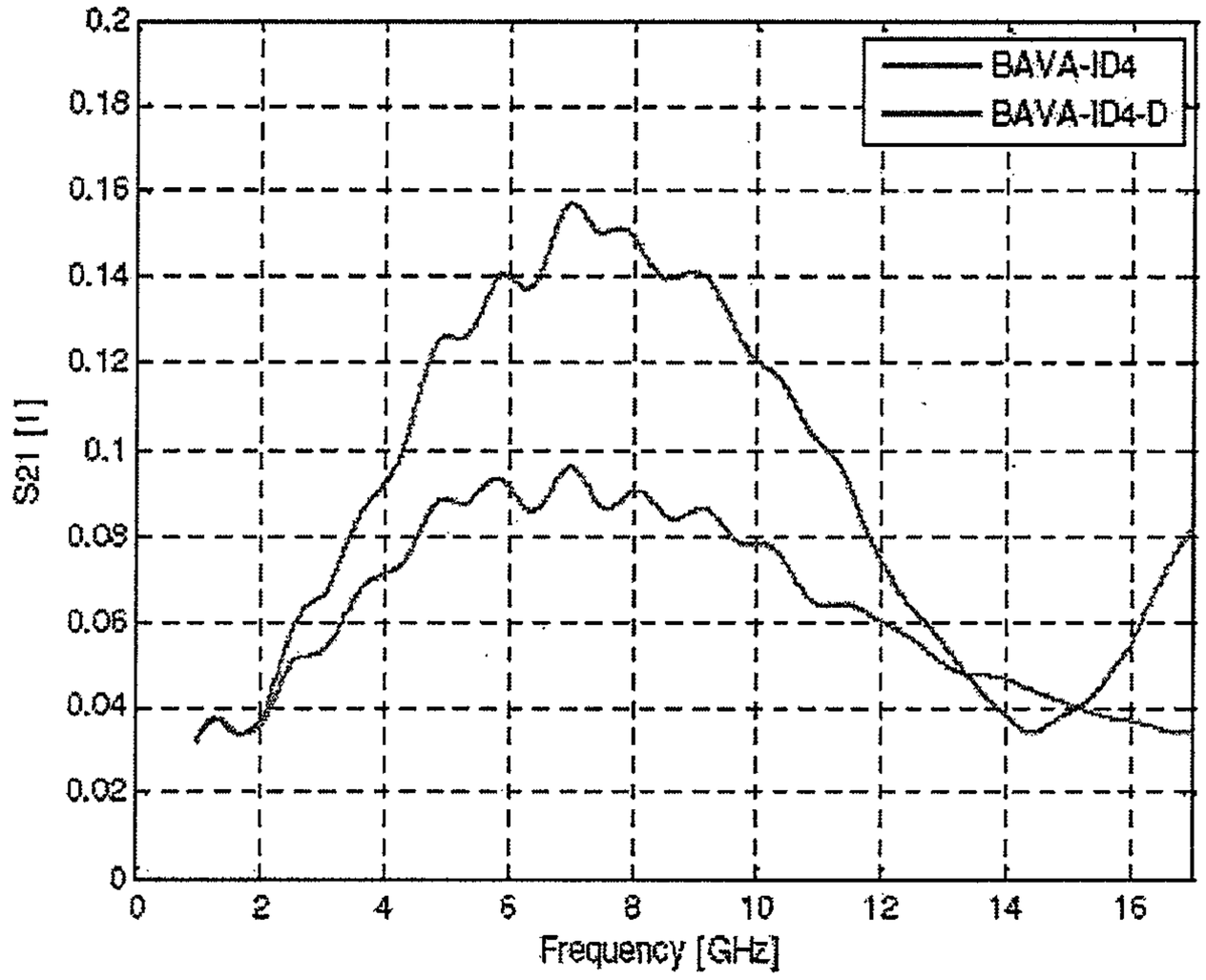
BAVA-ID4
BAVA-ID4-D
S21 [-]
Frequency [GHz]
0.2
0.18
0.16
0.14
0.12
0.1
0.08
0.06
0.04
0.02
0
0
2
4
6
8
10
12
14
16

FIG. 17

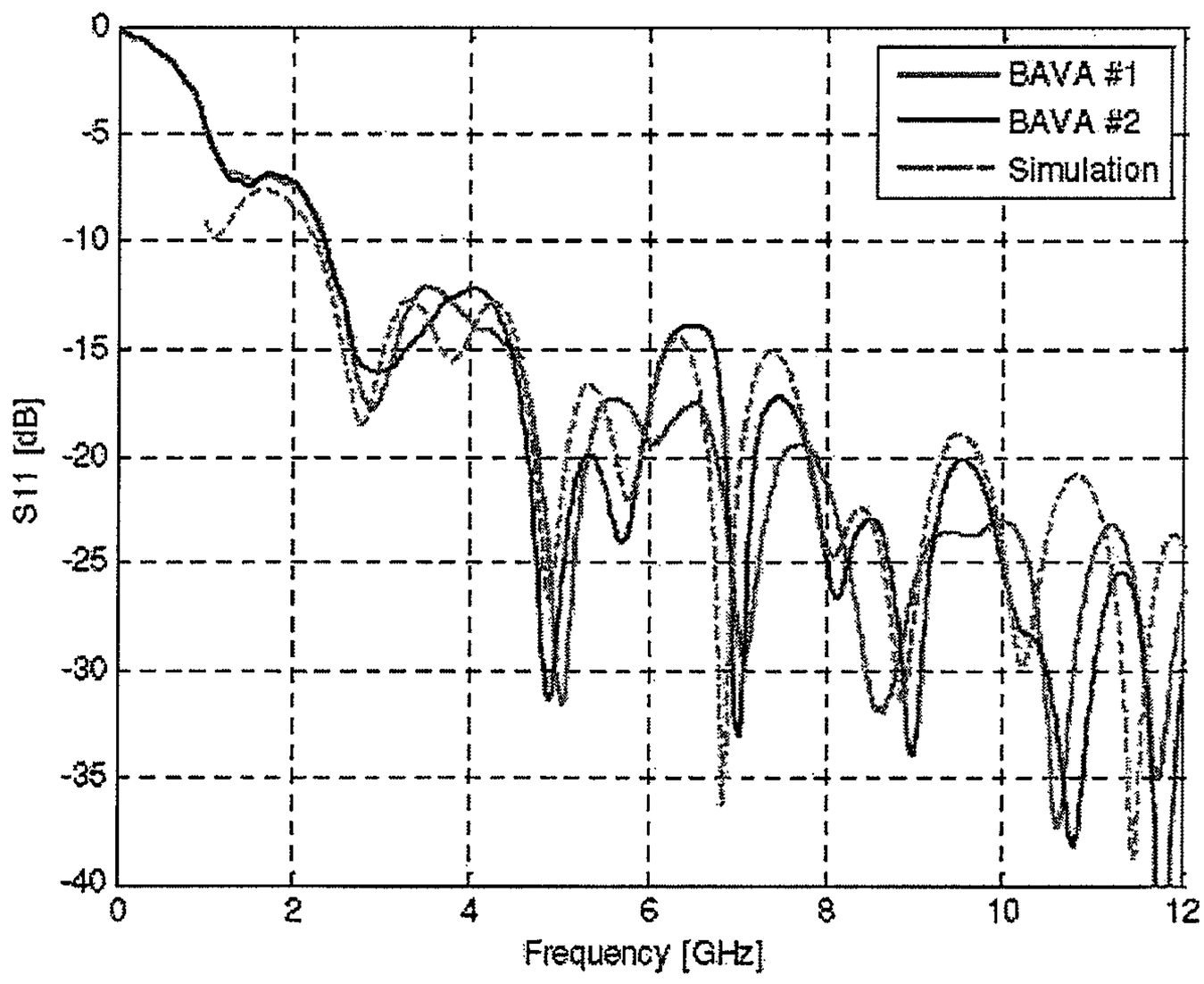
BAVA #1
BAVA #2
Simulation
S11 [dB]
Frequency [GHz]
0
-5
-10
-15
-20
-25
-30
-35
-40
0
2
4
6
8
10
12

FIG. 18

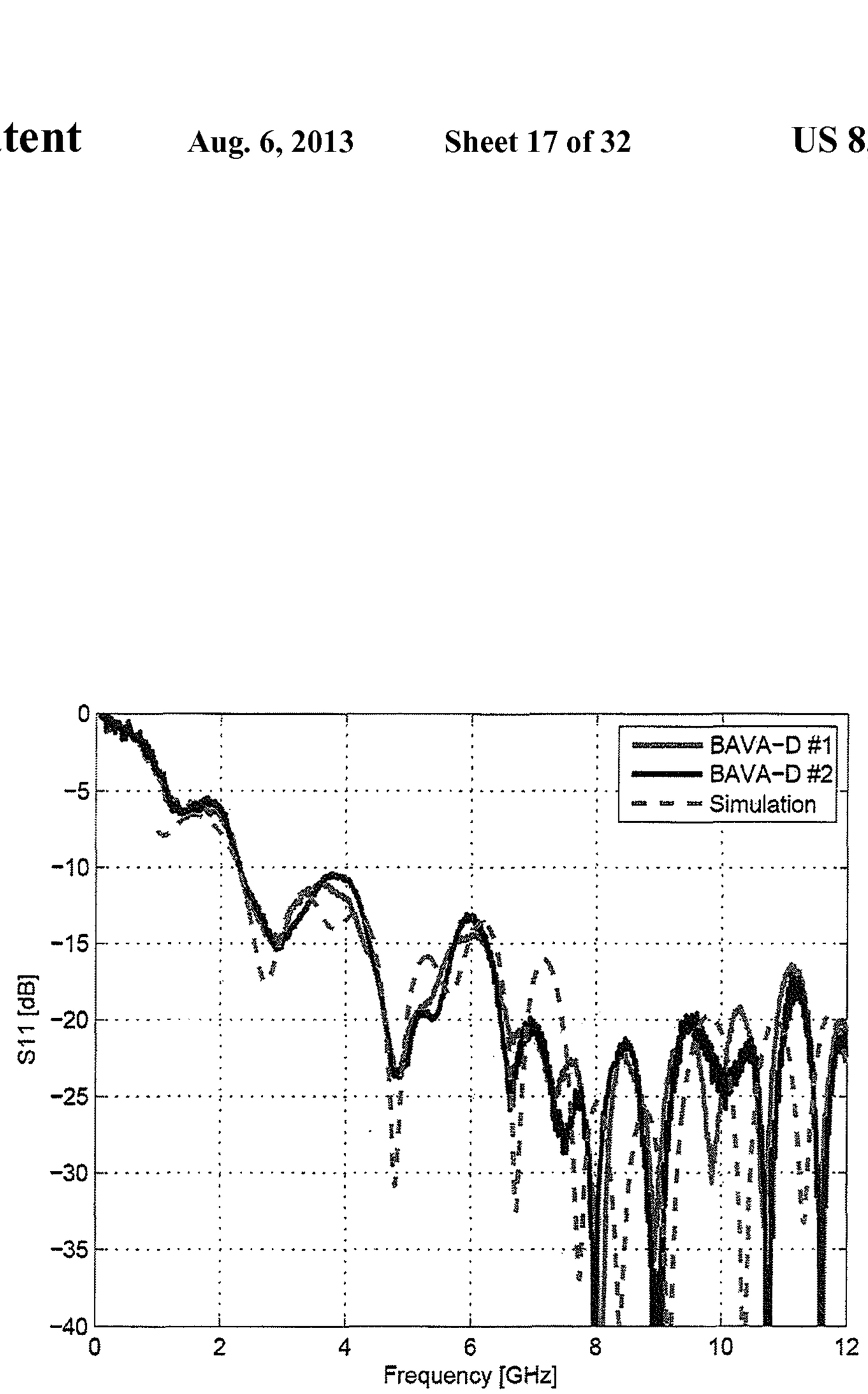
BAVA-D #1
BAVA-D #2
Simulation
S11 [dB]
Frequency [GHz]
0
-5
-10
-15
-20
-25
-30
-35
-40
0
2
4
6
8
10
12

FIG. 19

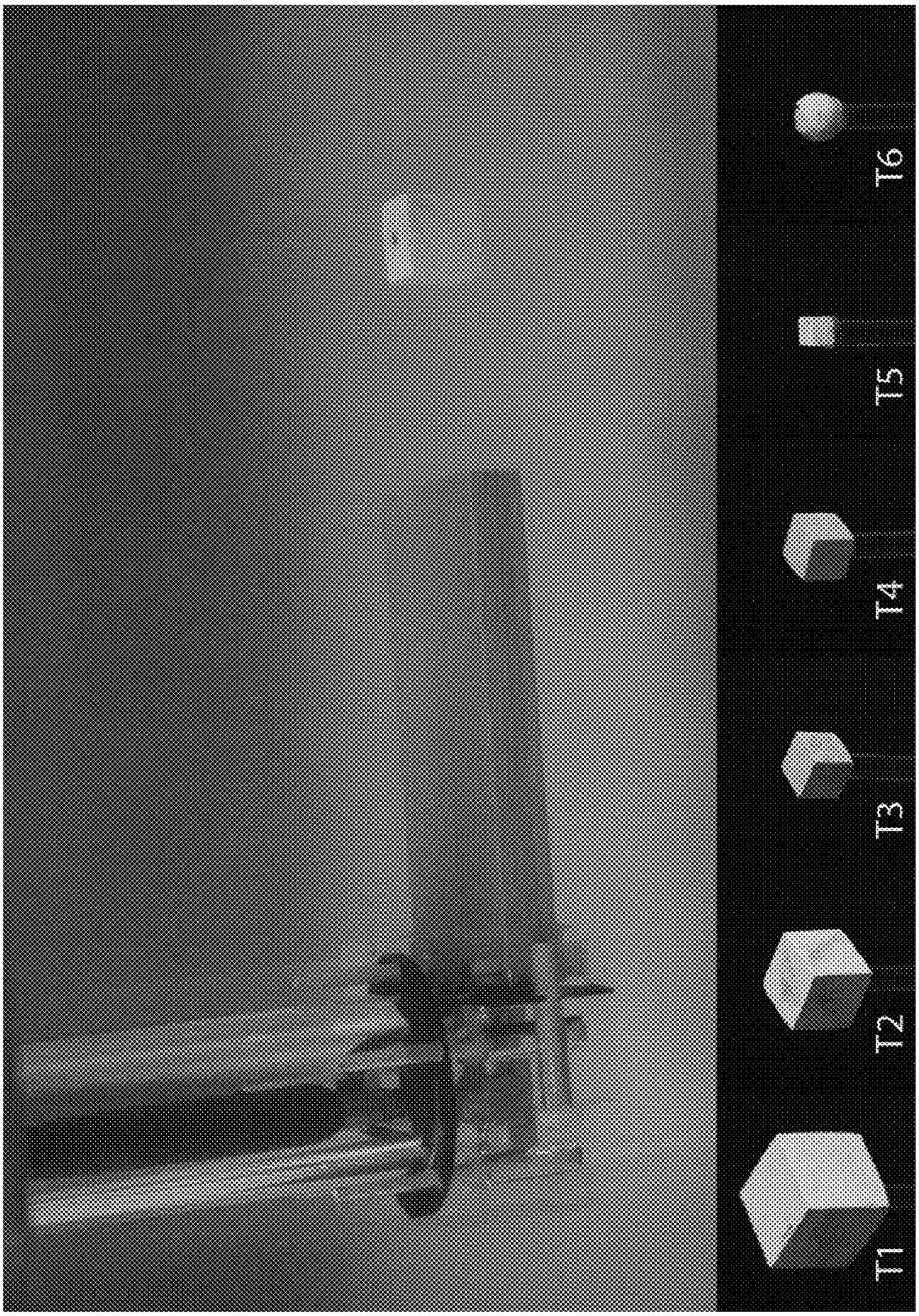

FIG. 20

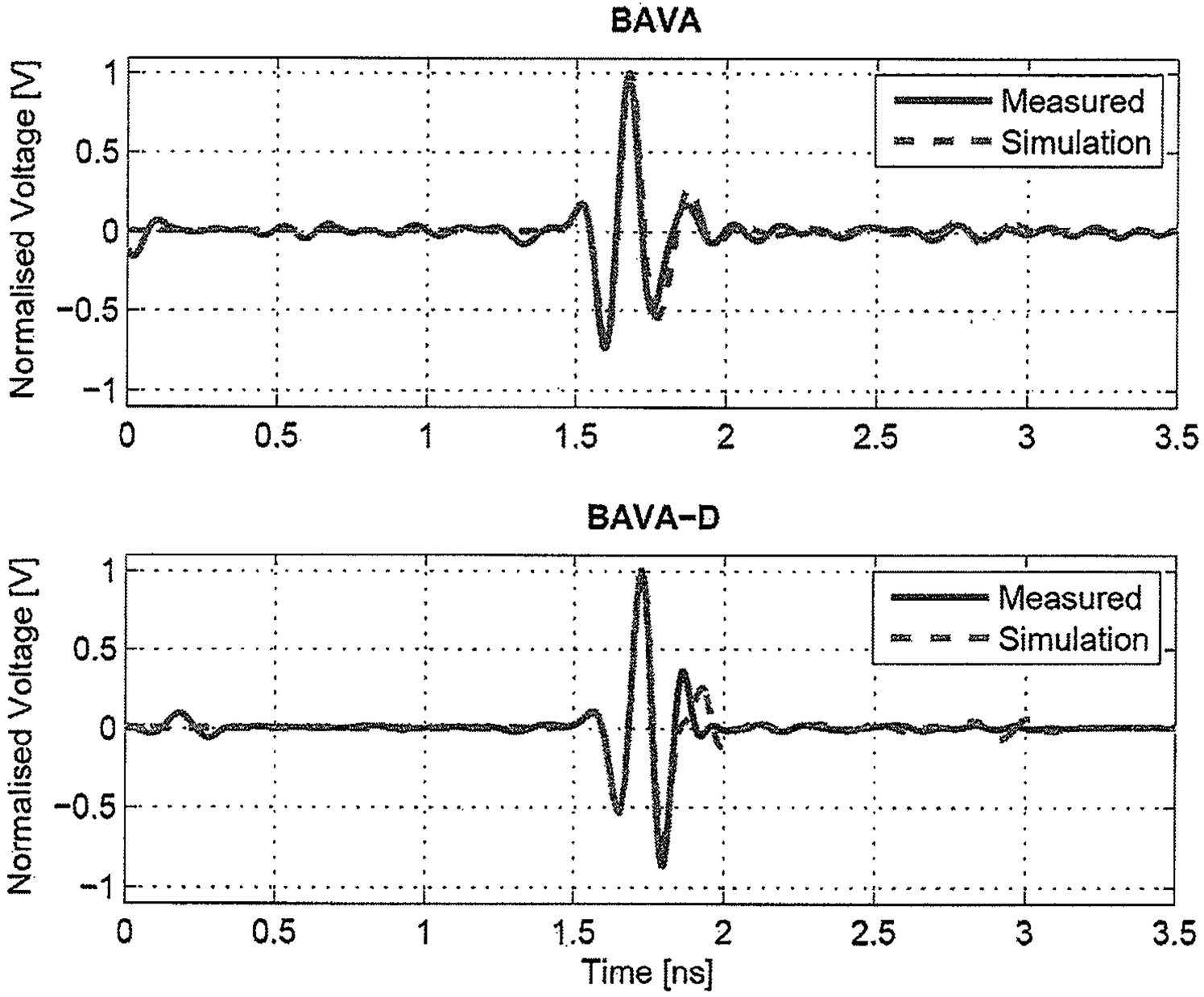
BAVA
Normalised Voltage [V]
Measured
Simulation
1
0.5
0
−0.5
−1
0
0.5
1
1.5
2
2.5
3
3.5
BAVA-D
Normalised Voltage [V]
Measured
Simulation
1
0.5
0
−0.5
−1
0
0.5
1
1.5
2
2.5
3
3.5
Time [ns]

FIG. 21

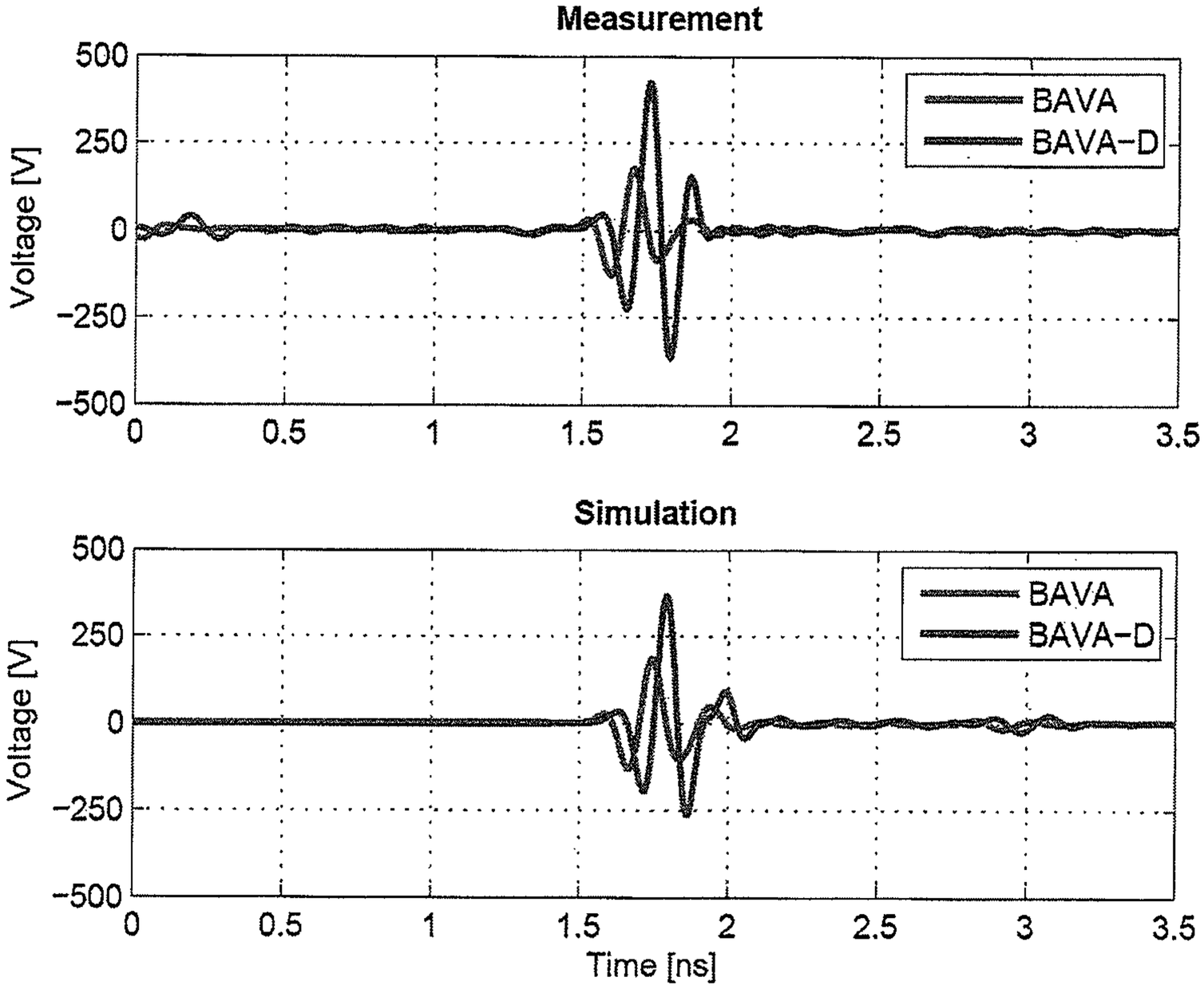
Measurement
500
250
0
−250
−500
Voltage [V]
0
0.5
1
1.5
2
2.5
3
3.5
BAVA
BAVA−D
Simulation
500
250
0
−250
−500
Voltage [V]
0
0.5
1
1.5
2
2.5
3
3.5
BAVA
BAVA−D
Time [ns]

FIG. 22

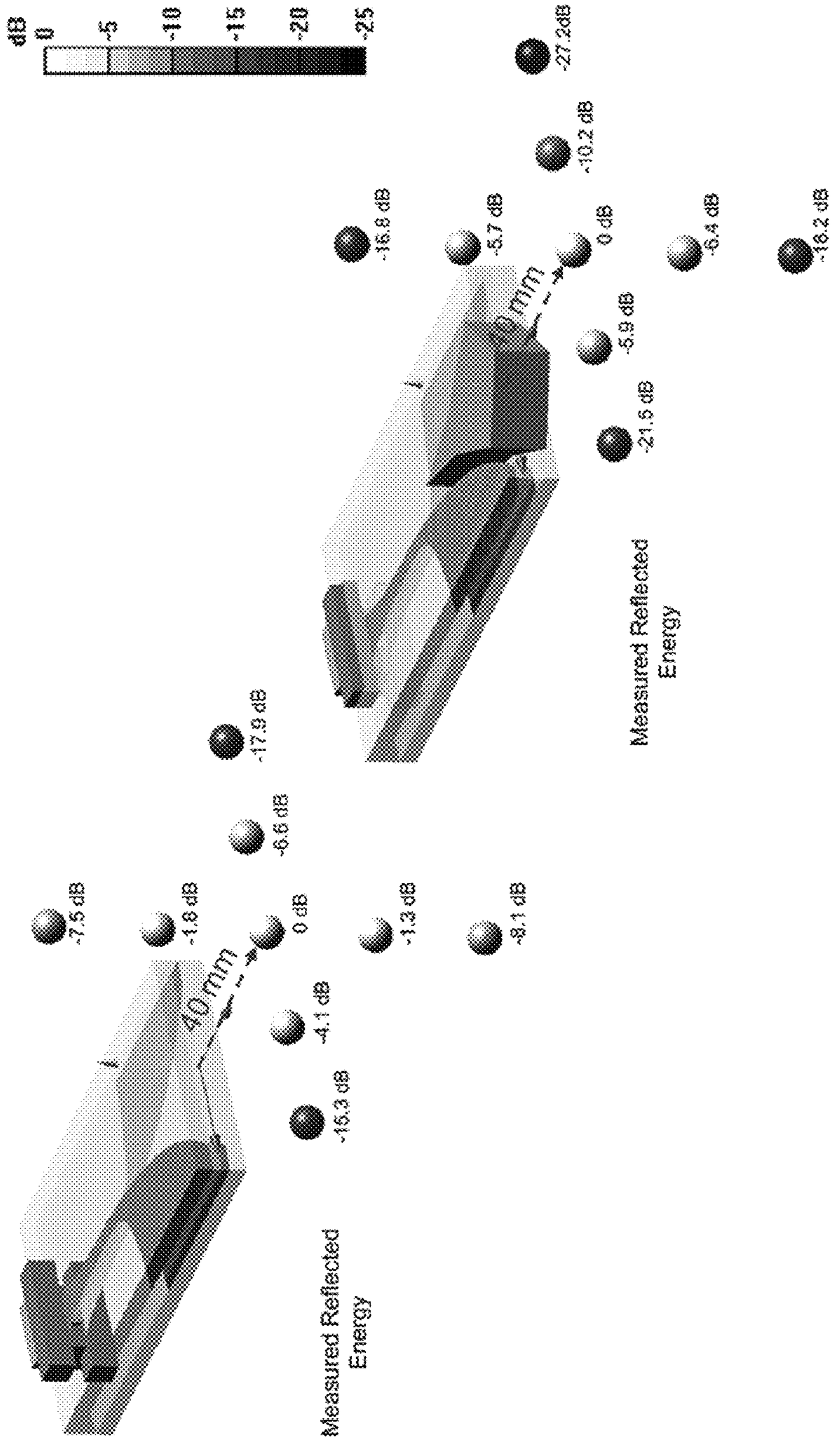
dB
0
-5
-10
-15
-20
-25
-27.2dB
-10.2 dB
-16.8 dB
-5.7 dB
0 dB
-6.4 dB
-18.2 dB
40 mm
-5.9 dB
-21.6 dB
Measured Reflected Energy
-7.5 dB
-1.8 dB
0 dB
-6.6 dB
-17.9 dB
-1.3 dB
-9.1 dB
40 mm
-4.1 dB
-15.3 dB
Measured Reflected Energy

FIG. 23

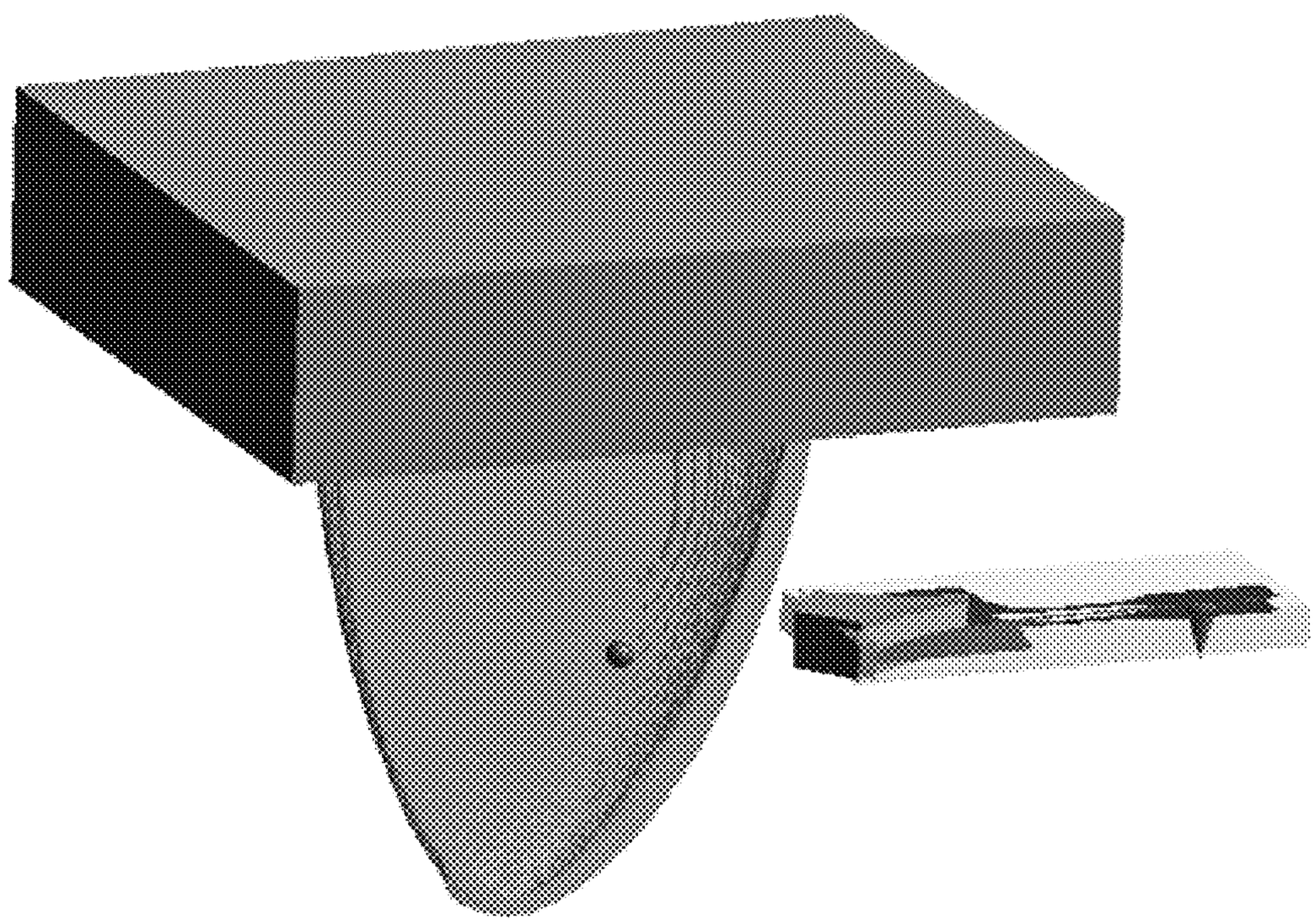

FIG. 24

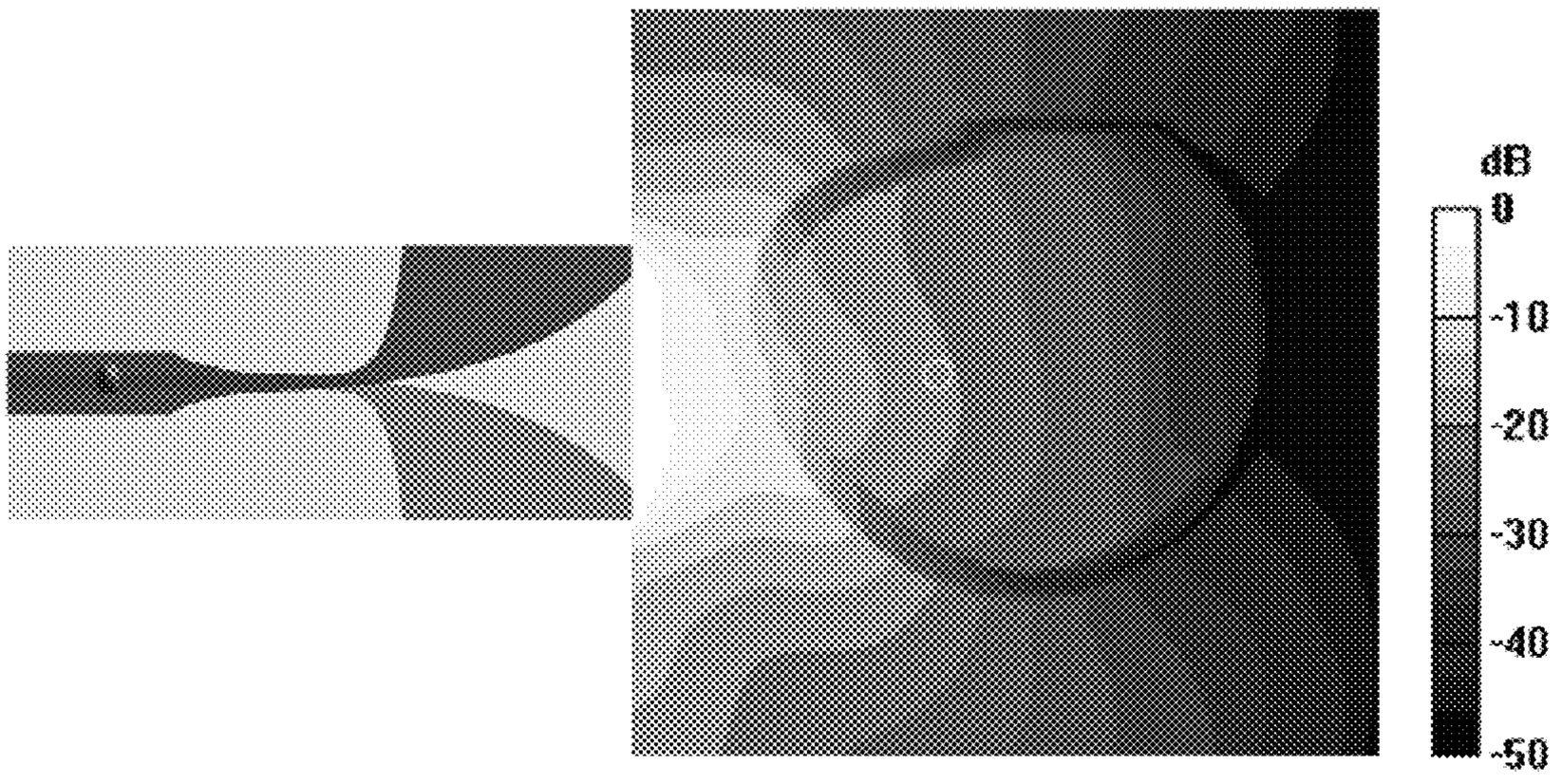

(a)
Energy Flux Density (x,y,z) in dB

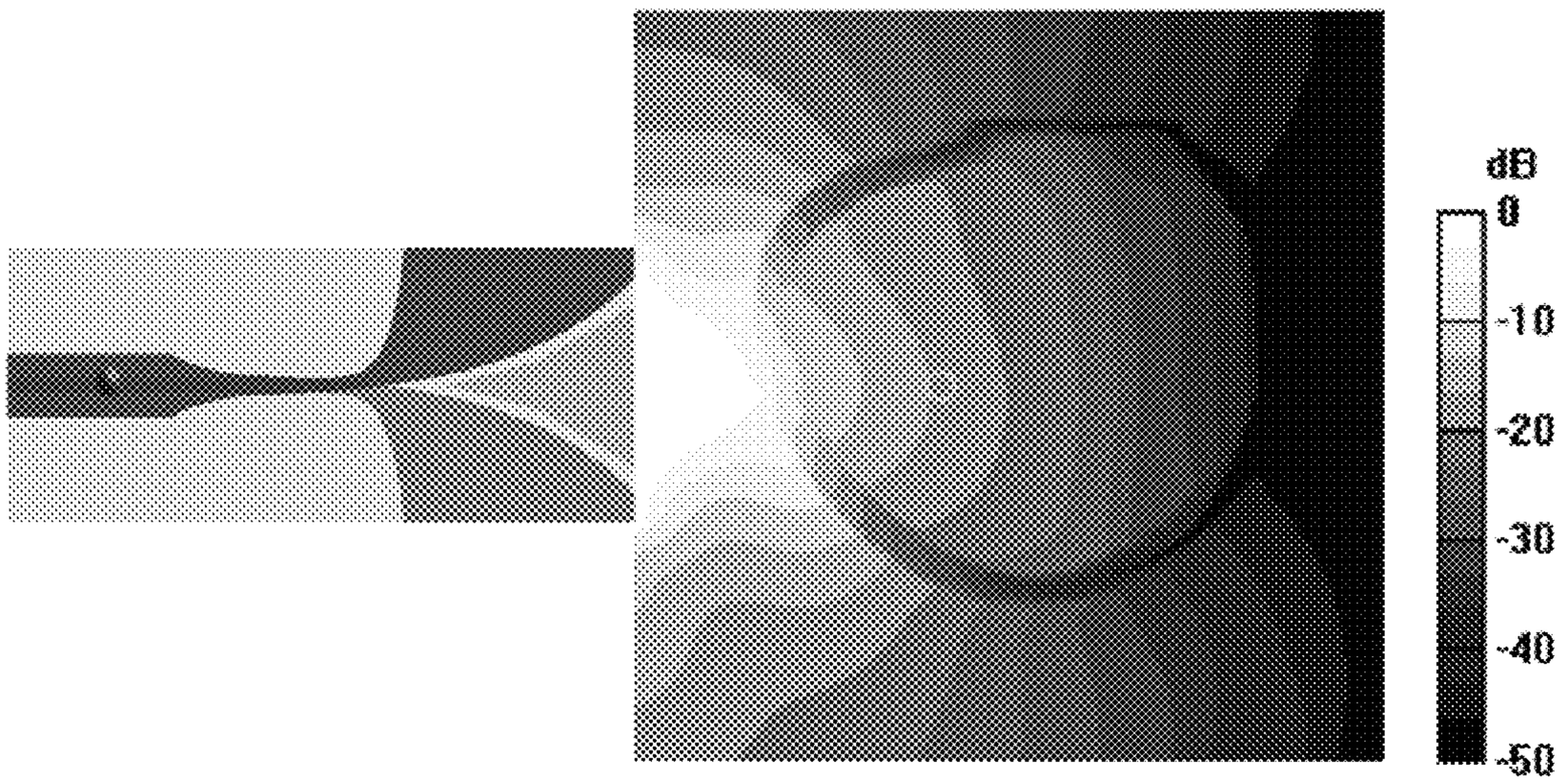

(b)
Energy Flux Density (x,y,z) in dB

FIG. 25

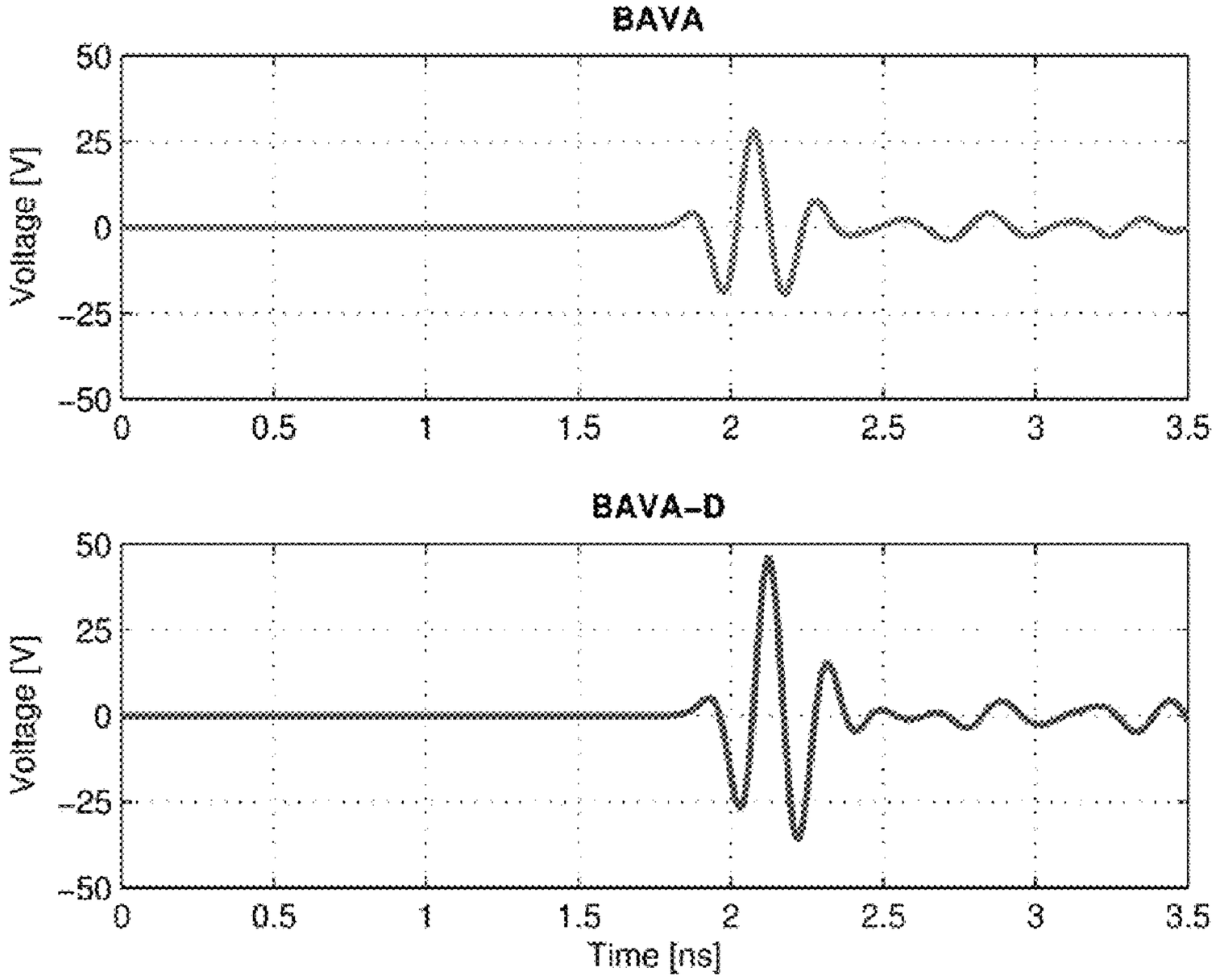
BAVA
50
25
0
−25
−50
Voltage [V]
0
0.5
1
1.5
2
2.5
3
3.5
BAVA-D
50
25
0
−25
−50
Voltage [V]
0
0.5
1
1.5
2
2.5
3
3.5
Time [ns]

FIG. 26

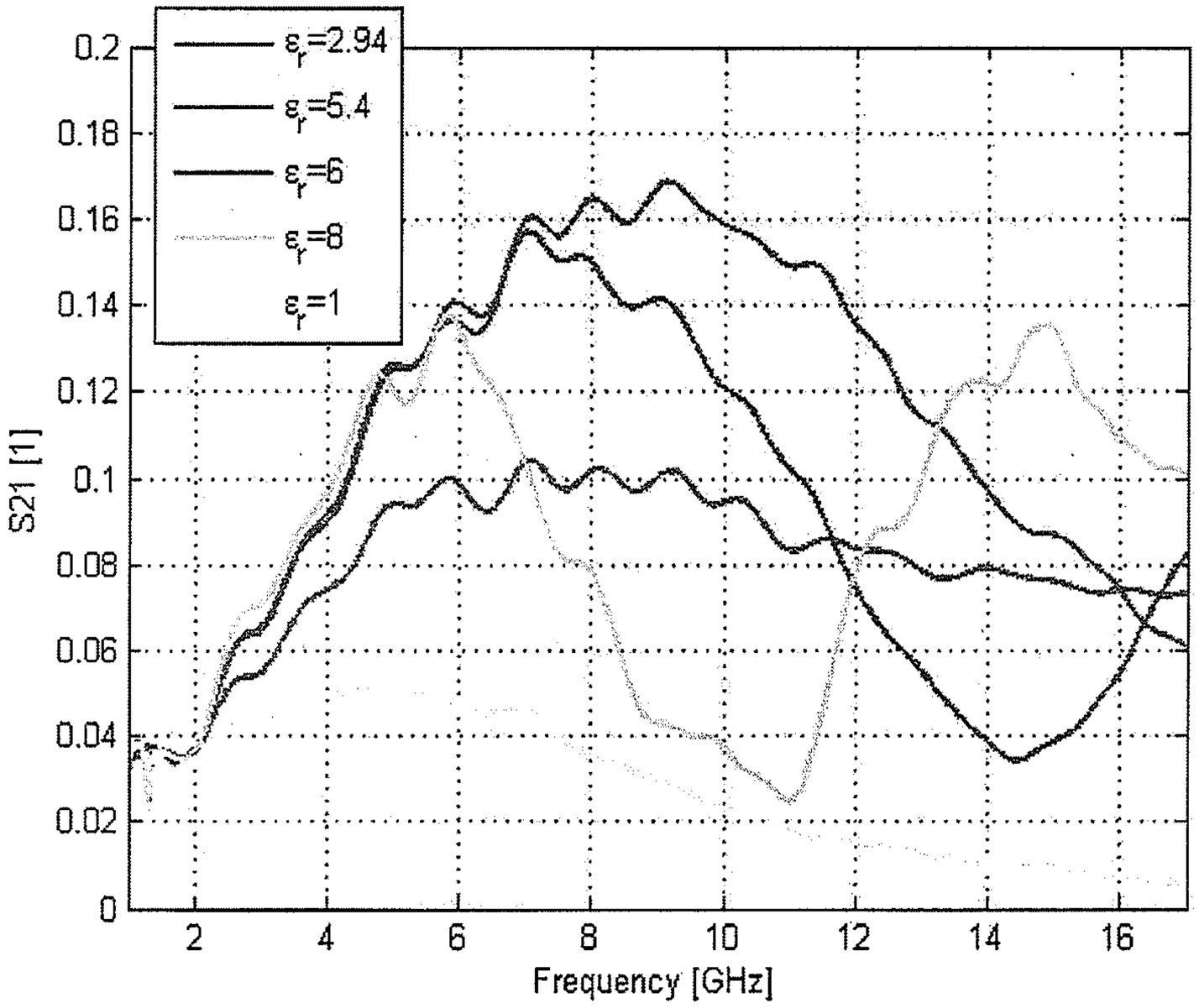
ε_r=2.94
ε_r=5.4
ε_r=6
ε_r=8
ε_r=1
S21 [1]
0
0.02
0.04
0.06
0.08
0.1
0.12
0.14
0.16
0.18
0.2
2
4
6
8
10
12
14
16
Frequency [GHz]

FIG. 27

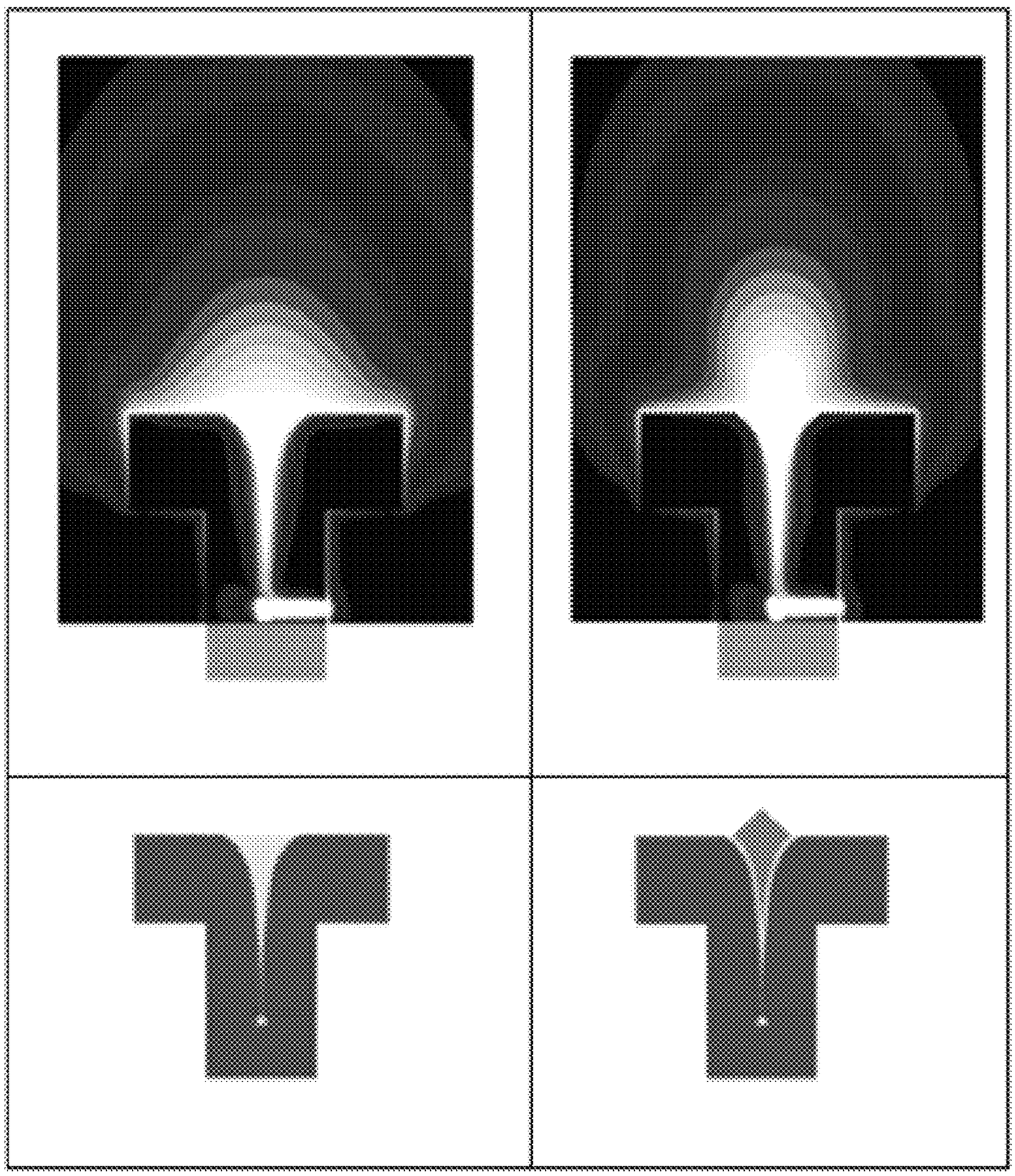

FIG. 28

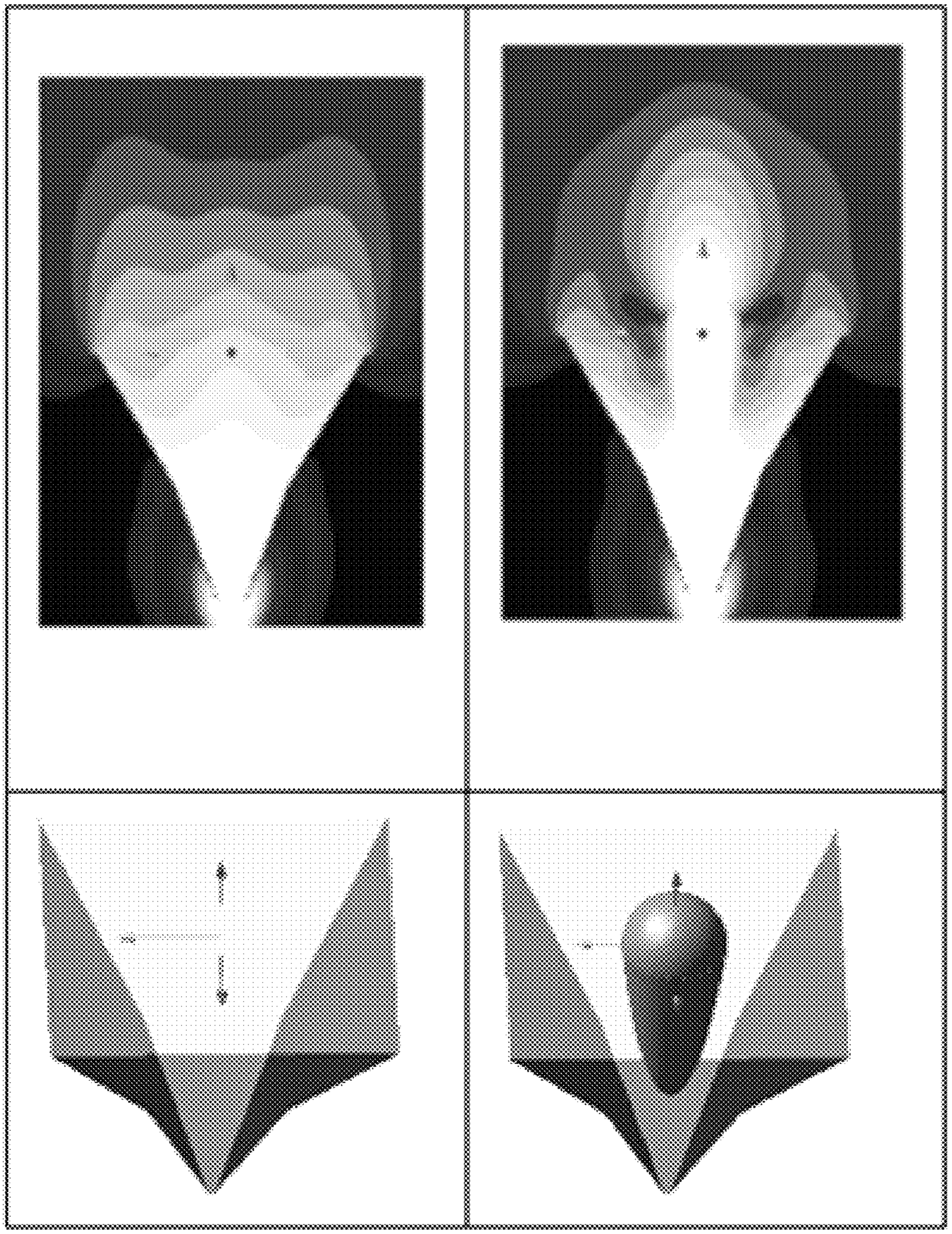

FIG. 29

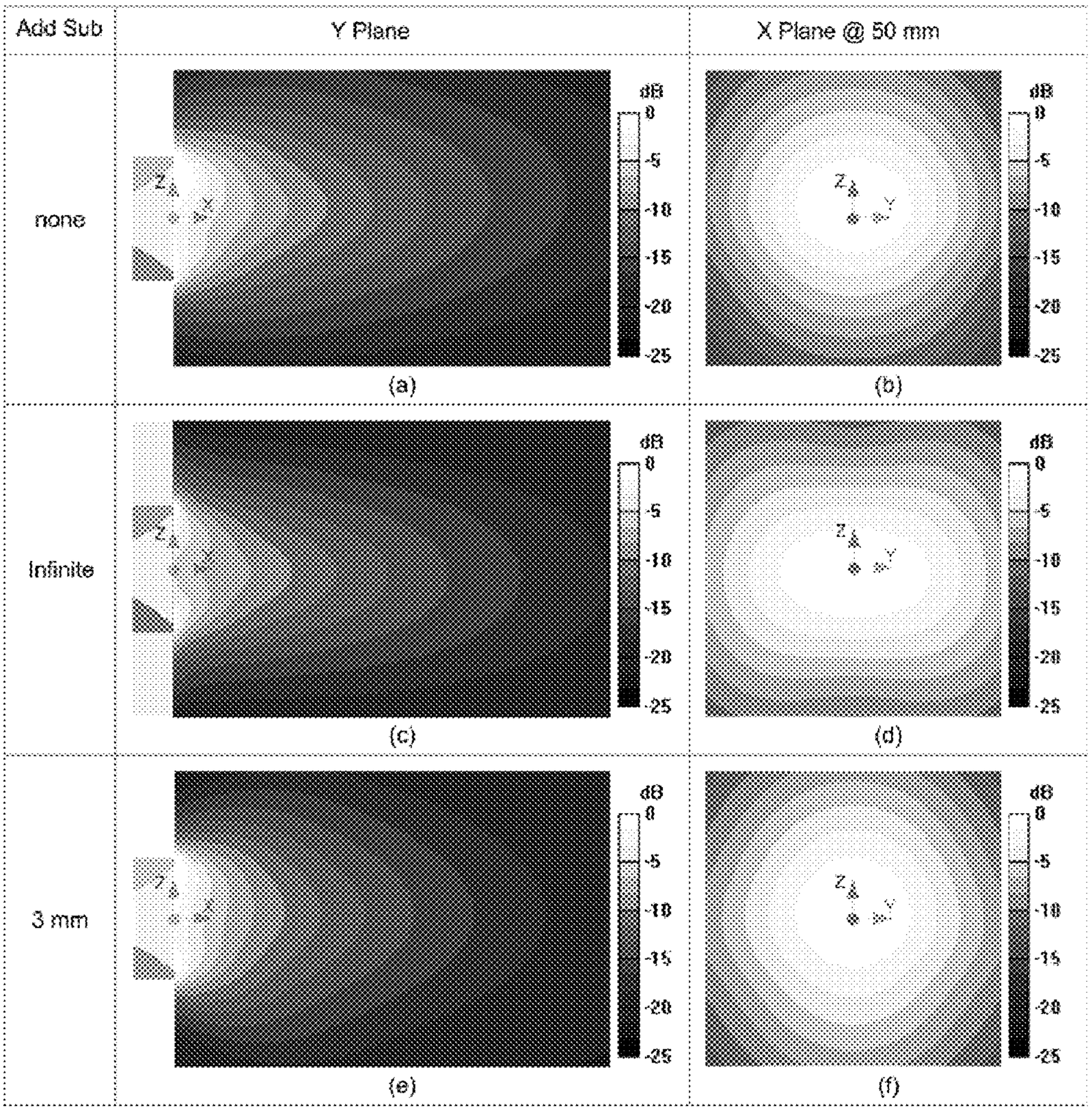
Add Sub
Y Plane
X Plane @ 50 mm
none
Infinite
3 mm
dB
0
-5
-10
-15
-20
-25
Z
Y
X
(a)
(b)
(c)
(d)
(e)
(f)

FIG. 30

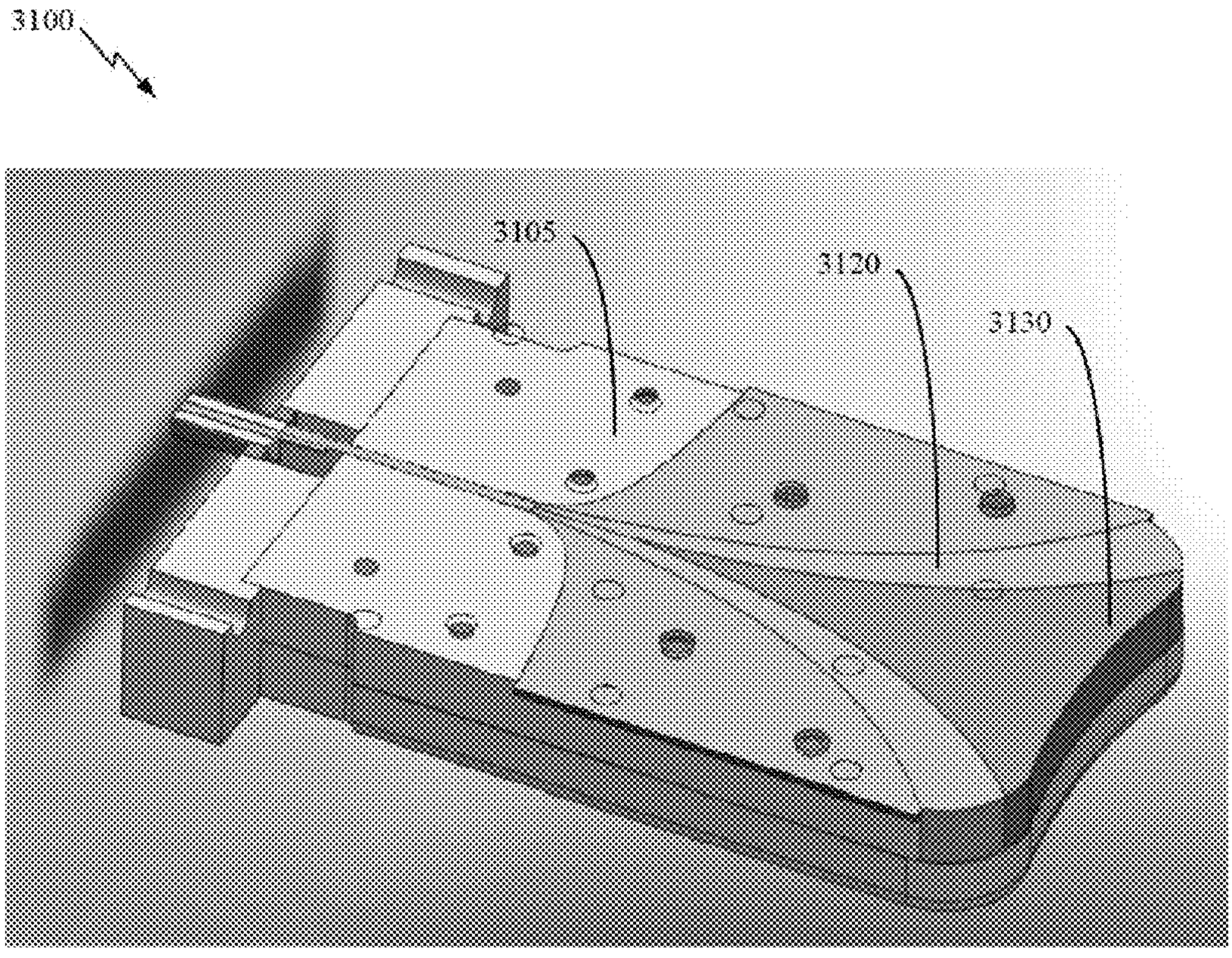

FIG. 31

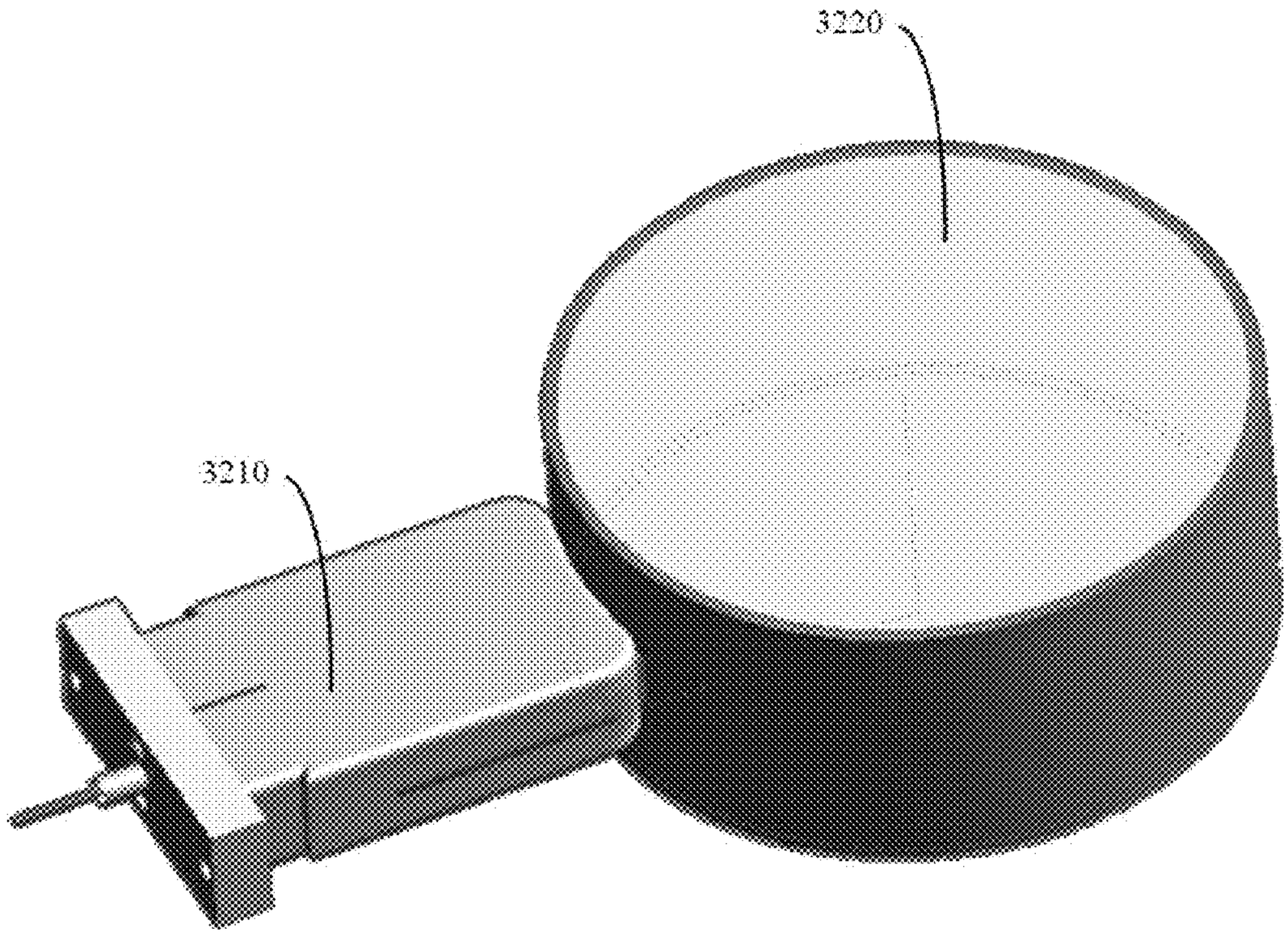

FIG. 32

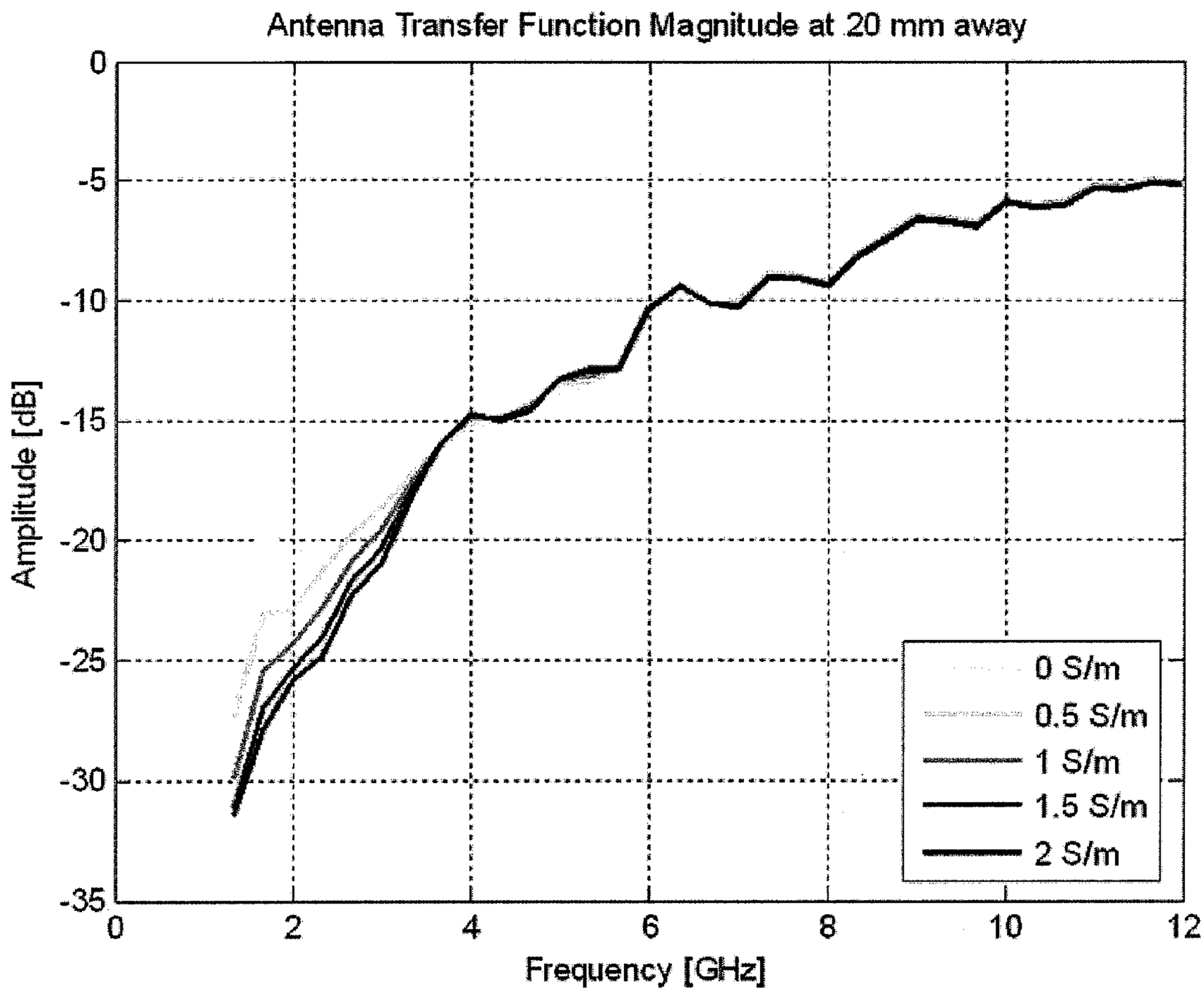

TATF for different immersion liquid conductivities

FIG. 33

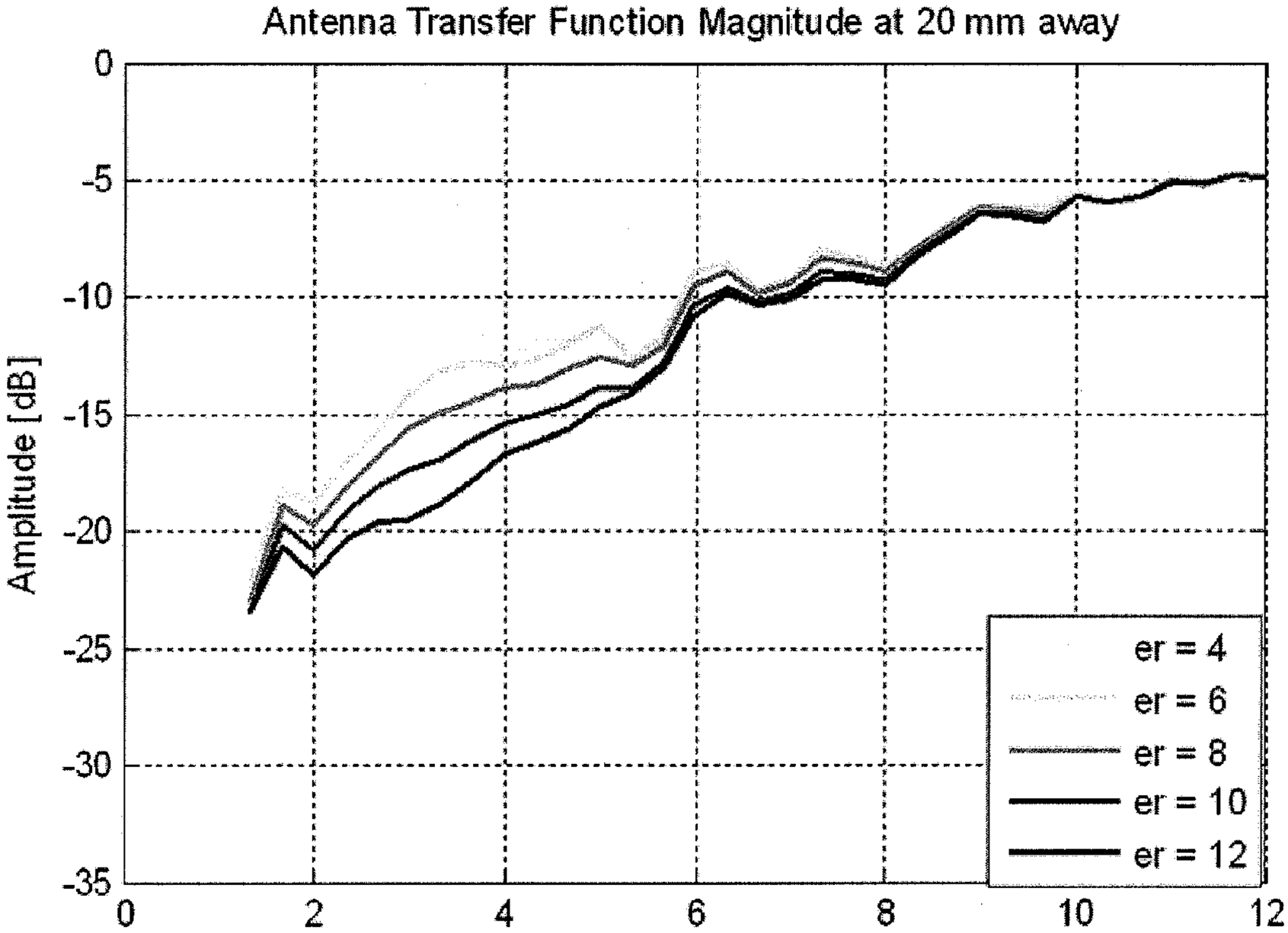

TATF for different immersion liquid relative permittivity

FIG. 34

TRAVELING-WAVE ANTENNA

CROSS-REFERENCE TO RELATED APPLICATIONS

This application claims the benefit of U.S. Provisional Patent Application No. 61/197,560 filed on Oct. 27, 2008, the entire contents of which is specifically incorporated herein by reference without disclaimer.

TECHNICAL FIELD

This disclosure relates to traveling wave antennas and, more specifically, traveling wave antennas having enhanced directivity.

BACKGROUND OF THE INVENTION

Generally, antennas can be configured to transmit and/or receive energy in the form of electromagnetic waves. In many cases, antennas are coupled with one or more electrical device components and can be configured to transmit and receive signals over a distance, e.g., to relay information. In some cases, antennas are carefully engineered so that signal communication between the antenna and the other device components proceeds with minimal loss in signal integrity, e.g., fidelity. For example, medical imaging devices, such as magnetic resonance imaging machines or microwave imaging systems, can transmit energy and receive corresponding signals through use of specialized antennas. In such applications, signal fidelity can be an important aspect of device operation.

SUMMARY OF THE INVENTION

In general, this document describes endfire aperture-based traveling wave antennas, such as Vivaldi antennas. In some embodiments of the Vivaldi antenna, a director is incorporated into the aperture region of the antenna to provide enhanced radiation directivity. In various embodiments, the director can be a shaped dielectric that interacts with an electromagnetic field to reduce the divergence of the resultant beam as it exits the antenna. In some embodiments of a Vivaldi antenna, additional substrate layers are stacked on both sides of the antenna in order to balance the dielectric loading between the different conductors. The substrates may also eliminate contact between the antenna metallization and the lossy environment.

In a first aspect, an endfire aperture-based traveling wave antenna includes a plurality of conductors separated by a dielectric material and coupled to the antenna feed structure to cooperatively transmit and receive electromagnetic radiation, the plurality of conductors including at least a first flared conductor that flares outwardly from a longitudinal axis and a second flared conductor that flares outwardly from the longitudinal axis in an orientation opposite from the first flared conductor so as to at least partially define an aperture region therebetween. The antenna further includes a director arranged in the aperture region between the first flared conductor and the second flared conductor to provide a concentrated radiation pattern when transmitting the electromagnetic radiation. The director includes a material having a dielectric permittivity higher than the dielectric material that separates the conductors.

Implementations can include any, all, or none of the following features and configurations. The first flared conductor and the second flared conductor can be at least partially defined by an aperture curve and a flare curve. The first and second conductors can curve outwardly, away from the longitudinal axis so as to exhibit separation variations along a length of the first and second conductors. The plurality of conductors can include a third flared conductor that curves outwardly from the longitudinal axis in an orientation opposite the first flared conductor. The first flared conductor can include a central conductor and the second and third conductors can include ground conductors. The first conductor can be separated from the second conductor by a first substrate layer of dielectric material and the first conductor is separated from the third conductor by a second substrate layer of dielectric material. The director can be shaped to substantially conform to a surface of an object for illumination.

In a second aspect, an endfire aperture-based traveling wave antenna includes ground and conductor electrodes each having a flared contour and configured to cooperatively emit radiation in a selected propagation direction, the ground and conductor electrodes being separated by one or more dielectric substrates. A director is configured to at least partially focus the radiation in the selected propagation direction and is arranged at least partially between said ground and conductor electrodes.

Implementations can include any, all, or none of the following features and configurations. The endfire aperture-based traveling wave antenna may be a Vivaldi antenna or an antipodal Vivaldi antenna. The antipodal Vivaldi antenna can be a balanced antipodal Vivaldi antenna. The radiation can be broadband radiation. The broadband radiation can be within a frequency range of about 2 to 18 GHz. The dielectric permittivities of the director can be higher than the dielectric substrate. The configuration to focus or direct said radiation in said selected propagation direction can include the director having dielectric permittivities and a shape that affects propagation of an electromagnetic pulse or wave traveling along the ground and conductor electrodes in a determinable manner. The antenna is immersible in an immersion medium, and in one embodiment, the immersion medium is oil, such as canola oil. In another embodiment, the antenna is immersible in glycerin.

In a third aspect, a method for detecting objects beneath or disposed in biological tissue includes providing the Vivaldi antenna described above and configured for use in a tissue sensing adaptive radar (TSAR) system, and using the TSAR system to detect an object beneath or disposed in said biological tissue.

Implementations can include any, all, or none of the following features and configurations. The Vivaldi antenna can be contacted to a breast.

In a fourth aspect, an antenna includes a plurality of planar ground conductors each having a feeding line ground plane, a planar conductor electrode having a signal conductor on a feeding line, a connector for connecting the ground conductors and the conductor electrode to an external assembly capable of transmitting or receiving electromagnetic energy; and a director, disposed in an area between where a first ground conductor and a first conductor electrode curve away from one another. The planar ground conductors and the planar conductor electrode are separated by one or more dielectric substrates, each dielectric substrate having a dielectric permittivity. The director is formed of a material having a dielectric permittivity higher than that of the one or more dielectric substrates.

In a fifth aspect, a balanced antipodal Vivaldi antenna includes a plurality of ground and conductor electrodes each having a flared contour and configured to cooperatively emit radiation in a selected propagation direction. The ground and

conductor electrodes are separated by one or more dielectric substrates having a first dielectric permittivity. Two of the ground conductor electrodes are external layers of the balanced antipodal Vivaldi antenna. The balanced antipodal Vivaldi antenna further includes one or more additional dielectric substrates having a second dielectric permittivity and stacked with the external layers, wherein the one or more additional dielectric substrates are configured to balance a dielectric loading between one or more central conductors and the external layers.

In certain embodiments, the balanced antipodal Vivaldi antenna described above can further include a dielectric coating applied to metallic parts of the antenna that come into contact with a surrounding environment. The dielectric coating can be applied and configured to attenuate electromagnetic losses introduced by a lossy environment.

Unless otherwise defined, all technical and scientific terms used herein have the same meaning as commonly understood by one of ordinary skill in the art to which this disclosure belongs. Although methods and materials similar or equivalent to those described herein can be used in the practice or testing of the present disclosure, suitable methods and materials are described below. In addition, the materials, methods, and examples are illustrative only and not intended to be limiting. All publications, patent applications, patents, and other references mentioned herein are incorporated by reference in their entirety. In case of conflict, the present specification, including definitions, will control.

The term "coupled" is defined as connected, although not necessarily directly, and not necessarily mechanically.

The terms "a" and "an" are defined as one or more unless this disclosure explicitly requires otherwise.

The term "substantially" and its variations are defined as being largely but not necessarily wholly what is specified as understood by one of ordinary skill in the art, and in one non-limiting embodiment "substantially" refers to ranges within 10%, preferably within 5%, more preferably within 1%, and most preferably within 0.5% of what is specified.

The terms "comprise" (and any form of comprise, such as "comprises" and "comprising"), "have" (and any form of have, such as "has" and "having"), "include" (and any form of include, such as "includes" and "including") and "contain" (and any form of contain, such as "contains" and "containing") are open-ended linking verbs. As a result, a method or device that "comprises," "has," "includes" or "contains" one or more steps or elements possesses those one or more steps or elements, but is not limited to possessing only those one or more elements. Likewise, a step of a method or an element of a device that "comprises," "has," "includes" or "contains" one or more features possesses those one or more features, but is not limited to possessing only those one or more features. Furthermore, a device or structure that is configured in a certain way is configured in at least that way, but may also be configured in ways that are not listed.

The details of one or more embodiments are set forth in the accompanying drawings and the description below. Other features, objects, and advantages will be apparent from the drawings and detailed description, and from the claims.

BRIEF DESCRIPTION OF THE DRAWINGS

FIG. **1** is an illustration of a Balanced Antipodal Vivaldi Antenna (BAVA), according to one embodiment.

FIG. **2** shows various design parameters of a BAVA, according to one embodiment.

FIG. **3** shows a perspective view of a BAVA, according to one embodiment.

FIG. **4** is a photograph of a BAVA and references to the BAVA scale.

FIGS. **5**A-**5**C show various perspectives of a BAVA with director ("BAVA-D"), according to one embodiment.

FIG. **6** is a photograph of a BAVA-D and references to the BAVA-D scale.

FIG. **7** illustrates various field sensor reference planes.

FIGS. **8**A and **8**B show simulation results illustrating the concept of the half-energy beamwidth in the near field.

FIGS. **9**A and **9**B show simulation results illustrating the concept of half-energy beam in the near field.

FIG. **10** shows charts of permittivity and conductivity versus frequency for canola oil.

FIG. **11** is a chart of the simulated S_{11} versus frequency for one embodiment each of a BAVA and a BAVA-D.

FIG. **12** is a chart of the simulated fidelity versus distance for one embodiment each of a BAVA and a BAVA-D.

FIGS. **13**A and **13**B show simulation results of energy flux density for one embodiment of a BAVA and BAVA-D over the Y-plane.

FIGS. **14**A and **14**B show simulation results of energy flux density for one embodiment of a BAVA and a BAVA-D over the Z-plane.

FIGS. **15**A and **15**B show simulation results of the half-energy beam from one embodiment of a BAVA and BAVA-D over the Y-plane.

FIGS. **16**A and **16**B show simulation results of the half-energy beam from one embodiment of a BAVA and BAVA-D over the Z-plane.

FIG. **17** is a graph of the simulated S_{21} versus frequency for one embodiment each of a BAVA and a BAVA-D.

FIG. **18** is a chart of S_{11} versus frequency for various embodiments of a BAVA and a simulation.

FIG. **19** is a chart of S_{11} versus frequency for various embodiments of a BAVA-D and a simulation.

FIG. **20** is an illustration of various objects that can be used to test BAVA operability.

FIG. **21** includes charts of normalized voltage versus time for a simulation, and signals obtained using one embodiment each of a BAVA and a BAVA-D to illuminate the same test object.

FIG. **22** includes charts of voltage versus time for measured and simulated results of a system incorporating one embodiment each of a BAVA and a BAVA-D when the same test object is illuminated.

FIG. **23** includes measured reflected energy values of an object at various locations using one embodiment each of a BAVA and a BAVA-D.

FIG. **24** is an illustration of a breast model, according to one embodiment.

FIGS. **25**A and **25**B show the energy flux density induced by one embodiment each of a BAVA (a) and a BAVA-D (b) and according to the model shown in FIG. **24**

FIG. **26** is a chart of voltage versus time for a simulated tumor, obtained by one embodiment each of a BAVA and a BAVA-D.

FIG. **27** shows the effect of a director with different permittivity value on the transmission parameter S_{21} obtained with two embodiments of a BAVA-D, separated by 100 mm and facing each other.

FIG. **28** presents the application of a director to a tapered slot antenna.

FIG. **29** presents the application of a director to a TEM horn antenna.

FIGS. **30**A-**30**F illustrate the radiated energy flux density in front of the antenna when A-B no stacking substrate layers

are used, C-D infinite stacking layers are used, E-F 3 mm thick stacking layers are used.

FIG. **31** is a block diagram illustrating a Cassiopeia antenna according to one embodiment.

FIG. **32** is a block diagram illustrating a Cassiopeia antenna placed in front of a breast model according to one embodiment.

FIG. **33** is a graph illustrating the Transmitting Antenna Transfer Function (TATF) variation of the Cassiopeia antenna for various liquid conductivities.

FIG. **34** is a graph illustrating the Transmitting Antenna Transfer Function (TATF) variation of the Cassiopeia antenna for various liquid permittivity.

Like reference symbols in the various drawings indicate like elements.

DETAILED DESCRIPTION OF ILLUSTRATIVE EMBODIMENTS

In one general aspect, a balanced antipodal Vivaldi antenna (BAVA) is provided. A BAVA can, in some embodiments, include three conductors separated by dielectric layers, the configuration of which will be known to those skilled in the art of balanced antipodal antenna design and function. In certain implementations of a BAVA, the BAVA includes a director, a shaped dielectric located in the antenna aperture that can provide enhanced radiation directivity in the near field, by providing a more directional or concentrated radiation pattern than a BAVA without a director. In certain implementations of a BAVA, the BAVA includes stacking substrates in order to balance the dielectric loading or reduce contact with lossy media in which the antenna may operate.

Referring now to FIG. **1**, one embodiment of a BAVA includes three copper conductors **105***a-c*; two of the conductors **105***a* and **105***c* are connected to feeding line ground planes **110***a* and **110***c*; the central conductor **105***b* is connected to the signal conductor of the feeding line **110***b*. The copper conductors **105***a-c* are separated by dielectric substrates **120***a-b*. Dielectric layers **125***a-b* (stacking substrates) are positioned on the sides of the conductors **105***a* and **105***c* opposite the dielectric substrates **120***a* and **120***b*. Thus, an exemplary stacking structure of a BAVA **100** includes (e.g., from top to bottom) a first stacking substrate **125***a*, a first conductor **105***a*, a first dielectric substrate **120***a*, a second conductor (e.g., the central conductor **105***b*), a second dielectric substrate **120***b*, a third conductor **105***c*, and a second stacking substrate **125***b*. In one embodiment, the dielectric substrate **120***a-b* may be air.

The antenna feed structure **110** can be a gradual transition between a stripline to a tri-strip transmission line (TL), although other configurations are contemplated. The conductor layer width increases linearly while the widths of the ground conductors decrease exponentially to keep constant impedance along the transition. The tri-strip TL extends for a short distance and then the ground and conductor layers start to flare in opposite directions with exponential curvatures to create an antenna aperture, generally indicated at **130**.

Still referring to FIG. **1**, in general, the assembled BAVA **100** can be configured so that the ground layers are in electrical communication with parts of a connector such as SMA attachment elements **150**. An SMA connector **155** is in electrical communication with the SMA attachments **150** and the feeding line **110***b*. The SMA connector **155** is configured to provide an SMA connection (not shown in FIG. **1**) so that electrical signals can be transmitted to and from the BAVA to external components. Contact between the ground layers and the SMA attachment elements **150** can be made by applying pressure thereto using, e.g., two screws (not shown in FIG. **1**). The contact between the SMA connector **155** and the feeding line **110***b* is also achieved when pressure is applied, e.g., with the two screws. Other attachments may be used in place of the SMA connector.

In general, one or more layers of supportive substrate (e.g., substrate **120***a-b*) can be disposed adjacent to, and in-between the conductor layer **105***b* and ground layers **105***a*, **105***c*. Substrates **120***a-b* can be formed from materials providing select electrical characteristics that can optimize the function of the BAVA; some of those characteristics are described herein. In one embodiment, the substrates can be formed of materials with permittivity similar to the surrounding environment and very low conductivity. This eliminates contact between the antenna conductors and a lossy medium in which the antenna operates. The substrate **120***a-b* may have one or more recesses on a surface of the substrate **120***a-b*. This can allow one or more of the ground layers **105***a*, **105***c* or the conductor layer **105***b* to lay flush within the recess, which may provide advantages for assembly and function.

In general, one or more of the stacking substrates **125***a-b* can conjoin one or both of the external ground layers (**105***a* or **105***c*). The material properties of the one or more stacking substrates **125***a-b* are described herein. Generally, the material can be chosen to be the same as the supportive substrate layers in order to balance the dielectric loading between the central conductor and the external ground plates. It can also be chosen to effect a desired electromagnetic interaction between the ground layers and the environment such as reducing the loss induced by a lossy environment.

Referring now to FIG. **2**, some of the geometric parameters of a BAVA **200** referenced herein include: W, L and T as variables representing the overall width, length and thickness respectively; Ws and Wg corresponding to the width of the stripline and corresponding ground planes **205***a* and **205***c* (note that only one ground plane is depicted in the side-view of the BAVA **200** for clarity); Wts is the width of the tri-strip TL; Wa defines the actual aperture **230** width; and Lt, Lts and La correspond to the transition, tri-strip TL, and aperture length respectively. The dielectric thicknesses are defined by T**1** for the supportive substrates and T**2** for the stacking layers.

In one embodiment, when the conductors are stacked layers, a longitudinal axis **240** is arranged in a longitudinal cross-sectional plane between the curved conductors as shown in FIG. **2**. In preferred embodiments, the orientation of the ground conductors **105***a*, **105***c* are mirror opposites (ignoring the vertical displacement of the conductors in the stacked arrangement) of the central conductor **105***b* about the longitudinal cross-sectional plane.

The exponential curves for the transition, flare and aperture (Et, Ef, Ea respectively) can be defined by:

$$z = \pm A \cdot e^{P(x-B)} + C \quad [1]$$

where A is a scaling factor, P the magnification factor, B the shifting value, and C an offset. Exemplary parameters for one implementation of a BAVA are given in Table 1. Other flaring shapes are also contemplated in addition to the embodiment described herein.

TABLE 1

Exponential curve parameters based on a system coordinate origin of FIG. 2

Curve	A	P	B	C
Et	$\frac{Wts - Wg}{2(e^{P_t L_t} - 1)}$	P_t	0	$\frac{Wg}{2} - A_t$
Ef	A_f	P_f	Lt + Lts	$\frac{Wts}{2} - A_f$
Ea	$\frac{Wts + Wa}{2(e^{P_t L_a} - 1)}$	P_a	Lt + Lts	$-\frac{Wts}{2} - A_a$

Referring to FIG. **2**, in one embodiment of a BAVA, the overall length (L) is selected to be 74 mm with Lt=23 mm, Lts=1 mm and La=50 mm. In some cases, choosing a substrate dielectric with a permittivity slightly higher than the surrounding environment can produce favorable radiation behavior while the thickness of the supportive substrate (T**1**) has been shown to not significantly influence the antenna performance. In one embodiment of a BAVA, the substrate dielectric has E_r=2.94. In some cases, a thicker substrate can lead to better antenna operation.

A BAVA of the type described herein, e.g., BAVA **100**, can be manufactured or produced by methods known in the art. In one approach, a photolithography process can be used to pattern the copper conductor layers (e.g., ground and conductor layers **105***a-c*). The layers can be bonded using Rogers 3001 bonding film, available from Rogers Corporation (Rogers, Conn.). The bonding film has a relative permittivity of 2.28, similar to the substrates. The feeding structure (e.g., feed **110***a-c* in FIG. **1**) can be a custom-made SMA-to-stripline transition having an overall length of 6 mm, excluding the connector. A photograph of a BAVA is shown in FIG. **4**.

Stacking Substrate Layers

In general, stacking substrate layers may be placed in contact with the external ground layers of a BAVA. In some cases, when the supporting substrate layers of a BAVA have a permittivity different than the surrounding environment, a squint of the radiation pattern can result. Without wishing to be bound by theory, this behavior seems to originate from an unequal dielectric loading between the conductor and ground plate. One solution that restores symmetry involves stacking an additional substrate layer on the external side of the antenna.

Referring now to FIG. **30**, as proof of concept, a BAVA structure with supportive layers of relative permittivity of 5 has been evaluated (where the surrounding environment has a relative permittivity of 2.5). Without any additional substrate, a squint was observed in the main radiation beam (FIGS. **30**A-B). The structure was simulated with an infinite substrate coating having the same permittivity as the supporting substrates and then a practical case with a 3 mm thick substrate layer on both sides of the antenna. The infinite substrate coating seemed to cause the radiation squint to vanish, as observed in FIGS. **30**C-D. The 3 mm thick additional substrates reduced the original squint by moving the maximum field intensity from z=3.8 mm to z=1.6 mm at 50 mm (FIGS. **30**C-D).

When the stacking layers were used, the antenna efficiency was increased. In one BAVA implementation, an increase in efficiency of 20% was observed between antennas with and without stacking substrates and immersed in lossy canola oil.

BAVA-D

In general, a director can be incorporated into the aperture region of an antenna, e.g., a BAVA (BAVAs that incorporate a director are hereinafter referred to as a BAVA-D). It will be understood that the directors discussed herein are framed in various embodiments of BAVA's, however, the use of dielectric directors is equally contemplated in other types of traveling wave antennas, for example, a TEM horn antenna, and various tapered slotline antennas. In general, a director can provide advantages when, for example, a narrow or more focused radiation beam is preferred. Some of the geometric details of an exemplary director are shown FIGS. **5**A-C, and a photograph of the constructed BAVA-D is shown in FIG. **6**.

Referring now to FIGS. **5**A-C, in one embodiment of a BAVA-D **500**, a BAVA director **510** can be a shaped dielectric (e.g., substantially diamond-shaped) positioned at least partially within the aperture **520**. In some embodiments of a BAVA-D **500**, the director **510** may be positioned completely within the area defined by the aperture region plus any portion of the stacking or dielectric layers that may extend beyond the aperture region. In yet another embodiment of a BAVA-D **500**, the director **510** may be positioned such that a portion of the director **510** is within the aperture region while another portion extends beyond the area of the aperture region and the dielectric and stacking substrates, as best illustrated in the top-down perspective view of FIG. **5**A. The director **510** can include a profile that reduces the likelihood of creating radiation reflections from the lower and upper boundaries, i.e., the start **505** and the end **535** of the aperture **520** respectively. The portion of the director in the antenna structure can substantially follow a curvature (generally indicated at **540**) of the conductor **525** on one side and that of the ground plates **530***a*, **530***b* on another side. A portion of the director **510** extending outwardly from the aperture (generally referred to by indicator number **550**) can include a triangle-like shape **555** that reduces the likelihood of creating reflections within the aperture **520**. In general, curved portion **540** in FIG. **5**A illustrates a flared portion that extends from the start **505** to a distal portion of the antenna.

In some cases, the director can be a material having a select dielectric permittivity, and can generally be enclosed in the BAVA aperture, e.g., aperture **130** in FIG. **1**. In some embodiments of a BAVA-D, the director is made of a material having higher dielectric permittivity than that of the surrounding dielectric layers. In some embodiments of a BAVA-D, the director is made of multiple materials with a range of dielectric constants.

In one exemplary embodiment of a BAVA-D, the maximum width is 26 mm and the total length of the director is 40 mm, which includes 10 mm of director material that protrudes outside of the original antenna (e.g., that indicated by reference numeral **550** in FIG. **5**). In this embodiment, the substrate length of the BAVA can be extended to accommodate the mechanical placement of the director. The director can be made, for example, from Eccostock HIK material, having a relative permittivity of 6 (double that of the original substrate) from Emerson and Cuming (Billerica, Mass.). Other suitable permittivities and/or materials may be used for the director, however.

In general, a director may be incorporated into the BAVA aperture by various methods. For example, a director may be machined out of a selected dielectric material such that the contours of the flared portions of the ground and conductor planes match a portion of the director. In some embodiments, a small recess may exist in-between the director and the conductors, i.e., the director can be fixed at a selected distance

from the metallization. In some embodiments the director may be affixed to the BAVA aperture using a selected adhesive, for example Eccostock cement from Emerson and Cuming Microwave Products.

Simulations

Prior to implementation of a physical device, the performance of a particular BAVA or BAVA-D design can be assessed using computer simulations, for example using the SEMCAD X computer program available from SPEAG AG, Switzerland. When such simulations are performed, a coaxial TL can be connected to the stripline to represent the SMA-to-stripline transition used in the physical implementation of a BAVA or BAVA-D. Referring now to FIG. **3**, an exemplary modeled antenna **300** may have ground planes **305***a*, **305***c* and conductor **305***b* as indicated.

In some cases, the performance of a BAVA or BAVA-D can be evaluated in terms of S_{11}, the half energy beamwidth (HEBW) and fidelity.

Without wishing to be bound by theory, in some cases, for a classical narrow band application, the power radiated away from the antenna can be used to evaluate the radiation pattern. In the case of a pulsed signal a consideration of the energy content of the signal is preferred. The radiated energy pattern can be calculated using [2] where the radiated electric field ($E_{rad}(\theta,\phi,t)$) is squared and integrated over time before division by the intrinsic impedance of the medium η_0 which is usually air.

$$U_T(\theta,\varphi)=\frac{1}{\eta_0}\int_{-\infty}^{\infty}|E_{rad}(\theta,\varphi,t)|^2\,dt\left[\frac{Ws}{m^2}\right] \quad [2]$$

This equation is defined for the far field, while the fields examined to evaluate the BAVA and BAVA-D are closer to the antenna, or in the near field. In addition, the far field concept assumes an infinitely small antenna situated at the spherical coordinate origin, and is valid in a far-field scenario but may not be valid in the near field. It can be difficult, therefore, to define an appropriate axis origin as reference over the antenna structure. A practical disadvantage may arise if the medium is not uniform, as a specific intrinsic impedance may be needed for each data point.

A Poynting vector (S) can be used to calculate the radiated energy which may provide advantages over the approach described above. In a time-harmonic problem, the vector can represent the density of power flux of an electromagnetic wave, with the vector directed toward the traveling direction. For a time harmonic wave, the vector can include the cross product between an electric field and the complex conjugate of a magnetic field, E and H* respectively:

$$S=\frac{1}{2}\mathrm{Re}\{E\times H^*\}\left[\frac{W}{m^2}\right] \quad [3]$$

Equation [3] can also be used with real time domain data. By integrating the result over time, the EFD(x,y,z) can be obtained:

$$\vec{EFD}(x,y,z)=\int_{-\infty}^{\infty}\vec{E}(x,y,z,t)\times\vec{H}(x,y,z,t)\,dt\left[\frac{Ws}{m^2}\right]. \quad [4]$$

The final result is a vector that can indicate the direction of energy flow, which is useful in the near field, while the norm of the vector can correspond to the value that would be calculated using [2], if considered at the same location. In most cases the intrinsic impedance term is not a required variable since the magnetic field can be used to compute the energy.

Simulated 'field sensors' can be used to record a field value during a simulation at certain points in space. The sensors may record the field along a line, in a plane, or even an entire volume. Line and plane sensors used for the simulations described are herein referred to 'X line' or 'Y plane' as illustrated in FIG. **7**. The fields recorded along a line or in a plane may be processed as appropriate to calculate EFD. For example, practical calculation of EFD results in the following equation:

$$\overline{EFD}(x,y,z)=\int_0^{T_{sim}}\vec{E}(x,y,z,t)\times\vec{H}(x,y,z,t)\,dt\left[\frac{J}{m^2}\right], \quad [5]$$

where E and H are the field values in the time domain from the simulation and T_{sim} is the total simulation duration.

To assess the radiation pattern in the near field, the EFD can be computed over adequate areas of interest around the antenna, without having to be related to the axes origin. A qualitative view of the energy pattern for a BAVA is illustrated in FIG. **8**A. The pattern can be produced in a post-processing step based on the data recorded by the field sensors; this step can be programmed into SEMCAD X using the Python scripting environment, for example. Since, in most cases, the propagation direction of the energy is known, an additional feature that records the total energy entering and leaving the sensor boundaries can be added into the algorithm. For example, if an X plane sensor is placed away from the antenna, it is possible to record how much energy goes through the sensor in one direction or the other. In some cases, if an antenna is surrounded by sensors, antenna efficiency can be computed.

The Half Energy Beamwidth (HEBW) can be an acceptable way to quantify a radiation pattern. In the far-field, the HEBW can be the angular separation of the points on a specific plane where the radiated energy is one half of the maximum. The HEBW can be defined in the near field by measuring the half energy contour on a plane normal to the main radiation direction, using the maximum energy located on the same plane as reference. The half energy contour is usually elliptical and the HEBW can be quantified by measuring its two axes as shown in FIG. **8**A. In some cases the HEBW can be evaluated at different distances from the antenna aperture as illustrated by FIG. **8**B.

In some cases, a drawback of this method is that the resulting HEBW can depend on the distance from the antenna, which can complicate the performance comparison between two antennas. FIG. **8**B shows that when the HEBW is measured at many different locations away from the antenna, the beam spreads out in a conical shape. In this case, the beam could be modeled using an equivalent angular beamwidth in conjunction with a corresponding beam origin.

In order to implement this method according to one embodiment, the EFD values located at a common distance from the antenna aperture can be normalized to the maximum energy recorded at the same distance. FIG. **9**B shows a result including a Half Energy Beam (HEB) which was produced using a Python script based on the EFD data shown in FIG. **9**A. The half energy contour and the maximum energy path can be fit to linear functions that are used to define the beam origin location, HEB and beam deviation, as shown in FIG.

9B. A beam deviation metric may be needed when the direction of the main beam is not aligned with the coordinate axis.

FIG. **10** shows that canola oil is a dispersive material whose permittivity and conductivity can vary with frequency. For most simulations incorporating canola oil as the background, the average permittivity value of ϵ_r=2.5 and the maximum conductivity of 0.04 S/m can suffice. In some cases, however, such as when reflections from an object placed away from the antenna are received, it may be necessary to simulate the oil as a dispersive material. This can be accomplished, e.g., using the 'Dispersive Model Parameter Optimization' tool available in SEMCAD X; a single pole Debye model was found to be suitable to fit most canola oil properties.

The representation of the HEB in the near field can be very useful since it models the actual radiation behavior and therefore allows straightforward comparison between different antennas or different antenna configurations. It should be noted that, in some cases, this representation of the radiation beam becomes accurate only at a certain distance from the antenna aperture. In the examples given herein, the representation can be considered correct beginning at a distance of 30 mm from the antenna aperture.

In one approach to antenna assessment, the antenna fidelity can be a measure of how faithfully an excitation pulse is transmitted or received by the BAVA, and can reflect the distortion due to the frequency band limitation and phase non-linearity. The transmission fidelity (F(x,y,z)) can be calculated using [6]. In one approach, the calculation can include maximizing a cross correlation between a component of the electric field measured at a specific position (E(x,y,z,t)) and a reference signal r(t) which is the time derivative of the excitation signal. Both signals are normalized according to [7] and [8]. In some cases, the z-component of the electric field dominates the radiated field, and therefore the fidelity can be calculated using only the z-component:

$$F(x,\ y,\ z) = \max_{\tau}\left(\int_0^{T_{ref}} \hat{E}_z(x,\ y,\ z,\ t+\tau)\hat{r}(t)\,dt\right); \quad [6]$$

$$\hat{E}_z(x,\ y,\ z,\ t) = \frac{E_z(x,\ y,\ z,\ t)}{\left[\int_0^{T_{sim}} |E_z(x,\ y,\ z,\ t)|^2\,dt\right]^{1/2}}; \quad [7]$$

$$\hat{r}(t) = \frac{r(t)}{\left[\int_0^{T_{ref}} |r(t)|^2\,dt\right]^{1/2}}; \quad [8]$$

where T_{ref} is the time length of the reference signal and T_{sim}, remains the total simulation time.

In one approach, reflections from the antenna (S_{11}) can be simulated using a broadband excitation, such as the signal provided by the SEMCAD X software package. The simulations for the EFD and fidelity, however, can be computed using an ultra-wideband pulse excitation of the form:

$$V(t)=V_0(t-t_0)e^{-(t-t_0)^2/\tau^2}, \quad [9]$$

where V_0 is used to adjust the amplitude of the pulse, τ=62.5 ps, and $\tau_0=4\tau$. In some cases, a disadvantage of a time based characterization includes its dependency on the antenna excitation waveform. The use of different pulses will produce different energy radiation pattern(s).

In some implementations of a BAVA or a BAVA-D, the antenna can be used in an immersion medium. One exemplary immersion medium is oil, e.g., canola oil, however other immersion media are equally contemplated. Tissue sensing adaptive radar imaging for breast tumor detection, U.S. patent application Ser. No. 10/942,945, now fully incorporated by reference, describes an implementation of a submersible antenna where a BAVA or BAVA-D is contemplated for use. A tissue sensing adaptive radar (TSAR) system can utilize canola oil as a preferred immersion medium, thus the electrical properties can be applied and integrated into simulations of a BAVA or BAVA-D.

In one embodiment of a BAVA, the transition dimensions Wg, Ws and Wts (FIG. **2**) are selected to provide TLs having 50 Ohms characteristic impedance at both ends and P_t is selected to get the best transmission coefficient (S_{21}) when two transitions are placed back to back. The dielectric is RT/Duroid® 6002 from Rogers Corporation, which has a relative permittivity of 2.94. The thickness T**1** is 1.524 mm, which was purposefully chosen to accommodate the coax-stripline transition, and T**2**=3.048 mm, which was the thickest material available. The various lengths are: L=74 mm, Lt=23 mm, Lts=1 mm, and La=50 mm. The remaining parameters are: W=44 mm, Wa=34 mm, Wg=10, Ws=2 mm, Wts=2.24 mm, T=~9.2 mm, P_t=–0.15, P_f=0.4, P_a=0.05 and A_f=0.1.

For this embodiment of the BAVA, a director is designed out of an Eccostock HIK material with a relative permittivity of 6. The director generally follows the shape of the aperture, as described previously. The director dimensions are shown in FIG. **5**, and include maximum width of 26 mm and total length of the director of 40 mm. This results in 10 mm of director material that protrudes outside of the original antenna (e.g., that indicated by reference numeral **550** in FIG. **5**). In addition, the substrate length of the BAVA is extended by an additional 4 mm to accommodate its mechanical placement.

Simulations of a BAVA and BAVA-D are performed with the antennas immersed in canola oil. Referring now to FIG. **11**, there are no substantial differences in reflections (S_{11}) between the two versions, except slightly higher reflections are observed at lower frequencies for the BAVA-D. The antennas show better than –7 dB reflection between 1 and 12 GHz.

To evaluate the radiation pattern in the near-field, the HEBW can be defined on a plane orthogonal to the endfire direction (+X in FIG. **7**) that is positioned a given distance from the antenna aperture. To compute the HEBW, the EFD can be computed on a series of planes orthogonal to X and ranging from the antenna feed to a distance of 70 mm away from the aperture. The EFD calculations are shown for both a BAVA and a BAVA-D in FIGS. **13** and **14**, indicating endfire radiation behavior and the effect of the director on the radiation directivity for the BAVA-D. Specifically, the EFD plots in FIGS. **13**A-B indicate a narrower beam and increased intensity at a selected distance away from the antenna with the director present. The EFD plots in FIGS. **14**A-B show that the director contains the fields closer to the antenna structure when compared to the director-free case. The HEB was computed based on the EFD data for qualitative purposes and the results are shown in FIGS. **15**A-B and **16**A-B. This involves fitting curves to points where the EFD distribution is half of the maximum value, then tracing the curves to an intersection point located in the antenna aperture. The angle between the curves is taken as the half-energy beamwidth. The beam origin, or intersection of the curves, is also noted.

TABLE 2

Simulated beamwidth dimensions for the BABA and BAVA-D.

	Parameters				
	Y plane		Z plane		
	Antenna				
	BAVA	BAVA-D	BAVA	BAVA-D	Unit
HEB	32	34	60	51	[°]
Beam Deviation	3	4	0	0	[°]
Beam origin	x = −28 z = −2	x = −15 z = −1.3	x = −17 y = 0	x = −8 y = 0	[mm]
HEBW (20 mm)	34	23	45	42	[mm]
HEBW (50 mm)	44	40	80	58	[mm]

Referring now to FIGS. **16**A-B, the pulse energy appears more concentrated in the center of the antenna structure when the director is present. The HEB substantially follows the edges of the substrate until the end of the structure for a BAVA-D while the HEB begins to expand outside the substrate boundary around 15 mm before the end of the BAVA. Referring now to Table 2, calculated numerical HEB values for a BAVA and BAVA-D, the effect of the director on the beamwidth can include an overall narrowing on both axes as demonstrated by the usual HEBW values at 20 and 50 mm from the antenna aperture. Without wishing to be bound by theory, the improved radiation patterns that result from director use may not necessarily be due to a smaller HEB angle; instead, the advantages may be mostly due to a shift of the beam origin towards the antenna aperture. For example, the HEB on the Y plane increases from 32° to 34° when the director is used. The HEBW measured at 20 and 50 mm, however, are smaller because the energy starts to expand further away in the x direction, as expressed by the shift of the beam origin from x=−28 to x=−15 mm when using the director. On the Z plane the director reduces the HEB from 60 to 51° while moving the focal point from x=−17 to x=−8 mm. The beamwidth on the Y axis, therefore shrinks as indicated by the HEBW value at 20 and 50 mm.

The simulated fidelity is approximately 0.9 at the aperture and above 0.96 at distances of 20 mm, as shown in FIG. **12**. This order of magnitude is considered as high fidelity for an antenna that radiates electromagnetic pulses. The fidelity is not deteriorated when the director is present, in fact it is higher closer to the antenna. This effect is due to a more constant endfire radiation behavior across the frequency band when the director is used.

In one approach, the transmission parameter (S_{21}) is a parameter that can be used to better understand the director effect in the frequency domain. The information given by S_{21} is the amount of energy that is transmitted between the two antennas. The higher the value of S_{21}, the better the transmission of the energy, and more focused the beam. As shown by FIG. **17**, the presence of the director increases dramatically the S_{21} magnitude between 2 to 12 GHz while a null appears at 14 GHz. An antenna with higher S_{21} will receive more reflected energy from an object placed in front of the antenna. In other words, the BAVA-D is expected to provide a larger amplitude response for the same object.

Measurements

Simulations have shown that the director effects a noticeable improvement in the radiation patterns produced from a Vivaldi antenna. The following measurements were obtained to compare actual signals with the simulations; the antennas were immersed in canola oil and data were recorded by an Agilent 8719ES Vector Network Analyzer (VNA). The time signals were synthetically created from the frequency domain S parameter using an inverse Chirp-Z transform approach.

FIGS. **18** and **19** illustrate that the measured reflection coefficients of two different BAVA and BAVA-D's are within agreement to their corresponding simulated data. One known source of error in the measurements arises from the thermoplastic (Rogers 3001 bonding film) used to bond the different layers together because the adhesive does not match the substrate permittivity exactly. The discrepancy remains acceptable, however, since the bandwidth is not altered to an appreciable extent.

Referring now to FIG. **20**, one way to measure and verify the improved directionality in the BAVA-D radiation pattern is to measure the reflections from an object placed in front of the antenna aperture and compare the results with simulations. In one approach, small cubes and spheres of different shape and permittivity can be used (FIG. **20**).

In a general approach, the shape of the backscatter signal can be first compared between two simulations performed with a BAVA and BAVA-D illuminating an object with the same size and properties. Then the intensity of the backscatter energy received can be compared between the two antenna versions, and finally a similar object can be measured at various locations along the projected radiation path to assess the directivity of the antennas.

In one approach, such a measurement setup can include of a tank of canola oil that accommodates placement of the antenna and the object (which can be attached to a Plexiglas rod ($\in_r$=2.6)). A reference measurement of the antenna with only the Plexiglas rod present can be subtracted from each measurement taken with the object so as to obtain a measurement of the object exclusively.

Referring to FIG. **21**, overall the shapes of the measured backscatter signals are very consistent with their simulated counterpart for both the BAVA and BAVA-D. Concerning the main reflection between 1.5 and 2 ns, it can be observed that the signals overlap almost perfectly for the first part while discrepancies appear in the second part (after t=1.8 ns) (referred to as the "late time response"). This discrepancy can be more accentuated for the BAVA-D yet still provides acceptable results.

The simulated results obtained for the different objects demonstrate intensity ratios ranging from 2.6 to 3.6. It was observed that smaller objects tend to exhibit larger ratios; without wishing to be bound by theory, differences in reflections resulting from illumination by two different beams are expected to be more pronounced for smaller objects when the objects are placed directly in the line-of-sight of the beam. Additionally, the director has a more significant impact on focusing the energy of higher frequencies which may also contribute to the larger reflections observed from smaller objects. The measurements confirm the increase in reflected energy observed with the director and its dependency on the object size. However the measured reflected energy is increased from 4 to 8 times when the BAVA-D is used to detect the different objects, which is more or less twice as much as in simulation. Referring to FIG. **22**, the director significantly magnified the tumor response in simulation and measurement.

In another approach to comparing BAVA and BAVA-D data, a spherical object was used. The experimental procedure included measuring backscatter energy from an object at different locations on a common plane. Measurements were taken on an X plane 40 mm away and at 5 different positions along the Y and Z axis spaced by 20 mm. The backscatter energies were normalized to the central measurement point

and converted to dB. Referring now to FIG. **23**, a narrowing of the beamwidth, presumably resultant from the director, is most noticeable along the Y axis where the furthest measurement points (y=40 and y=−40 mm) indicate a backscatter energy of approximately −8 dB with the BAVA and approximately −18 dB with the BAVA-D. The backscatter energies are larger toward the positive Z direction which seems to confirm the beam deviation and its orientation observed in simulation.

BAVA and BAVA-D for use in Breast Tumor Detection

A BAVA and/or a BAVA-D may be used in systems configured to detect objects beneath a surface, e.g., tumors located within biological tissue. One implementation of a BAVA or BAVA-D has been mentioned herein with respect to the TSAR system. In some cases, it can be advantageous to conduct computer simulations to assess the functionality of a BAVA or BAVA-D for this particular application.

In one simulation approach, a realistic breast model, derived from a MRI scan, can be imported into, e.g., SEMCAD X. A 40 mm thick object representing an artificial chest wall can be added to the upper part of the breast model to simulate the human breast anatomy. Referring now to FIG. **24**, the inside of the breast is homogeneous and simulated as adipose tissue with a 6 mm tumor aligned with the antenna. Breast tissue at microwave frequencies is dispersive and modeled in SEMCAD X using single pole Debye models. The Debye parameters are used for the adipose tissue and tumor are found in a reference paper (Lazebnik et al., "Highly Accurate Debye Models for Normal and Malignant Breast Tissue Dielectric Properties at Microwave Frequencies," IEEE_J_MWCL, Vol. 17, pp. 822-824, 2007) while data from a second paper were used to simulate dry skin (Winters et al., "Estimation of the Frequency-Dependent Average Dielectric Properties of Breast Tissue Using a Time-Domain Inverse Scattering Technique," IEEE_J_AP, Vol. 54, pp. 3517-3528, 2006). The chest wall, with a relative permittivity of 50 and electrical conductivity of 4 S/m, is not modeled as a dispersive material. The parameters for the different Debye models are shown in Table 3.

TABLE 3

Debye parameters used to model the properties of different breast tissues.

Parameter	Dry skin	Adipose tissue (group 3)	Tumor	Unit
Epsilon static	37	4.74	54.66	
Epsilon infinity	4	3.14	6.75	
Dispersive conductivity	1.1	0.036	0.79	S/m
Pole amplitude	1	1	1	
Pole relaxation time	7.23	13.56	10.1	ps

The simulations are performed with and without the tumor present so that the tumor reflection could be extracted from the overall signal by a simple subtraction. Additionally, Y and Z Plane sensors are placed in front of the antenna to assess field penetration into the simulated breast. FIG. **25** shows the EFD induced by both antennas on these planes and indicates that more energy is penetrating into the breast when the director is used. This observation is corroborated by the recorded tumor signals shown in FIG. **26**. The energy contained in the main tumor reflection (i.e. without the tail) is 2.6 times larger with the BAVA-D compared to the BAVA. The director may therefore dramatically improve tumor sensing when utilizing a BAVA.

Cassiopeia Antenna with Shaped Director Element

According to one embodiment, a variation of a tapered slot antenna including a director is a Cassiopeia antenna and illustrated in FIG. **31**. A Cassiopeia antenna **3100** has nearly constant radiation performance independent of the surrounding environment. That is, similar performance is achieved by the Cassiopeia antenna **3100** with different dielectric properties in the environment surrounding the Cassiopeia antenna **3100**. A material **3105** includes low permittivity material and isolates the antenna structure from potential conductive environments surrounding the Cassiopeia antenna **3100**. The material **3105** may be, for example, Delrin, which has a relative permittivity of approximately 3. The Cassiopeia antenna **3100** also includes an aperture **3120** having a director **3130** inside the aperture **3120**. According to one embodiment, material in the director **3130** is of higher permittivity than the aperture **3120**. For example, the aperture **3120** may be Eccostock Cement with a permittivity of approximately 10, and the director **3130** may be Eccostock HiK with a permittivity of approximately 12. The relatively high permittivities of the aperture **3120** and the director **3130** concentrate electromagnetic energy inside of the Cassiopeia antenna **3100**.

The director **3130** may be shaped to approximately conform to contours of a surface the object of interest for measurement. For example, a Cassiopeia antenna **3210** for illuminating a breast according to one embodiment is illustrated in FIG. **32**. A Cassiopeia antenna **3210** may include a director shaped to conform to a surface of a breast model **3220** or of a human breast (not shown). Contact between the breast model **3220** and the Cassiopeia antenna **3210** during illumination and measurement may confine electromagnetic energy and substantially prevent deterioration in electromagnetic energy caused by changes in a surrounding environment.

FIGS. **33** and **34** are graphs demonstrating simulated Transmitting Antenna Transfer Functions (TATFs) for the Cassiopeia antenna. The TAFT is a ratio of the power density of the radiated field at a selected position to the excitation power of the antenna. The breast model used for simulation of FIGS. **33** and **34** is a 12 cm diameter cylinder enclosed in a 2 mm layer of skin. The simulated relative permittivity of skin is 36 and of fat is 9. The simulated conductivity of skin is 4 S/m and of fat is 0.9 S/m. FIGS. **33** and **34** are graphs illustrating simulated TATF for different conductivities and permittivities, respectively, for an observation point immediately in front of the Cassiopeia antenna and 20 mm inside the cylindrical breast model.

It is to be understood that while certain concepts have been described in conjunction with the detailed description thereof, the foregoing description is intended to illustrate and not limit the scope of this disclosure, which is defined by the scope of the appended claims. For example, while the discussion above has been mainly presented with reference to BAVA antennas, the disclosed addition of a director may be reasonably expected to perform advantageously in any travelling wave antenna or any other applications necessitating transmission or reception of a short pulse with a narrow beamwidth. Other shapes and permittivity values for the director than those disclosed herein have the potential to produce similar or better results. Referring to FIG. **27**, S_{21} parameters for BAVAs with varying director permittivities are contemplated. It can be observed that a director with different permittivity can improve or degrade the performances at certain frequencies. Referring now to FIGS. **28** and **29**, different director shapes can be used for different types of endfire aperture-based traveling-wave antennas, for example, a tapered slot antenna (FIG. **28**) and a TEM horn (FIG. **29**). In

both cases there is a higher concentration of radiated energy in the endfire direction when the director is present.

Computational techniques and software packages other than those disclosed herein, yet known to those skilled in the art can be used to determine and model the radiation pattern in the near field. For example, options available in SEMCAD X, can create highly realistic simulations. Other aspects, advantages, and modifications are within the scope of the following claims.

What is claimed is:

1. An endfire aperture-based traveling-wave antenna comprising:

a plurality of conductors separated by a dielectric material and coupled to an antenna feed structure to cooperatively transmit and receive electromagnetic radiation, the plurality of conductors including at least a first flared conductor that flares outwardly from a longitudinal axis and a second flared conductor that flares outwardly from the longitudinal axis in an orientation opposite from the first flared conductor so as to at least partially define an aperture region therebetween; and

a dielectric director arranged in the aperture region between the first flared conductor and the second flared conductor to provide a concentrated radiation pattern when transmitting the electromagnetic radiation;

wherein the dielectric director comprises a material having a dielectric permittivity higher than the dielectric material that separates the conductors.

2. The antenna of claim **1**, wherein the first flared conductor and the second flared conductor are at least partially defined by an aperture curve and a flare curve.

3. The antenna of claim **1**, wherein the first and second conductors curve outwardly away from the longitudinal axis so as to exhibit separation variations along a length of the first and second conductors.

4. The antenna of claim **1**, wherein the plurality of conductors comprises a third flared conductor that curves outwardly from the longitudinal axis in an orientation opposite the first flared conductor.

5. The antenna of claim **4**, wherein the first flared conductor comprises a central conductor and the second and third conductors comprise ground conductors.

6. The antenna of claim **5**, wherein the first conductor is separated from the second conductor by a first substrate layer of dielectric material and the first conductor is separated from the third conductor by a second substrate layer of dielectric material.

7. The antenna of claim **1**, wherein the dielectric director comprises several materials, each material having a dielectric permittivity higher than the dielectric material that separates the conductors.

8. The antenna of claim **1**, wherein the director is shaped to substantially conform to a surface of an object for illumination.

9. A Vivaldi antenna, comprising:

ground and conductor electrodes each having a flared contour and configured to cooperatively emit radiation in a selected propagation direction, said ground and conductor electrodes being separated by one or more dielectric substrates; and

a dielectric director configured to at least partially focus said radiation in said selected propagation direction, arranged at least partially between said ground and conductor electrodes.

10. The Vivaldi antenna of claim **9**, wherein said Vivaldi antenna is an antipodal Vivaldi antenna.

11. The antipodal Vivaldi antenna of claim **10**, wherein said antipodal Vivaldi antenna is a balanced antipodal Vivaldi antenna.

12. The Vivaldi antenna of claim **9** wherein said radiation is broadband radiation.

13. The Vivaldi antenna of claim **12**, wherein said broadband radiation is within a frequency range of about 2 to 18 GHz.

14. The Vivaldi antenna of claim **9**, wherein said dielectric director has a dielectric permittivity higher than said dielectric substrate.

15. The Vivaldi antenna of claim **9**, wherein said configuration to at least partially focus said radiation in said selected propagation direction comprises said dielectric director having dielectric permittivities and a shape that affects propagation of an electromagnetic pulse or wave traveling along said ground and conductor electrodes in a determinable manner.

16. The Vivaldi antenna of claim **9**, wherein said antenna is immersible in an immersion medium.

17. The Vivaldi antenna of claim **16**, wherein said immersion medium is oil.

18. The Vivaldi antenna of claim **17**, wherein said oil is canola oil.

19. A method for detecting objects beneath or disposed in biological tissue, comprising:

providing a Vivaldi antenna configured for use in a tissue sensing adaptive radar (TSAR) system; and

using the TSAR system to detect an object beneath or disposed in said biological tissue;

wherein the Vivaldi antenna comprises:

ground and conductor electrodes each having a flared contour and configured to cooperatively emit radiation in a selected propagation direction, said ground and conductor electrodes being separated by one or more dielectric substrates; and

a dielectric director configured to at least partially focus said radiation in said selected propagation direction, arranged at least partially between said ground and conductor electrodes.

20. The method of claim **19**, wherein using the TSAR system comprises contacting the Vivaldi antenna to a breast.

21. An antenna, comprising:

a plurality of planar ground conductors each having a feeding line ground plane;

a planar conductor electrode having a signal conductor on a feeding line;

a connector for connecting said ground conductors and said conductor electrode to an external assembly capable of transmitting or receiving electromagnetic energy; and

a director, disposed in an area between where a first ground conductor and a first conductor electrode curve away from one another;

wherein said planar ground conductors and said planar conductor electrode are separated by one or more dielectric substrates; and

wherein said director is formed of a material having a dielectric permittivity that is higher than a dielectric permittivity of said one or more dielectric substrates.

* * * * *